Submitted to Annual Review of
Nuclear Science

LBL-2952
Preprint

IDENTIFICATION OF NUCLEAR PARTICLES

Fred S. Goulding and Bernard G. Harvey

February 1974

Prepared for the U. S. Atomic Energy Commission
under Contract W-7405-ENG-48

DISCLAIMER

IDENTIFICATION OF NUCLEAR PARTICLES*

Fred S. Goulding and Bernard G. Harvey

Lawrence Berkeley Laboratory
University of California
Berkeley, California 94720

February 1974

I. INTRODUCTION

The past few years have seen a rapid development of techniques by which the identity of species produced in nuclear reactions may be established. There has been an almost equally rapid improvement in the energy resolution that can be obtained from semiconductor detectors and magnetic spectrometers. The present review is limited to techniques for the determination of the atomic number Z and mass number A of nuclear species. Writing a nuclear reaction in the usual way --X(a,b)Y-- we shall review methods for the identification of b and the measurement of its energy. We shall consider only on-line techniques, ignoring methods based on radiochemistry, photographic plates or track detectors. These latter were reviewed by Price and Fleischer (1).

In addition to the determination of A and Z, it is almost invariably required that the energy E of the particle shall be simultaneously measured with the best possible resolution. In many experiments it is sufficient to

*Work performed under the auspices of the U. S. Atomic Energy Commission.

measure the kinetic energy differences between more or less sharp lines in the energy spectrum of particle b, corresponding to the formation of discrete energy states of the residual nucleus Y. If the energies of the states of Y are well known from previous work, even the energy differences need only be measured with sufficient precision to be sure that lines in the b spectrum are correctly associated with states of Y. Nuclear energy levels, however, are frequently spaced very near to each other so only a small spread in the E measurement can normally be tolerated even though the absolute value of E may not be important.

A complete determination of Z, A and E requires the measurement of three quantities that are different functions of Z, A and E. No measurable quantities depend directly upon A, but for the non- or only slightly relativistic particles typically encountered in nuclear physics experiments, A is very nearly equal to the mass of the particle M (in atomic mass units), which is measurable. For non-relativistic particles, M has only near-integral values. It is therefore sufficient that M and Z be determined only with enough accuracy to separate them from adjacent integral values. For light particles (H and He isotopes, for example), this is very easy because the fractional differences between adjacent small

integers are large. For heavy particles, the necessary resolution becomes difficult or even impossible to achieve.

Several classes of measurements that can be made on charged particles provide results that depend on various functional combinations of M, Z and E, but no one measurement uniquely determines these parameters. The value of E is nearly always required in an experiment but individual values of M and Z are often not needed. For example, the quantity MZ^2 can be obtained from a telescope that measures the energy loss of a particle passing through a thin detector into a second detector where its residual energy is deposited and measured. For light ions, e.g. protons, deuterons, tritons, ^{3}He and ^{4}He, the values of MZ^2 are respectively 1, 2, 3, 12 and 16. Therefore the value of MZ^2 determines M (or A) and Z unambiguously. For heavier ions, though, successive values of MZ^2 become closer together so that more elaborate identification measurements must be made. To provide perspective on later portions of this paper, a simplified view of the various methods and the information they yield will now be given:

i) Total absorption in a detector (or detector telescope)

Measurement of the total ionization produced in the detector(s) provides a measure of the particle energy E. An ideal detector produces an output signal linearly related to E.

ii) Energy absorption in a thin detector

A thin transmission detector, included in a detector telescope, provides a direct measure of a particle's rate of energy loss for a particular segment of its track. The energy of the particle on leaving the transmission detector can be determined by summing ionization signals from the later detectors in the telescope. The rate of energy loss is approximately given by the simplified Bethe-Bloch (2) equation:

$$- dE/dx = (aZ^2c^2/v^2) \ln[bv^2/(c^2 - v^2)] \qquad 1.$$

where v is the particle velocity, c is the velocity of light and a and b are constants dependent only on the detector material. Although the Bethe-Bloch equation is tradionally written in terms of the atomic number Z, the rate of energy loss actually depends on an effective charge state q_{eff} of the moving ion, which may not be fully stripped of atomic electrons ($q_{eff} \leqslant Z$).

Since the logarithmic term varies only slowly with energy (or velocity) its effect will be neglected in this approximate

discussion. Also, for non-relativistic particles, $v^2 = 2E/M$. therefore Equation 1 can be simplified to:

$$dE/dx \propto MZ^2/E \qquad 2.$$

As stated earlier, E can be computed by summing the detector telescope signals, so the measurement of dE/dx provides a measure of MZ^2.

iii) Time-of-flight measurement

Measurement of the time of flight (TOF) of a particle through a known flight path in vacuum determines the particle velocity v. We have:

$$v^2 = 2E/M \qquad 3.$$

If the value of E is known, then the TOF determines M. If this measurement of M is combined with a dE/dx determination, Z can be determined.

In principle, therefore, a detector telescope measuring TOF, E and dE/dx uniquely identifies a reaction product particle. Unfortunately, limitations in the accuracy of determination of E, dE/dx and v blurr the results and prevent unique identification for the heavier isotopic species.

iv) Bending in a magnetic field

Magnetic spectrometers provide yet another determination of a combination of the particle parameters M, Z and E. In a fixed magnetic field B, the radius of curvature ρ of a particle is given by:

$$B\rho \propto Mv/Z \qquad 4.$$

Light particles, or heavy ions at high energies, emerge from a target fully stripped of electrons so that q is equal to Z. Measurement of $B\rho$, TOF and dE/dx is, in this case, equivalent to a complete identification and energy measurement. For heavy ions at lower energies, $q \leqslant Z$ and there may be ambiguities in the identification: these are discussed in Section IV.

Other physical effects that depend on M, Z and E can also, in principle, be used for particle identification. The deflection of a particle in an electric field is one example, but this effect is so small for the high-velocity particles of interest that it has not yet been used.

II. IDENTIFICATION BY ABSORPTION IN A DETECTOR TELESCOPE

Basic ΔE,E Systems

As indicated earlier, signals obtained from detectors in a telescope can be used, either alone or, where necessary, together with another measurement (e.g. time of flight), to identify the fragments produced in a nuclear reaction. The simplest type of telescope and the essential elements of the associated electronics are shown in Figure 1. In such a ΔE,E telescope, the detector thicknesses are chosen so that the particles of interest pass through the front ΔE detector, providing a ΔE signal, then stop in the rear E detector. The total energy signal can be derived by adding the two signals, and particle identification can be obtained from the individual signals.

Referring to Figure 1, signals from the detectors are amplified to a convenient level and, providing that they satisfy certain energy (i.e., amplitude) and timing requirements, they are allowed to pass into the signal adder to generate the total energy signal. They also feed an identifier which develops an output signal whose size is ideally determined only by the type of particle--independent of its energy. The identifier function may be performed by a special-

purpose analog computer unit, or by a digital computer--or sometimes by both. In general, analog calculations can be performed in a very short time while digital operations are slower, but offer more flexibility and accuracy. As shown in Figure 1, signals from the two detectors must be coincident in time and fall into energy windows defined by the single-channel analyzers. These two requirements reduce the chance that the summation of signals generated by two fragments will produce a particle identifier output that corresponds to a third type of ion. Narrowing the energy acceptance windows to the minimum values consistent with detecting the rare events, and reducing the resolving time of the fast coincidence circuit to its minimum tolerable value, reduces the chance of false identification.

Identification Algorithms

As shown in the Introduction, knowledge of dE/dx and E is adequate to establish the quantity MZ^2 for an ion. In principle, therefore, a table look-up procedure can be used to identify the particle--or at least to identify its MZ^2 value. When a computer is available, this technique is sometimes used (3,4), but it is often simpler, using the ΔE and E signals, to generate a function whose

value is characteristic of a particular type of ion and independent of its energy. The purpose of the algorithms to be discussed here is to provide suitable readily-computable analytical functions that come close to achieving this ideal.

Identification of ions by a $\Delta E,E$ detector telescope depends on the deposition of energy by an ion passing through the detectors, and the resulting ionization that creates the output signals. Therefore, we must consider the energy loss - ionization process. The complete Bethe-Bloch equation which describes a charged particle's rate of energy loss by ionization is:

$$- dE/dx = 4\pi n(e^4/m)(q^2/v^2)\ \ln\{[2mv^2/I(1 - \beta^2)] - \beta^2 - S - D\} \qquad 5.$$

where:

n is the number of electrons/cm^3 of the absorber,

e and m are the charge and mass of the electron,

q is the charge (in electronic units) on the ion. (Note: in cases where q is constantly changing; its mean square value at the appropriate energy should be used in Equation 5.)

v is its velocity,

β = v/c where c is the velocity of light,

I is the mean ionization potential for the absorber.

The value of I is often taken as being equal to approximately $13Z_A$eV, but a more accurate value (5) is $Z_A(9.76 + 58.8Z_A^{-1.19})$ when the atomic number Z_A of the absorber is greater than 13.

S is the shell correction which allows for the fact that the electrons from different shells do not all equally participate in the ionization process,

D is a density correction.

The corrections S and D are minor and will be neglected in the following discussion. Furthermore, in most nuclear reaction experiments, the ions are non-relativistic (i.e., $\beta^2 \rightarrow 0$). In these cases, Equation 5 can be reduced to a simpler form.

A better perspective on the basis and limitations of various methods of identification results from examination of the variation of stopping power (i.e., dE/dx) over a wide range of energies. The curves given in Figure 2, adapted from Northcliffe (6,7), show the behavior of various ions in an aluminum absorber. Since the stopping power (see Equation 5) is basically

dependent on velocity rather than energy, and ions of different mass all have the same velocity when they have the same value of E/M, it is convenient to plot the curves in terms of E/M.

The vertical scale of Figure 5 is in terms of $(1/Z^2)$ dE/dx, where Z is the nuclear charge of the ion. In Equation 5 , however, the ion charge q is the effective charge state of the ion. For a proton, q = Z over most of the energy range shown in Figure 2, but for very heavy ions, the atom is only fully stripped at the very highest energies. For this reason, the curves of stopping power/Z^2 for heavy ions depart from those for protons except at the highest energies. At the lower velocities, ions capture sufficient electrons to become neutral at least part of the time. In this region, collisions of the neutral atom with electrons and nuclei become the dominant energy loss mechanism. Collisions with electrons produce a variation in stopping power proportional to the ion velocity (shown dotted for the heavier ions), while nuclear collisions become dominant at very low velocities (full lines for the heavier ions).

A useful practical feature of the stopping power curves of Figure 2 is that, for all ions of $Z < 10$, a power-law approximates the curves over a useful part of the range of energies. Thus, we have:

$$\text{Stopping Power}/Z^2 \propto (E/M)^n \qquad 6.$$

where the value of n varies from about -0.75 for a proton, to -0.5 for a very heavy ion, for the energies commonly encountered in nuclear reactions. The validity of the power-law approximation for protons stems from the 1/E behavior of the main term in the right-hand side of Equation 5 , combined with the fact that the slow variation of the logarithmic term can be closely represented by a $E^{0.3}$ law over the energy range of interest. For heavy ions, charge exchange processes at low energies modify the energy dependence resulting in a change in the exponent n.

Particle identifiers generally use one of two basic algorithms. The earliest identifiers (8-13) are based directly on simplified versions of Equation 5. For non-relativistic particles we may write:

$$-dE/dx = a(q^2M/E)\ \ln(bE/M) \qquad 7.$$

where a and b are constants depending on the absorber material. If a detector of thickness Δx absorbs a very small fraction of the incident energy of a particle to produce a signal proportional to the loss ΔE, and if a second detector then absorbs the remainder of the energy E to produce a signal proportional to E, according to Equation 5 , the signals are related as follows:

$$E\Delta E \propto \Delta x\ (Mq^2)\ \ln(bE/M) \qquad 8.$$

Neglecting the slow variation with energy of the logarithmic term, we see that the product of the total energy signal and the signal in the ΔE detector is a measure of Mq^2. This product can readily be computed by a computer or by the analog circuits described in the next section to yield the required identifier output signal which depends, to first order, only on the value of Mq^2 for the detected particle.

In practice, two modifications to the basic multiplier method are necessary in applications where a broad range both of energies as well as of types of particle is to be analyzed. First, the assumption of constancy of the logarithmic term with energy is invalid. Consequently, use of the simple multiplier algorithm produces identifier output signals that vary with energy, as well as particle type, as shown schematically in curve (a) of Figure 3. To partially correct for the fall-off in identifier output at low energies, it is common to add a term proportional to ΔE to the $E\Delta E$ product. Since the ΔE signal rises at low energies, choice of an appropriate multiplying factor E_o causes the resulting identifier output $(E + E_o)\Delta E$ to remain relatively constant with energy. This

also provides some correction for the change in the effective charge state of the ions at low velocities. A second correction is necessary to compensate for the fact that the energy loss in the ΔE detector is not infinitesimally small--and may become quite a large part of the total energy E for some of the particles detected by the E,ΔE detector telescope. Providing that the energy loss ΔE is much less that the energy E remaining after passage of a particle through the detector, it is reasonable to calculate the energy loss in the ΔE detector by assuming an average energy between E and E + ΔE. To allow for this in the identifier algorithm, the term $E\Delta E$ is modified to $(E + k\Delta E)\Delta E$ where the constant k is adjusted for best identification. If the energy increment ΔE is very small compared with E, ionization will be uniform through the ΔE detector so that 0.5 is the correct value for k. The final form of the function used in 'multiplier' types of identifiers is therefore:

$$(E + E_o + k\Delta E)\Delta E \propto Mq^2\Delta x \qquad 9.$$

where E_o and k are parameters adjusted experimentally for optimum constancy of the identifier output as a function of energy.

The second basic type of identifier (14-19) largely avoids the need for experimental adjustment of parameters. Since a major difficulty with the multiplier type of identifier results from its dependence on measurement of an incremental energy loss, it appears that a more suitable method might be based on a range function. For a given ion, and over a limited range of energies, the curves of Figure 2 can be represented by the relationship

$$- dE/dx = E^n/a \qquad 10.$$

where $n \approx -0.7$ for protons, becoming smaller for low velocity ions. The value of a will be roughly proportional to $1/Z^2M^{-n}$, or even more approximately, $1/MZ^2$. The range R of an ion entering an absorber with energy E can be calculated by integrating the incremental elements of the path corresponding to incremental energy losses. Thus:

$$R = \int_{E_1}^{E} (dx/dE)dE + R_1 \qquad 11.$$

where E_1 represents the energy at which the simple relationship of Equation 10 breaks down and R_1 represents the remaining range at energy E_1. For the high-energy particles commonly studied in nuclear reactions $R_1 << R$ and $E_1 << E$. Neglecting these terms we have:

$$R = \int_0^E aE^{-n}dE$$

i.e.,

$$R \propto a\, E^{1-n} \qquad 12.$$

For a proton, $n \simeq -0.7$ so the range R_p is given by

$$R_p \propto a\, E^{1.7} \qquad 13.$$

Similar relationships, but with slightly smaller values of n apply to other ions. More generally, we will write

$$R \propto a\, E^{b} \qquad 14.$$

where $b = 1 - n$.

If we again suppose that an ion deposits energy ΔE in the first detector of thickness Δx of a telescope, then stops in the second detector, depositing energy E, it is obvious that the range of the particle with energy $E + \Delta E$ is Δx longer than the range of the same particle with energy E. Therefore:

$$\Delta x/a \propto [(E + \Delta E)^b - E^b] \qquad 15.$$

Since a is approximately proportional to $1/MZ^2$, the left-hand side of this equation is roughly proportional to MZ^2. Δx is a known quantity, while E and

ΔE are determined by measuring the amplitude of the detector signals. Therefore, Equation 15 provides a direct determination of MZ^2 that involves no arbitrary constants and no limitation on the fraction of the incident energy deposited in the ΔE detector. These factors make identification based on Equation 15 more generally useful that the method based on Equation 9.

As with the multiplication operation involved in identifiers based on Equation 9, the exponentiation involved in those based on Equation 15 is readily performed by either analog or digital methods. These methods will be discussed in the next section.

In view of the simplicity of the power-law relationship it is surprising how accurately it predicts the range of ions of widely differing type and energy. Skyrme (20) has shown that the errors amount to no more than a few percent over the energy range of 5 to 50 MeV for particles ranging from protons to alphas; as seen by inspection of Figure 2, the errors should not increase significantly up to much higher energies. Figure 2 indicates that the situation is not so favorable for heavy ions, and energy-dependent corrections (e.g. making b a function of E) are often made. Examples of such corrections have appeared in the literature (21).

Chaminade et al. (22) have used an approximation to the relationship of Equation 15 that is more tolerant of imperfections in identifier circuits when ΔE is very small compared with E. Bird and Ollerhead (23) have extended the use of the range algorithm to low energies where the power-law approximation to the range-energy relationship is no longer valid. In order to achieve this they generalize the range-energy relationship to:

$$R = a\ F(E) \qquad 16.$$

Consequently Equation 15 is replaced by

$$\Delta x/a = [F(E + \Delta E) - F(E)] \qquad 17.$$

By storing range-energy tables (which represent F(E)) in a computer, and by using a table look-up method, they identify any particle registering in the detector telescope. Other computer methods (24) have appeared in the literature.

Identifier Circuits

The availability of medium-size on-line computers at accelerator laboratories has resulted in increasing use of digital calculations (by table look-up, or using the algorithms described in the previous section, or more complex ones) for identifying particles. The detector pulses, suitably amplified and

shaped, are digitized by an analog-to-digital converter (ADC) and fed to the computer for processing. Use of a temporary analog storage device (often called an analog-multiplexer) permits the two signal channels to share the same ADC. Depending on the speed of the computer, the processing of each event, to identify a particle, may take a time ranging from a few tens to a few hundred microseconds. Since the optimum shaping time in the signal paths prior to digitizing is only a few microseconds or less, computer processing of each event seriously reduces the data acquisition rate. If the ions of interest are rare, and are accompanied by a large flux of less interesting particles, the rate limitation imposed by computer identification of each event is unacceptable. In these cases, it is convenient to use an analog identifier, which identifies particles in a few microseconds, to select only interesting events for processing by the computer. Of course, the analog identifier can also be used alone without the help of a computer, whose main virtue is its ability to subject an event to more critical evaluation before deciding upon its type. Typically, for example, the computer might employ a modified form of the simple power-law algorithm to compensate for the change in b (in Equation 14) that occurs for low-energy heavy ions.

Analog identifiers utilize circuit techniques to achieve the multiplication operation required by the function $(E + E_o + k\Delta E)\Delta E$ of Equation 9, or the exponentiation required in the range algorithm represented by Equation 15. The following basic methods have been employed:

i) Circuit elements whose output is proportional to the square of their inputs can be used to process two signals A and B to generate the functions $(A + B)^2$ and $(A - B)^2$. By taking the difference between these outputs, a final result proportional to AB is produced. This method, which commonly used the Raytheon QK329 square-law tube, has now been superseded by some of the following techniques, so we will not discuss it further. Another element that exhibits almost a square-law characteristic is a field-effect transistor (FET). This has also been used (18,25) as a function generator in identifiers.

ii) By converting the amplitude of one of the signals to a time proportional to amplitude, then integrating the other signal for this time, an output proportional to the product AB is produced $\left(\int_0^A B\, dt = AB\right)$. While this method has been employed in identifiers (9), its application is

limited to the multiplier algorithm technique. Also the rate limitation caused by using time as an intermediate parameter in the calculation is not desirable.

iii) The most versatile method of performing the analog calculation required in an identifier is based on the use of elements exhibiting a logarithmic or exponential relationship between input and output. The most convenient element is a semiconductor junction whose characteristics are given (26) by:

$$i = i_o(\exp(eV/nkT) - 1) \qquad 18.$$

or:

$$V = (nkT/e)\ \ln(i + i_o)/i_o \qquad 19.$$

where:

V and i are the voltage and currents,

i_o is the diode saturation current (determined by the junction doping, carrier lifetimes, etc.),

k is Boltzmann's constant,

T is the temperature (°K),

e is the charge on the electron,

n is a factor (between 1 and 2) which represents the effects of recombination, generation and trapping in the junction region.

The saturation current i_o is very small ($< 10^{-12}$A) and can often be neglected. Also, for reasonable forward current levels $n \cong 1$, so, for practical purposes, Equation 19 can be simplified to:

$$V(\text{millivolts}) = 70 \log(i/i_o) \qquad 20.$$

The restraints imposed, on the one hand, by series resistance, and, on the other, by response time, limit the dynamic range of semiconductor junction logarithmic elements to about 100:1 or at the most 1000:1 in input current. Fortunately this range is sufficient to cover the range of E and ΔE signals encountered in particle identifiers.

At high current levels Equation 20 must be written:

$$V(\text{millivolts}) = 70 \log(i/i_o) + iR \qquad 21.$$

where R is the bulk resistance (in milliohms). If R = 10 ohms, a value typical of semiconductor signal diodes, the current change from 1 to 10 mA would produce a 90 mV drop in R -- larger than the 70 mV change

in the junction voltage drop. Using the emitter-base junction of a transistor rather than a simple diode, drops the effective value of the series bulk resistance well below 1 ohm, but compensation for its effect is still required if adequate logarithmic characteristics are to be achieved at high current levels (i.e., ~ 10 mA).

At low current levels, the speed of response is limited by the junction capacitance shunting the diode. The incremental diode resistance is given by:

$$r = kT/ei \qquad 22.$$

The small signal response time constant is therefore:

$$t = rC = kTC/ei \qquad 23.$$

where C is the junction capacitance and r is its incremental resistance. For i = 1 mA and C = 100 pF, t = 2.5 ns, and time constants approaching a microsecond, the normal signal pulse width, occur for currents of 10 μA.

Figure 4A shows one implementation of a logarithmic function generator. The base-to-emitter junction of transistor Q forms the logarithmic element. The high gain operational amplifier forces the emitter voltage of Q to a value where

its collector current equals the input pulse current plus a very small standing current i_1. The standing current must be much smaller than any signal current of interest if the output voltage pulse is to be a reasonable approximation to the logarithm of the input current. Figure 4B shows an exponential function generator. Transistor Q is the exponential element whose standing current i_2 is stabilized by feedback to the base of Q. A voltage pulse V on the base of Q produces a change in the collector current proportional to exp(V) which, in turn, produces a proportional voltage across R. The high input impedance output amplifier allows the output to be scaled by an appropriate factor.

Logarithmic and exponential elements can be used to perform both the multiplication operation required when using the multiplier algorithm, or the exponentiation required by the range algorithm. Figure 5A shows schematically the use of the logarithmic and exponential generators to perform the exponentiation operation. The variable gain amplifier permits adjustment of the power b in the range equation. When both a logarithmic element and an exponential element are used in sequence, as shown in Figure 5A, the temperature dependence of the output, inherent in Equations 18 and 19, may be shown (14) to cancel out.

Therefore a relatively drift-free function generator results. The experimentally measured performance of a function generator based on these principles is shown in Figure 6.

Figure 5B shows one arrangement that is used in identifiers. It has the virtue of requiring only a single function generator -- thereby avoiding relative gain and zero drifts that would be present if two function generators were used. In this arrangement, the ΔE signal is mixed with the E signal after a short delay time. By measuring the height of the output step that occurs when the ΔE signal is allowed to enter the system, the required particle identifier output is produced.

These are only a few examples of the circuits used in particle identifiers. This brief description omits many circuit details and does an injustice to the ingenuity employed in identifier circuits. Questions of counting-rate performance, speed, linearity, stability and accuracy are all important in these designs. The interested reader should refer to the quoted references for more details.

Detectors

Requirements on detectors and signal processing electronics for use in particle identification systems are generally similar to those imposed on

detectors for nuclear spectroscopy. In the case of ΔE detectors, however, in addition to requiring good energy resolution, it is necessary to have near-zero dead layers at both the particle entrance and exit windows. Furthermore, the required ΔE detector thicknesses range from about 1 gm/cm^2 to 0.1 mg/cm^2 depending on the types of ions being measured. The very thin detectors required for low-energy and/or heavy-ion measurements naturally present serious problems in design, construction and handling.

Many early identifier experiments employed scintillation detectors using plastic or inorganic scintillators. The requirement for thin windows in ΔE detectors eliminated the possibility of using materials such as NaI which require to be protected from the atmosphere. Consequently, CsI was used in some experiments. However, the rather poor energy-resolution capabilities of all scintillation detectors, and the non-linearity of output signal as a function of the absorbed energy (particularly for the heavier ions), seriously limited the identification capabilities of scintillation detector telescopes. Furthermore, efficient light collection from thin ΔE scintillator foils presented serious difficulties. Despite these drawbacks, scintillation detectors were used in

most of the early particle identification experiments and have been used in fission experiments quite recently (27).

The advent of semiconductor detectors with their excellent energy resolution and linearity, and the relatively easy fabrication of thin silicon detectors has improved the capability of particle identifiers to resolve adjacent isotopes up to the Z = 10 range. Scintillation detectors were able to resolve only the lightest isotopes; adequate separation even of ^{4}He from ^{3}He ions was not possible. For some low-energy heavy-ion identification problems, even the thinnest available silicon ΔE detectors (five microns) absorb too much energy; in these cases, a gas proportional ΔE detector has been used together with a silicon E detector (28). However, techniques of particle identification still largely depend on silicon detectors, so we will concentrate our attention on these.

The reader not familiar with semiconductor detector techniques is referred to one of the many treatises on the subject (29-37). Here we will emphasize those parts of the topic related to particle identification. Figures 7 and 8, which show the range of various ions in silicon, illustrate the wide range of detector

thicknesses required for particle identification in typical nuclear reaction experiments. E detectors for use with light ions having energies of up to 50 MeV/amu must have thicknesses as large as 1 cm, while those ΔE detectors intended to absorb only a fraction of the energy of heavy ions of 1 MeV/amu energy must have thicknesses well below 10 microns.

Thick detectors require very pure silicon, or the compensation of impurities by lithium-drifting. Therefore, either surface barriers on very high resistivity silicon or lithium-drifted silicon detectors may be used. In either case, 5 mm represents a practical limit to the thickness of silicon detectors. If thicker detectors are required, germanium (either high-purity or lithium-drifted) must be employed. These detectors require cooling near to liquid nitrogen temperature with the attendant problem of providing thin entry windows to the cryostat. Unless a very clean vacuum exists in the reaction scattering chamber, it is essential to provide a barrier window between the scattering chamber and the detector cryostat vacuum. The extreme sensitivity of semiconductor surfaces to contaminants prohibits germanium detector operation in a typical scattering chamber vacuum. Even thick silicon detectors may require cooling to improve hole- and electron mobilities and thereby to reduce the collection time and signal rise-time.

At the other end of the range of detector thicknesses, very thin detectors are difficult to fabricate and to handle. Minor thickness variations across the detector area cause position-dependent variations in the ΔE signals even for a single type of particle, thereby resulting in poor particle identification. Consequently, very uniform thickness across the area is essential. With present fabrication techniques, which require etching of silicon wafers from both sides, it is difficult to provide detectors whose thickness is uniform to better than 0.5 microns over an area of 0.25 cm^2. In the future, epitaxial-growth and preferential etching (38,39) may provide better detector thickness control.

Thin detectors exhibit large electrical capacities which limit the electronic resolution of the detector and its associated preamplifier. The capacity C of a totally-depleted silicon detector of thickness T and area A is approximately given by:

$$C = 1.1\ A/T\ pF \qquad 24.$$

where A is measured in cm^2 and T in cm.

A 10 micron thick detector of 0.5 cm^2 area therefore exhibits a capacitance of almost 600 pF. Using a high transconductance FET (g_m = 50 mA/V),

and assuming 1 μs pulse shaping (differentiation and integration), the full width at half maximum (FWHM) noise limit on resolution is typically given by:

$$R = R_o + 0.04\ C\ keV \qquad 25.$$

where R_o is the resolution with no added capacitance (typically 3 keV). We see that the overall electronic resolution of such a system can be no better than approximately 30 keV FWHM. The use of thinner detectors of large area further degrades this resolution. This fact, together with the problems of handling large area, thin silicon wafers causes a severe constraint on the area (and therefore efficiency) of a detector telescope. Consequently, it is not unusual to find two or more independent telescopes being used to improve the geometrical efficiency of particle identifier systems.

Another important aspect of detector performance, particularly for heavy-ion measurements, is the thickness of dead layers on either side of transmission detectors, or on the particle-entry side of E detectors. Since low-resistance evaporated metal layer contacts must be used across the entire face of a detector in order to achieve fast timing when necessary, these metal layers constitute a part of the dead layer. Many detectors use evaporated gold

layers for this purpose -- at least 0.02 microns is required to achieve the desired low resistance. Added to the metal layer, the true detector dead layer must include a thin layer of silicon in which charge produced by ionization is not completely collected. For diffused detectors, the heavily-doped diffused layer partially acts as such a dead layer--typically a 950°C, 30 min phosphorus diffusion in silicon produces an effective dead layer of about 0.3 microns of silicon. For surface barrier detectors, the silicon dead layer is controlled by poorly understood parameters, such as recombination effects at the silicon-metal interface. A recent paper (40) details results on several types of surface-barrier detector.

The whole question of dead layers is confused by the fact that results of measurement of dead-layer thicknesses depend upon the type of ion measured and on the applied detector voltage (41-43). Increasing the bias causes the plasma column of hole and electrons to erode more quickly, thereby reducing the probability of recombination in the dense plasma. Since the plasma density increases as dE/dx increases (i.e., for low-energy heavy ions), detectors capable of withstanding high overvoltages (i.e., much more voltage than required

to deplete their full thickness) should be used for heavy-ion identification. In many surface-barrier detectors a static field inversion beneath the silicon surface tends to act in the opposite direction from the normal detector junction reverse bias. Increasing the bias overcomes this tendency and, if sufficient bias can be applied, the thickness of the silicon dead layer approaches zero. In practice, fields of about 50,000 volts/cm just beneath the surface appear to be required to achieve this result.

The ion-channelling phenomenon (44-46) whereby ions may be 'focussed' through regions in a crystal having low electron density can also cause serious changes in signals from thin transmission detectors. As indicated in Equation 5, the stopping power depends on the electron density in the region of the track of an ion. Therefore, 'channelled' ions deposit less energy when passing through a detector than those not 'channelled', which encounter the normal random distribution of electron densities along their track. The probability that ions will follow preferred channels becomes greater for highly charged ions, and clearly also increases as detector thickness is decreased. Therefore, the effects of this phenomenon become very important in heavy-ion experiments. Figure 9

shows the distribution of energy losses for 100 MeV alpha particles passing through a 100 micron silicon detector in two directions. The normal distribution of signals is produced when the beam is oriented essentially at random with respect to major axes of crystal symmetry but, when the beam is parallel to the < 110 > axis, a skewed distribution with many small signals is observed. The effect of channelling on identifier performance is illustrated by the identifier output spectrum seen in Figure 10. The valley between the ^{3}He and ^{4}He peaks is filled in when the detector is cut normal to the < 111 > axis. It is prudent to employ ΔE detectors cut off-axis in all particle identifier experiments, and to test for the effects of channelling prior to a lengthy experiment.

Since the literature contains many discussions of the signal processing electronics for nuclear spectroscopy (33,47-49), and the problems there are the same as those encountered in particle identification using ΔE,E absorption measurements, we will not dwell on this topic. Fast timing aspects of the electronics will be discussed in Section III.

Resolving Power of E,E Identifiers

Apart from the requirement that the median value of an identifier output be constant and independent of energy for a given type of ion, we must also be concerned with fluctuations and errors in the measurement of ΔE and E and their effect on identification. These errors limit the ability of the system to resolve one type of ion from others having nearly the same value of MZ^2.

Figure 11 illustrates the accuracy required in the MZ^2 determination in order to identify unambiguously the known stable isotopes with $Z < 10$. Plotted in this manner, a certain fractional error in determining MZ^2 represents a fixed vertical error. We note first the existence of overlapping isotope series -- for example, the range of values of MZ^2 for B isotopes overlaps that for both Be and C isotopes. Secondly, the percentage separation of the MZ^2 values of adjacent isotopes decreases as Z increases. In the region where the isotopes of F and Ne overlap (i.e., $MZ^2 \simeq 1700$), the separation between adjacent stable isotopes (either F or Ne) corresponds to a change of about 1% in MZ^2. On the other hand, the stable He isotopes are separated in their MZ^2 value by about 25%. We see that identification of heavy isotopes by measurement of MZ^2 alone demands very small fluctuations (or errors) in determination of ΔE and E.

The wide range of types and energy of particles measured during even a single experiment makes a general statement of the measurement uncertainties impossible. We can only cite the various factors responsible for errors or fluctuations in the ΔE and E signals and indicate cases where the various factors assume importance. Some of these factors are:

a) Electronic noise causes a Gaussian fluctuation in both ΔE and E signals. The effect of these fluctuations on energy resolution (FWHM) can be calculated approximately using Equation 25. This equation assumes a pulse-shaping time near to 1 μs. Speeding up the signal-processing system degrades the resolution almost in inverse proportion to the measurement time.

Since the ΔE detector in a detector telescope is usually considerably thinner than the E detector, its capacitance is higher, and the resolution of the ΔE system is consequently worse. Fortunately, there are only a few cases where electronic noise is the main limitation in particle identifier experiments, and these cases usually involve light ions depositing very little energy in the ΔE detector. Since the

difference in MZ^2 between one type of light ion and its neighbors is large, these experiments rarely impose a very severe demand on energy resolution.

b) Statistics of the charge production process in a detector (50-52) result in a spread in the signals produced by a detector even when particles deposit a fixed amount of energy. The FWHM spread introduced by this effect is given by:

$$< E > = 2.35\sqrt{FE\ \varepsilon} \qquad 26.$$

where:

E is the energy deposited

ε is the average energy required to produce a hole-electron pair in the detector material ($\varepsilon \simeq 3.7$ eV for silicon)

F is the Fano factor ($F \simeq 0.12$ for silicon)

While the absolute value of the spread increases with absorbed energy, the fractional spread decreases as the energy increases. For this reason, this factor is rarely a serious limitation in identifier experiments where substantial amounts of energy are deposited in detectors. For example, the spread in a 20 MeV signal is only about 6 keV (FWHM) or .03%.

c) Channelling effects in the ΔE detector may cause a significant fraction of the incident ions to deposit less than the normal amount of energy in this detector--and, in consequence, a larger amount in the E detector. Channelling effects become increasingly important for heavier ions and when thin ΔE detectors are employed. Using detectors fabricated from wafers cut at a suitable small angle from the normal to a major crystal axis largely avoids these effects, but this phenomena must always be considered a potential source of fluctuations in ΔE signals.

d) Fluctuations in the charge state of heavy ions passing through a ΔE detector constitute another source of fluctuation in the energy loss in this detector. These fluctuations are zero for very high velocity ions, which are fully stripped, but they can become important at energies where ions are only partly stripped--which is a typical situation in heavy-ion experiments.

While the average charge state of heavy ions has been studied (53,54) and the results have been used to generate stopping power data (see Figure 2, for example), very little theoretical or experimental

work on the effect of fluctuations in charge state on ionization in detectors is available. This is clearly one area where more detailed work is needed to elucidate the effects in identifier systems.

e) Even when the charge state of the incident ion remains constant, the energy exchanges between the ion and electrons in the detector material occur as discrete events and statistical fluctuations both in the number of these events, and in the nature of the energy exchange process itself, cause a spread in absorption when a large number of particles pass through a thin absorber such as a ΔE detector. If the number of exchanges along a particle's track through the detector is large, details of the individual events are insignificant, and an average value can be assumed for the discrete energy exchanges. In this regime, a Gaussian distribution of the energy losses is produced. At the other extreme, when the detector is very thin and the incident ions are lightly ionizing, only a few discrete interactions of the ion with electrons take place in the material. Fluctuations in the energy exchange process itself then become the

dominant factor determining the distribution of energy losses. The rare high-energy exchanges (head-on collisions) of the ions with electrons cause a skewed distribution of losses with a high-energy tail. This is the Landau (55) collision regime. Between these two extremes, a complex mixture of the two statistical processes occurs. This intermediate regime can be analyzed using an approximate method of Symon (56) or the more exact approach of Vavilov (57). Experimental results (58,59) agree closely with predictions of the Vavilov theory.

The magnitude of the spread in energy absorption can be calculated using tables (4,20,60) based on the Vavilov theory. When the number of interactions in the ΔE detector is large, and a Gaussian distribution occurs (a typical case in identifiers), the width of the distribution can be calculated using Bohr's theory (61). According to this theory, a very thin absorber of thickness dx will introduce a spread given by:

$$d(\sigma^2) = 4\pi e^4 q^2 n \, dx \qquad 27.$$

(using the same nomenclature as in Equation 5). Combining this with Equation 5, and assuming $\beta = 0$, it can be expressed in the form:

$$d(\sigma^2) \simeq 2(m/ML)E\ dE \qquad 28.$$

where:

L = ln(4 mE/IM) which is a slowly varying function of E,

dE is the energy loss in element dx,

m is the mass of the electron.

Assuming that the total spread in energy absorption in a ΔE detector is much smaller than the average energy loss E, Equation 28 can be approximately integrated to yield a value for the spread:

$$\sigma^2 = (m/ML)\ \{(E_o + \Delta E)^2 - E_o^2\} \qquad 29.$$

where E_o is the energy of the ion on exit from the ΔE detector. If $\Delta E << E$, this equation simplifies to:

$$\sigma^2 = 2(m/ML)\ \Delta E.E_o \qquad 30.$$

The FWHM spread can be obtained by multiplying the calculated value of σ by 2.35.

As an example, we can consider a 30 MeV α particle beam losing an average of 3 MeV in a silicon ΔE detector. In this case, L $\simeq$ 5, m/M $\simeq$ 1/8000, so $\sigma \simeq$ 70 keV, and the FWHM spread will be almost 250 keV.

This is an 8% error in the ΔE measurement--clearly a very significant error in identification. Fortunately, the fractional error decreases as M increases and also as the energy loss ΔE increases; otherwise heavy-ion identification would be impossible using the ΔE,E detector telescope method.

Fluctuations in discrete interactions of ions passing through a detector therefore become a serious problem when thin ΔE detectors are used to identify lightly ionizing particles such as high-energy hydrogen and helium ions. Several studies (4,20) have been made of the effect of these fluctuations on identification of light ions. These fluctuations are generally of minor significance for heavy ions, although they become very important for the proportional gas chambers described in Section IV.

f) Thickness variations in the ΔE detector cause a fluctuation in the ΔE signals and an inverse fluctuation in E signals. The fabrication procedures for ΔE detectors tend to produce a fixed range of thickness variations ($\sim$ 0.5 microns), so the fractional spread of ΔE introduced by the thickness variations decrease as the ΔE detector thickness

increases. This problem becomes very important in experiments where heavy ions are identified with very thin ΔE detectors.

g) The errors introduced by the effects discussed so far are primarily in ΔE signals. Nuclear collisions occur, however, especially near the end of a particle's track where the ion becomes neutral. Fluctuations in these collisions therefore cause a spread mainly in E signals. The FWHM spread due to this effect (62) is approximately given by:

$$< E > = 0.7\ Z^{1/2}\ A^{4/3}\ \text{keV} \qquad 31.$$

This spread amounts to only 0.7 keV FWHM for protons, but it becomes quite large for heavy ions. When $Z \simeq 10$, the contribution is well over 100 keV--by no means insignificant for those ions that just succeed in penetrating through the ΔE detector and deposit very little energy in the E detector. This is not an unusual situation in heavy-ion experiments, since it is difficult to fabricate the very thin ΔE detectors that would ideally be used in these experiments.

h) The effects discussed so far produce fluctuations in signals from either the ΔE or E detectors. The two effects now to be discussed do

not cause signal fluctuations, but introduce an energy dependence in the identifier output over and above any energy dependence caused by the approximations involved in the identifier algorithm used. When a wide range of particle energies are present, this energy dependence results in a spread in identifier output. The first effect of this type, usually termed the 'pulse-height defect' (43,63-65), results in non-linearity in the response of detectors when measuring heavy ions. The defect is variously attributed to nuclear collisions near the end of the track of a heavy ion, or to recombination losses in the dense plasma column existing near the end of the track. In either case, the E detector output signal is not a linear representation of the energy deposited in it. The ΔE signal is not affected to the same degree since it is not subjected to the processes occurring near the end of the ion track.

The magnitude of this effect is difficult to assess since the range of cases encountered encompasses some where virtually no departure from linearity occurs to others where the departure can be very significant. However, the phenomena are essentially associated with the end of a

particle's track, either by virtue of recombination in the dense plasma existing there, or by the particle's capturing electrons to become neutral. It is therefore clear that, like the spread produced by nuclear collisions, the non-linearity becomes large for those heavy ions that reach the E detector with very low energy. Since the signal from the E detector then falls below its correct value, this effect produces a low value of MZ^2 from the identifier. From a practical point of view, a lower bound must be placed in the E signals to reduce this problem.

i) Another effect producing a reduction in the E detector signal is energy loss occurring in dead layers existing either on the back surface of the ΔE detector, or the front surface of the E detector. Since the energy loss in these dead layers increases rapidly for those particles that only just penetrate through the ΔE detector, but are usually negligible for the longer range particles, an energy dependence is introduced in the identifier output. Once again this is a serious effect for the heavier ions. From a practical point of view this consideration makes it essential for the experimenter to orient the two

detectors in the direction which produces the thinnest possible dead layers between them. In most identifier experiments, the total dead layer can then be kept below about 0.5 microns (silicon equivalent). This may not be true in multi-detector long-range particle telescopes where the relatively thick (~ 50 microns or more) lithium-diffused layer of lithium-drifted detectors cannot be avoided.

Multiple Detector Systems

In studies of relatively rare isotopic species accompanied by large numbers of more common particles, the errors of identification caused by the instrumental and basic physical effects discussed in the previous section become intolerable. Fortunately, for many of these experiments, the absolute yield of the particular species in a reaction is not of importance but, rather, identification is required to select some fraction of the rare particles so that their energy distribution can be determined. This is so, for example, in experiments to detect the particle-stable neutron-rich particles near the boundary of stability, or to measure their mass. It is for these experiments that the first multi-detector identifier systems (15,66) were devised. By allowing the ions to pass through

a series of detectors, several simultaneous calculations can be made of the particle's identity (i.e., MZ^2). Each calculation, in itself, is subject to the errors discussed in the previous section, but we can now place a criterion on the degree of agreement between the various answers before accepting a particle for energy analysis. Therefore, at the cost of rejecting all of the rare particles that deviate significantly from ideal behavior in any of the identifications, we reduce the chance of a neighboring isotope being falsely identified as the rare product.

A block diagram of a system commonly employed in these experiments is shown in Figure 12. In this system, the particles of interest must pass through two ΔE detectors, ΔE_2 and ΔE_1, and into the E detector. The detector thicknesses are chosen to satisfy this condition based on the predicted energies of the interesting types of particle. An E_{REJ} detector behind the E detector permits complete rejection of those particles that pass through the E detector. For this rejection to be efficient the dead layer on the rear of the E detector must be very small; therefore this detector must be fabricated as a transmission detector. As in the simpler identifier (Figures 1 and 5B), fast coincidence requirements and energy window limits are set on all signals in order to reduce background to a minimum.

The logarithmic function generator discussed in connection with Figure 5 provides a convenient method of processing the signals in a multi-detector system, since the time-share principle used in this circuit can easily be extended to sequencing more than one ΔE signal. For the triple-detector identifier, a three step waveform as shown in Figure 13 can be produced; measuring the height of the two steps on the top of the waveform developed by the function generator yields two separate identifications:

$$(E + \Delta E_1)^b - E^b = T_1/a \qquad 32.$$

and:

$$(E + \Delta E_2 + \Delta E_1)^b - (E + \Delta E_1) = T_2/a \qquad 33.$$

where a and b are the constants in the range-energy relationship (Equation 14) and T_1 and T_2 are the thicknesses of the two ΔE detectors. (Note: T_1 is the second detector in the telescope.) Using a logarithmic element, it is possible to determine the ratio of the two results which should be equal to T_1/T_2. It is then a simple matter to accept only those events for which this ratio falls in a limited range.

As with dual-detector identifiers, computer processing of the signals to select those particles that satisfy certain identity conditions can be performed as an alternative to analog identification. In practice it is often convenient to use an analog identifier to select interesting events for presentation to a computer, then to have the computer make a more rigorous investigation of the various signals to further check the particle's identity. In experiments designed to discover new isotopes, every precaution must be taken to eliminate chance pile-up of common types of particle from being recorded as the rare event. The computer, presented with signal amplitude (and sometimes time) information, is invaluable in this connection. Fortunately, very rare events can be examined individually in detail by the experimenter if all relevant information is recorded and if the bulk of the uninteresting events is eliminated by analog and/or computer processing.

A logical extension of the triple-counter identifier is the use of a telescope containing many detectors which permits recording the pattern of ionization along the whole length of a particle's track. This technique is, of course, limited to those higher-energy particles which will penetrate

most of the depth of a stack of detectors. Such telescopes are now being used (67) for measurements on the reaction products produced in targets by almost relativistic heavy-ion beams. In addition to providing a detailed fingerprint of a particle's track, particles that undergo nuclear reactions in the telescope itself can be observed and rejected. This feature suggests that thick detector telescopes, perhaps made of high-purity germanium detectors, may be a useful tool for high-energy light-ion experiments.

Experimental Results

Simple $\Delta E,E$ identifier telescopes have been used extensively since 1960, particularly in nuclear reaction experiments involving light ions. The first experiments used scintillation detectors and the multiplier type of algorithm. Adequate separation of protons, deuterons and tritons was achieved in these experiments, but separation of ^{3}He from ^{4}He was only marginally possible and became impossible if the yield of ^{3}He, in the reaction studied, was low compared with that of ^{4}He.

The improvement in identification resulting from the use of semiconductor detectors was quickly realized and exploited. The multiplier algorithm was used

exclusively in these early experiments. Unfortunately, fabrication of very thin ΔE detectors was not then practical so work on heavy ions required the use of other types of ΔE detectors. The first heavy-ion identification studies were carried out using a gas proportional detector for the ΔE detector with a silicon E detector. A result from these experiments (10) is shown in Figure 14.

The availability of thin silicon ΔE detectors quickly led to their use in identifier experiments. The first use of the range (power law) algorithm which imposed less restriction on the thickness of the ΔE detector resulted in a significant improvement in identifier performance. An early result achieved with this system is shown in Figure 15. As this system was applied to the search for rare neutron-rich isotopes, the need for better identifier resolution and lower backgrounds became evident. This led to the invention of the triple-detector telescope. A comparison between the results achieved with this telescope, with those from a simple ΔE,E telescope, is given in Figure 16. A direct comparison can be made between these results since the reaction is the same in each case (15).

This type of identifier has been used extensively for studies of the stability of neutron-rich isotopes near the boundary of stability. One example

is the measurement of the mass of ^{8}He. Figure 17 shows the identifier output in an experiment in which 80 MeV alpha particles bombarded a ^{26}Mg target. This figure illustrates the very large range of yields of the various isotopes. We estimate that a single ^{8}He particle was accompanied by 10^{8} to 10^{9} particles of other types. The small ^{8}He peak also includes some α-D coincident events in the telescope. Computer processing was used to eliminate most of these events. The final ^{8}He energy spectrum is shown in Figure 18. These events ($\sim$ 25) were accumulated in several days operation of a cyclotron.

While many experiments of this type continue to use detector telescopes in this manner, the addition of time-of-flight measurements as discussed in the next section has made studies possible on even more rare isotopes.

III. TIME-OF-FLIGHT IDENTIFIERS

General Considerations

As seen in the Introduction, a time-of-flight measurement determines the velocity of a particle and hence, in accordance with Equation 3, the ratio E/M. If a separate E measurement is made -- for example, by stopping the particle in a silicon detector located at the end of the flight path -- the mass of a particle can be determined. Sometimes this is adequate identification and systems of this type find application. On the other hand, if the mass is known, the measurement determines the energy E. Beam-energy measurements can be made by this method. When combined with a $\Delta E,E$ identifier, which determines both E and MZ^2/E, time of flight provides a complete determination of M, E and Z. This combination has been used in many recent experiments.

Unfortunately, the basic simplicity of time-of-flight methods is not matched by the hardware required to achieve the required timing performance. Since long flight paths necessarily involve serious efficiency problems due to the poor collection geometry, short paths are desirable and very fast timing circuits must be used. The velocity of an ion as a function of E/M is shown in Figure 19. It is given approximately by:

$$v = 1.4\sqrt{E/M} \text{ cm/ns} \qquad 34.$$

A heavy ion of 10 MeV/amu energy therefore has a velocity of about 4.5 cm/ns, and will travel through a 10 cm flight path in just over 2 ns. If a 10 cm flight path is used, and if the accuracy of the time measurement is 200 ps -- close to the best result yet achieved -- the velocity measurement is accurate only to 10%, and the error in E/M is 20%. Achieving the required timing accuracy has been the major problem in applying time-of-flight methods to identification of all but slow ions.

Since mass determination is usually the prime objective it is convenient to rearrange Equation 34 in terms of the mass;

$$M = 2\ E\ t^2/d^2 \qquad 35.$$

where t is measured in ns and d in cm. If statistical fluctuations occur in measuring E, t and d, the resulting fluctuation in mass determination is given by:

$$(\delta M/M)^2 = (\delta E/E)^2 + (2\delta t/t)^2 + (2\delta d/d)^2 \qquad 36.$$

where δE, δt, and δd represent the fluctuations in measurement of t, d and E and δM is the resulting fluctuation in M. $\delta E/E$ is much less than 1% in most

experiments (e.g. using a semiconductor detector to measure E), and the geometry can be designed to make $\delta d/d$ very small. Therefore $\delta t/t$ is commonly the most important measurement error. In this case, we have:

$$\delta M/M = 2.8\sqrt{E/M}\ \delta t/d \qquad 37.$$

This relationship is shown graphically in Figure 20. We see that ^{16}O ions with an E/M of 6 MeV/amu require a timing resolution of 9 ps/cm of flight path if they are to be resolved from other isotopes of mass 17 (i.e., $\delta M/M = 6\%$ or $\delta M \simeq 1$). The flight paths used in actual experiments range from a few centimeters to a meter or more depending on the timing accuracy of the detectors used and on the accuracy required in determination of M.

When a time-of-flight measurement is combined with a $\Delta E,E$ particle identification a very useful two-dimensional result is obtained which is more tolerant of fluctuations in both the mass and MZ^2 determinations than is a single-parameter experiment. One representation of the two-dimensional data provided by a time-of-flight and $\Delta E,E$ particle identifier is given in Figure 21. Allowing for reasonable spreads both in the particle identifier output and in the mass determination due to timing errors, and assuming that all particles have

100 MeV energy, the shaded regions, representing the errors in each determination, are well separated. Note that the series of carbon and boron isotopes overlap in the particle identifier dimension, so the resolution of ^{9}C from ^{14}B and ^{15}B depends on the mass identifying capability of the time-of-flight measurement. Here we see very clearly the power of the combined system, for those events poorly resolved by one system are well resolved by the other.

Achieving the necessary time resolution for these experiments has taxed the limitations of both detectors and electronic circuits. Since a time-of-flight measurement can be particularly useful for identifying low-velocity heavy ions, a prime requirement on any transmission detector used for timing is that it must be extremely thin so as to be penetrated by the ions of interest with very little energy loss. Three basic types of detectors have been used:

(i) Thin silicon detectors, which also provide a reasonably good ΔE signal but are relatively thick ($\sim$ 1 mg/cm^2).

(ii) Thin scintillator foils and photomultipliers which provide only a very crude ΔE signal but can be reasonably thin ($\sim$ 50 to 500 μg/cm^2).

(iii) Thin secondary electron foils which emit electrons that are detected by either electron multipliers or scintillator-photomultiplier combinations. These foils provide almost no ΔE information but can be extremely thin (10 to 50 $\mu g/cm^2$). The thinner foils are naturally rather fragile.

In the first of these cases, the small signals obtained from the silicon detector must be amplified by suitable circuits and timing limitations are caused by the charge collection time in the detector, by the rise-time of the amplifier pulse and by noise in the amplifier. In the latter two cases, the multiplier structures provide 'noiseless' amplification. Time jitter results from the statistics of emission from the foil, and from the front end of the multiplier, and also from the spread in transit time of electrons through the multiplier structure. Electronic considerations that limit the resolution of time measurements are therefore quite different in the last two cases from those in the first. Once signals of suitable size are realized, all systems can use the same timing discriminators, etc. for their timing channels. In the case of semiconductor detectors, where energy-loss information is also derived, a slow signal-processing channel, designed to optimize pulse-amplitude measurements, parallels the fast timing channel.

Since the design of the timing circuits for all systems is essentially the same once the timing signals reach a reasonable amplitude, we discuss here the basic features of such circuits before dealing separately with the various types of detector and front-end electronics.

The basic fast timing channel usually includes the following items:

a) A fast amplifier exhibiting the minimum possible rise-time and capable of developing an output pulse in the 1 V range. Using the best high-frequency transistors, rise-times (10 to 90%) of about 1 ns are achievable in the output signal if input signals to the amplifier are infinitely fast. It is important to note that the shape of the rise of the output pulse is the result, effectively, of multiple integrators in the amplifier -- therefore, the rise is almost Gaussian-shaped, starting slowly then achieving a rapid rate of change before levelling off slowly to the peak height. The design of fast amplifiers is discussed by Jackson (68).

b) Pulse-shaping circuits used to shape signal pulses for optimum processing. One function of these shaping circuits is differentiation

to limit the duration of pulses and thereby reduce pile-up probabilities. Also special operations, such as bipolar pulse-shaping, may be performed for feeding constant-fraction discriminators. In applications where the rise-time of the detector output signal is the dominant component in the overall rise-time, some integration can be used in the pulse shaper to reduce the effect of noise from the input stages of the amplifier. This is usually not the case in the fast timing systems described in this paper.

c) A fast discriminator which picks off the best possible timing information from the signal pulse at the output of the amplifier and produces an output pulse whose timing is an accurate measure of the time of the detected event. Fast discriminators may be designed to trigger at a fixed amplitude on the leading edge of signals (so called leading-edge discriminators), or to trigger at a time related to a point on the leading edge where the signal reaches a fixed fraction of the final signal amplitude (constant-fraction discriminators). The latter type of discriminator, in principle, develops a signal whose timing is independent of the amplitude of the signal. Since particle identification experiments

always involve a wide range of energy losses in detectors, and therefore widely varying signal amplitudes, constant fraction discriminators are universally used in these applications. The design of these discriminators is discussed in many papers (69-73). Generally speaking these designs use an input pulse shaped by double-differentiation to produce a zero-crossing point. The discriminator then triggers on the front edge of the pulse and retriggers on the zero-crossing point of the input signal. The timing signal is produced by the retriggering action -- whose time is independent of signal amplitude.

Delay lines are commonly used to achieve the differentiation and the bipolar signal is arranged to be asymmetrical with the negative undershoot constituting a preselected fraction of the initial positive portion of the waveform. Altering this undershoot changes the effective fraction of the signal rise at which the timing signal is developed. If it is set at too low a value, triggering may occur on the initial slow-rising portion of a signal; since noise on the signal modulates the triggering point, and the resulting fluctuation in triggering time is inversely

proportional to the rate of crossing of the triggering level, this is very undesirable.

A useful feature of a constant-fraction discriminator operating in this manner is that the output pulse width (i.e., leading edge triggering to cross-over) is changed by pile-up pulses occuring within the width. Thus, pulse-width discrimination can be used to detect pile-up on a short time scale (98). This is an important supplement to slower conventional pile-up rejectors. It can be particularly important in those accelerator experiments where intense short beam pulses are separated by long intervals with no particles.

d) A time-to-amplitude converter (TAC) is used to convert the time interval between timing pulses produced by two timing channels into a pulse whose amplitude is linearly related to the time interval. Since standard commercial TACs are readily available, they will not be discussed here.

Measuring the velocity of a particle requires that its time of passage at two points in its path be known. Sometimes the incident beam on a target is

pulsed so that the time when secondary particles can leave the target is known. In these cases a single detection of the secondary particles passing or reaching a detector is adequate to determine other velocity differences. In other cases, other radiation emitted from the target at the same time as the particle of interest can be detected and used to provide the fiducial signal (87). More generally it is necessary to interpose two or more detectors in the path of the particle, at least the first detector being thin enough for the particle to pass through it. Therefore, a wide variety of combinations of detectors is encountered in time-of-flight identifiers. Some of these combinations will now be discussed.

Thin Scintillators

A considerable program has existed for many years, in connection with high-energy particle physics, to produce scintillating materials with very fast decay times. A number of plastic scintillators, such as NE102, NE102A and NE111, with decay times in the 1 ns time region, have resulted from this program. These scintillators are commercially available in the form of thin foils down to about 5 micron thickness (i.e., 500 $\mu g/cm^2$), and can be produced by conventional methods (74) down to about 50 $\mu g/cm^2$. These foils have been shown to produce

sufficient light output when densely ionizing particles pass through them to provide timing signals from photomultipliers observing the light. Two methods of coupling to the photomultiplier have been used. In the first (75), the foil is clamped between the two halves of a split lucite light pipe which couples to a phototube. A two-ended version with two phototubes has also been used. The second basic arrangement (76) uses a hemispherical mirror to collect the light from a thin scintillator foil and direct it into a phototube.

The time resolution that can be achieved with these detectors is limited partly by the statistics of emission of electrons from the photocathode -- which is exaggerated by the poor light emission and collection from the scintillator. Another limitation is caused by the spread in transit time of electrons through the multiplier structure. The best time resolution achieved by these systems is about 0.7 ns and, more frequently, 1 ns is achieved. The time spread naturally increases as the foil is made thinner.

Electron-Emitting Thin Foils

The emission of secondary electrons (delta rays) from solid surfaces when charged particles enter them is a well known phenomenon. Since very thin

films of various materials are often used as targets in accelerator experiments and the technology of fabricating such films is well known to nuclear experimental groups, it is natural for such films, interposed in the path of nuclear particles, to be considered as potentially fast detectors. Detection of the secondary electrons with the necessary speed has proved to be a non-trivial problem, but this method is now beginning to realize its obvious promise.

The yield of secondary electrons from foils is a strong function of the type of film and its surface properties, of the type and velocity of the ion, and even of the angle of incidence of the ion passing into the foil. While low work function surface coatings increase the electron yield considerably, difficulties of preserving these surface properties have led to the use of plastic foils or, more commonly, carbon foils as thin as about 10 $\mu g/cm^2$. Electron yields from these foils range from approximately 10 for natural alpha-particles (77) to about 100 for fission fragments. Much of the early work using these foils was in the field of fission studies (78-80), but is has recently been extended to nuclear reaction product analysis (77,81-83).

Several types of electron detector have been employed to detect the electrons emitted by foils. Early systems employed scintillation or semiconductor

detectors. These detectors are insensitive to electrons having energies below 5 to 10 keV, so secondary electrons from the foil must be accelerated to this potential. Positive ions in the detector region are accelerated by the same electric field, strike surfaces in the vicinity and release electrons which are then attracted to the detector to produce spurious signals. Very careful design is required to avoid very high background counting rates with this type of detector.

A better situation prevails when the secondary electrons from the foil are accelerated directly onto an electron multiplier structure. In this case only a low accelerating voltage (< 1 kV) is required to achieve the full secondary emission ratio from the initial multiplying stage. At this potential, background is a much less serious problem and can largely be overcome with care in design of the detector chamber. The first work using open electron-multiplier structures (77) employed a commercial multiplier with Cu-Be-(BeO) dynodes (56P17-2). The multiplier structure in these tubes (as in the scintillation detector described in the previous paragraph) exhibits a time spread of about 1 ns which limits the particle timing to this value. In addition to this limitation, open-ended

electron multipliers are sensitive to contamination effects which degrade their gain, and are affected by magnetic fields. More recently channel electron multipliers have been employed (82). Time resolutions in the 400 to 700 ps range were obtained using these devices which are also less sensitive to contamination than the conventional multiplier surfaces. Finally, channel plates have now been used as the electron detector in particle timing experiments (83). These plates, about 1 mm thick and up to 3 inches in diameter, contain closely spaced microchannels only 50 microns in diameter in which electron multiplication occurs. Due to the short distance travelled by the electron cloud advancing down a channel, only a very small time spread (< 100 ps) is introduced by the electron multiplying process. Furthermore, the plates are rugged and rather insensitive to contamination problems. Unfortunately, the electron gain of a single channel plate is limited to about 10^4 by ion feedback effects. Consequently, where higher gains are required, two plates, one with holes biased at a small angle, are used in series. This so-called 'chevron' plate provides an electron gain of about 10^7 with a time spread below 100 ps. We note also that channel plates retain an image of the impact point of electrons on their front

face; if parallel field geometry is retained in the acceleration structure from the foil to the multiplier, the position of bursts of electrons emitted from the multiplier output side directly reflects the point of passage of the detected particle through the foil.

Figure 22A shows the arrangement employed in a foil-channel plate fast-timing detector. Plane-parallel field geometry is used partly to reduce electron transit time-spread to a minimum and partly to preserve the imaging capability of the system. Position information can be obtained by splitting the anode to give several separate signal outputs, or by replacing the final anode (collector) by a position sensitive semiconductor detector as shown in Figure 22B. In this version, it is necessary to accelerate electrons from the channel-plate onto the detector; also the inherent electron gain in the silicon detector permits the use of a simple plate instead of the chevron plate, as in Figure 22A. To reduce transit time spreads in the electron paths between the foil and the front surface of the channel plate, an open grid about 2 mm from the foil accelerates the electrons to about 1 keV very rapidly after their emission. A detector of the type shown in Figure 22A has exhibited a total timing spread (FWHM) below 150 ps

for natural alpha-particles passing through the foil. The combination of excellent timing and the small energy loss incurred by particles passing through carbon foils only 10 $\mu g/cm^2$ thick makes this type of detector a very important new tool in mass identifiers. The capability for location of the position of particles also offers the new potential of plotting the trajectory of particles entering a spectrometer magnet -- in itself suggesting a simplification in the design of such spectrometers, as discussed toward the end of this paper.

Thin Silicon Detectors

Thin silicon detectors are commonly used to provide ΔE signals for use in ΔE,E identifier systems which determine MZ^2. A natural extension of the technique is to separate the ΔE and E detectors by a suitable distance and to use the detector signals for timing purposes as well as energy measurements. In this manner the velocity, and hence mass, of the incident particle can be determined. A simpler version of this method, in which the time was measured between a cyclotron beam pulse and the signal from the ΔE detector of a detector telescope, was used by Parkinson and Bodansky (84). More recently the full technique has been used by a number of authors (85-87). Since thick detectors

exhibit intolerably long collection times, the technique is mostly restricted in practice to applications where the two timing detectors (these could be the ΔE_2, and ΔE_1 detectors of a triple-detector identifier) have thicknesses in the range below about 100 microns. Practical limitations (see Section II) restrict the minimum detector thickness to about 5 microns, although some experiments have been performed (85) with detectors as thin as 1.7 microns (i.e., about 400 $\mu g/cm^2$).

For the purpose of this discussion we will assume that the electric field through the whole thickness of the detector is greater than that required to achieve saturation of the velocity of holes and electrons. At room temperature, this demands an over-voltage of approximately 2 to 3 V/micron of detector thickness; the required over-voltage decreases rapidly with decreasing temperature, becoming 1 to 2 volts at -40°C. In the saturated condition, both holes and electrons travel at velocities of about 10^7 cm/s, independent of electric field and temperature. This corresponds to a collection time of 10 ps/micron of detector thickness. Therefore thin silicon detectors are potentially capable of extremely fast timing. Unfortunately, this simple picture is clouded by other

factors. The slow erosion of the dense plasma produced in heavy-ion tracks significantly retards the signal produced by such particles. Furthermore, thin detectors necessarily exhibit large electrical capacitances (see Equation 24), which degrade the signal/noise ratio of the detector amplifier system, and also make the effect of any series resistance or inductance in the input circuit very serious. Despite these effects, the timing capability of thin silicon detectors are almost equal to those of the best timing detectors (i.e., electron-emitting foils plus channel plates) while also providing accurate ΔE energy signals. Their main drawbacks, in some applications, are the limited minimum thickness and small area (< 0.5 cm^2).

The time resolution of a thin silicon detector system, neglecting plasma erosion times and series resistance in the detector and input circuit, is limited by the effect of electronic noise in the first stage of the amplifier required to amplify the relatively small detector signals. Noise fluctuations modulate the point on the signal rise where the timing discriminator fires which, since the signal rise-time has a finite value, causes a jitter in the triggering time. As discussed earlier, the signal rise-time is determined mainly by the

fastest achievable rise-time in the pulse amplifier. Commonly this is about 2 ns (10 to 90%). At high frequencies, noise is largely due to the random nature of electron flow through the input amplifier element (often called shot-noise).

Optimization of the input amplifier element which connects to the detector has received considerable study. The equivalent input noise voltage V_n of this element is given approximately by the equation:

$$< V_n^2 > = 4\ kT\ \Delta f/g \qquad 38.$$

where g is the transconductance of the device and Δf is the bandwidth of the system. On the other hand, the signal V_s developed at the input of the stage is given by:

$$V_s = Q/(C_D + C_I) \qquad 39.$$

where Q is the charge released by an event in the detector, C is the detector capacitance and C_I is the input capacity of the input amplifying stage. Assuming that a rise-time (10 to 90%) of τ is associated with a bandwidth (Δf) of $1/\pi\tau$, and assuming that the system is operated at room temperature, Equation 38 can be simplified to:

$$V_{n(RMS)} = 0.7 \times 10^{-4}/\sqrt{\tau g} \text{ volts} \qquad 40.$$

where τ is measured in ns and g in mA/V. Equation 39 can also be expressed in more practical terms:

$$V_s = 0.044\ E/(C_D + C_I) \text{ volts} \qquad 41.$$

where E is the energy deposited in the detector in MeV, and C_D and C_I are expressed in pF. Since the rise-time of the signal given by Equation 41 is τ (a linear rise is assumed for this approximate calculation) the fluctuation in timing caused by noise is given by:

$$\Delta t_{(FWHM)} = 2.35\ V_{n(RMS)}\ \tau/V_s \text{ ns}$$

i.e.,

$$\Delta t_{(FWHM)} = 3.7\sqrt{\tau/g}\ (C_D + C_I)/E \text{ ps} \qquad 42.$$

If τ = 2 ns, g = 50 mA/V $C_D + C_I$ = 500 pF and E = 10 MeV -- typical values in the ΔE detector of a particle identifier and in the associated input amplifier -- then $\Delta t_{(FWHM)}$ = 37 ps. Practical values of the timing limitation imposed by noise in properly designed systems approach this value but detector charge collection and series resistance effects in the detector-input circuit raise the

effective time resolution of a single detector, when timing actual particles, into the range near 100 ps. This means that the spread in timing the passage of particles between two detectors is in the 150 ps time range.

Equation 42 indicates that the time resolution is determined by the ratio $(C_D + C_I)/\sqrt{g}$ -- the other factors in the equation do not depend on the input amplifying element. Clearly the best timing would be achieved if an amplifying element with a very large ratio of g/C_I were used. Since this ratio is approximately 400 mA/V/3 pF for a bipolar transistor having a cut-off frequency f_T of 2 GHz, while the best field-effect transistors (FET) exhibit equivalent ratios of 50 mA/V/50 pF, it appears, at first sight, that a bipolar transistor should be used as the input amplifying element. However, the bipolar transistor, operating at a current of 10 mA to achieve the forementioned g/C_I ratio, exhibits an input resistance in the range of 30 ohms, so the voltage pulse at the input decays quickly with a time constant $(C_D + C_I)30$ -- i.e., 15 ns, if $C_D + C_I = 500$ pF. Such a rapid decay makes the slow signal processing, usually required for energy measurement, impossible. Therefore, a field-effect transistor is normally employed as the input amplifying element. The ratio g/C_I for a field-effect

transistor is determined by the ability of manufacturers to produce very small device structures; therefore while different values of g and C_I are available, their ratio tends to be constant for state-of-the-art devices. C_D is large for thin silicon detectors, so its value nearly always exceeds C_I in these applications. In this case a field-effect transistor having the highest practical value of g (and therefore C_I) will give the best timing performance. At the present time 50 mA/V and 50 pF are representative of suitable devices. Equation 42 predicts that the best timing would result from using an FET exhibiting $C_I = C_D$, but this condition can rarely be satisfied in practice.

Figure 23 shows the input circuit used with a fast timing silicon detector. This diagram emphasizes the requirement for very low-inductance connections around the entire detector loop. A wire 1 cm long and .05 cm in diameter exhibits an inductance of .01 μH, which will resonate at 250 MHz with a 300 pF FET input capacity. Clearly such a situation is intolerable if timing in the 100 ps range is to be achieved. Consequently, very short low-inductance connections should be used in the detector circuit. To avoid ringing in the input circuit a damping resistor ($\sim 10\Omega$) should also be included in the circuit.

A further timing limitation is imposed by the spreading resistance of the evaporated metal contact layers on the detector itself. If this resistance is not kept to a very low value (a few ohms), charge produced at different points across the detector area produces output signals that have been integrated to different degrees by the spreading resistance and detector capacitance combination. Since thick metal films constitute intolerably large dead layers on detectors used for heavy-ion measurements, a compromise must be made between their resistance and the dead layers they represent. Well-prepared gold films about 200 Å thick represent about the best compromise.

Typical Systems and Results

Simple time-of-flight mass measurements have been made for many years in a broad range of experiments. The types of experiment in which this simple measurement is adequate include some beam energy measurements (88), fission fragment mass distribution experiments (75), and some reaction experiments where the Z of the detected products was known or could be inferred. The more sophisticated systems, which depend on both MZ^2 particle identification using detector telescopes and time-of-flight measurement of mass have been used in

studies of heavy-ion transfer reactions (89,90) and of the fragmentation products of high-energy bombardment of heavy targets (91-98). These products provide the opportunity for studies of nuclei far from the normal region of stability and permit tests of the various theoretical mass-stability relationships.

For the purpose of illustrating particle identification using both the MZ^2 and time-of-flight methods we will briefly review the methods employed and some of the results achieved by Butler et al. (21) and by Bowman et al. (99), who used essentially the same system as Butler but with improved data processing methods. Figure 24 shows a block diagram of the electronic system used by these authors. The particle identifier signal fed to the computer is calculated by an analog identifier performing the power-law calculation $T/a = (E + \Delta E)^b - E^b$ (i.e., Equation 15). Events processed by the computer are selected on the basis of this signal, but a modified form of this algorithm is employed in the computer processing to make the identification less energy-dependent. The final identifier output P is given by:

$$P = [\{(E + \Delta E)/k\}^n - (E/k)^n]^{1/2} \qquad 43.$$

where:

$$n = b - c\ \Delta E/T \qquad 44.$$

The constants c and k are chosen empirically to realize the smallest energy dependence, and the square root of the whole expression is used to make the final output proportional to Z rather than Z^2, thereby producing a more convenient scale for output display.

The improved particle identifier behavior realized by this modification to the basic range algorithm is illustrated by the three cases shown in Figure 25. Using this method, elemental identification up to Argon (Z = 18) has been achieved. In the experiments described by Butler et al., this was combined with a time-of-flight measurement between a 22 micron ΔE detector and a 112 micron E detector. The time resolution achieved in these experiments was approximately 250 ps (FWHM). A two-dimensional counter plot of the resulting data is shown in Figure 26. In the more recent experiments by Bowman et al., amplitude-dependent time walk effects were reduced by computer processing with the result that a time resolution of about 150 ps (FWHM) was realized for the range of particles of interest. Using these methods the existence of approximately ten

new particle-stable neutron-rich isotopes of elements with $Z < 9$ has been demonstrated. Several other isotopes, whose stability was in question, have been shown to be unstable against particle break up. These methods clearly provide a powerful new technique to explore the boundary of the neutron-rich side of nuclear stability.

The range of isotopes that can be identified in practice is well demonstrated by Figure 27 taken from Butler et al. While recent improvements have altered this picture a little, the overall changes are not significant. Depending on the type of ion, different values are assigned to the minimum energies considered essential in the E detector -- these values are indicated on the horizontal axis. The curves then show the energy of those particles which pass through the ΔE detector with enough energy remaining to satisfy this condition. The dotted line is drawn to show the boundary of the range of isotopes practically resolvable at the present time by detector telescopes with combined MZ^2 and time-of-flight measurements. This figure shows the influence of energy on the ability to identify heavy ions.

IV. SYSTEMS INVOLVING MAGNETIC RIGIDITY

Fundamentals

The magnetic rigidity $B\rho$ is related by Equation 4 to the mass, velocity, and charge state q of the particle. If the residual gas pressure in a spectrometer is sufficiently low ($\lesssim 10^{-5}$ Torr) the probability that a particle will undergo a charge-changing collision is small. The value of q as well as the nuclear charge Z and mass M (for non-relativistic particles) is then restricted to integral values so that some of the measurements required for identification need only be made with sufficient precision to resolve adjacent integers. A precise measurement of $B\rho$ then yields the kinetic energy E with equal precision by setting M and q equal to their exact values and using

$$E = (B\rho)^2 q^2/(2M) \qquad 45.$$

This equation is, of course, non-relativistic.

If the spectrometer (deliberately or by accident) contains enough gas for a large number of charge-changing collisions to occur, $B\rho$ will be determined by the <u>average</u> charge state $\bar{q}$ of the ion, and of course $\bar{q}$ need not be integral. At intermediate pressures ($\sim 10^{-3}$ - 10^{-4} Torr), a few ions suffer a

single charge-changing collision. The detection system then identifies most ions as having discrete integral charges but there is a continuous background between one charge state and the next.

The energy loss in a detector is related to the quantity q_{eff} which is a function of Z and the velocity v. For light ions and high velocities $q_{eff} = Z$, but for heavy ions $q_{eff} \leqslant Z$. However, the velocity range observed in a focal plane at one magnetic field setting is usually small enough that q_{eff} is a function only of Z so that adjacent Z-values are separated by a measurement of dE/dx. At least for the lighter heavy ions, q_{eff} need therefore not be treated as an extra parameter to be determined. Since charge-state equilibrium is reached in passage through just a few $\mu g/cm^2$ of stopping material, the energy loss of a particle is virtually independent of the charge state with which it enters the detector.

In heavy ion experiments, particles leave the target in a variety of charge states that are separated in the spectrometer magnet. The fraction in a given state depends upon Z, v and the target element: this subject has been reviewed by Betz (54). In order to measure a reaction cross section, the fraction in the charge state detected must be known. Alternatively, all

charge states can be converted into the average state $\bar{q}$ in a gas-filled spectrometer, but then the multiple scattering and energy loss straggling will damage the resolution of the Bρ measurement.

Complete identification and energy measurement in a spectrometer thus requires that the five quantities E, Z, A, q and q_{eff} be determined, but as mentioned above, the measurement of q_{eff} is not essential. To determine the remaining four variables, the following five quantities are in principle measurable--Bρ, v, dE/dx, E and ρ_E (the radius of the orbit in an electric field). In fact, ρ_E has not so far been used because extremely strong fields are required to produce a useful deflection. Furthermore, no detectors are capable of measuring E with good resolution over the large areas of spectrometer focal surfaces. Plastic scintillators are used as stopping counters, but the energy resolution is typically about 20% and the very severe light quenching for heavy particles makes the response a poorly-known function of A, Z and E rather than of E alone. Particle energy can be measured in silicon or germanium detectors with excellent resolution, at least for short-range particles, but these detectors are only available with relatively small areas.

The remaining quantities, Bρ, v and dE/dx, can be measured with sufficient resolution (especially Bρ and v), but four unknowns cannot be determined

unambiguously by three measurements. Fortunately A, Z and q have integral values so that the ambiguity in their determination is usually not troublesome: it is discussed later.

Magnetic spectrometers and focal plane detector systems have been reviewed by Hendrie (100).

Measurement of Bρ

The magnetic rigidity Bρ is nearly always obtained by detecting the position at which the particle crosses the focal surface of a magnetic spectrometer. For adequate identification of the particle, the detection system does not need very good position resolution, but the requirement of good energy resolution for the particle spectra usually mandates that the position resolution shall be about 0.5 - 1 mm (FWHM).

Focal plane areas are typically 1 - 5 cm in the vertical dimension and up to 100 cm in the horizontal direction. Therefore for full exploitation of the momentum range of the focal surface, detectors of rather large area are required. Usually, only the position of a particle in the horizontal (radial) direction is measured, but several techniques permit a simultaneous measurement

in the vertical direction which can be used to correct for a curved or inclined line shape (101). Many spectrometers were designed for particle detection with photographic plates for which it is an advantage to make the particle trajectories strongly inclined (typically at 45°) to the focal surface (100). Unfortunately, the non-normal entry has a deleterious effect upon the position resolution obtained with nearly all types of detectors, especially in the measurement of particles with low specific ionization (see below). The same problem has been built into even quite recent spectrometer designs (102). When proper consideration (100) is given to the spectrometer system as a whole, it is evident that not only should the focal plane be normal to the trajectories, but it should also be flat since most detectors cannot be constructed to follow a curved surface.

Virtually every type of detector used in nuclear and high energy physics can form the basis of a position-measuring system provided that the units are cheap enough to be built into an array of large enough area. Matsuda et al. (103) built arrays of 250 Si detectors and 200 individual proportional counters. The reliability of such a large array must be questioned. Cohen and Rubin (104) used an array of plastic scintillators while Kobayashi and Takayanagi (105) put 1000 detectors on to 25 separate silicon wafers.

The multiwire proportional counter (MWPC) (106-107) and spark chamber (106, 108) with sonic read-out (109-111) have been used: they too are essentially arrays of detectors enclosed in a single large housing. They have the advantage over arrays of separated detectors that there are no gaps along the sensitive length, and that they can in principle be built along a curve adapted to a focal surface that is not flat. The low count-rate ($\sim$ 100 events/sec) of the spark chamber makes it unsuitable for use in nuclear physics spectrometers. Furthermore, high counting rates at discrete spots are known to cause insensitivity in these regions. The MWPC, though, offers many advantages and it is somewhat surprising that its use is not more common now that read-out systems are available that do not require an amplifier for each wire (112-114). However, it has not yet been demonstrated that the MWPC is capable of high-resolution energy-loss measurement.

In a second class of counters, a single long detector is used rather than an array, and inspection of pulses from one or both ends enables the position of particles to be determined. The long axis of the detector is positioned horizontally along the focal surface.

The position-sensitive silicon detector (115-166) has the advantages of commercial availability, and can measure both position and energy (for particles of short range) or energy-loss (for particles of intermediate range). Its many

disadvantages, though make it unsuitable for general application in a spectrometer. The counters are small--at best 1 cm high × 5 cm long in the position-sensitive direction, and they are rather expensive. An array is needed to cover the full focal plane (117). The best units are made by ion-implantation of boron into high-resistivity silicon to make a resistive front surface. One end of this surface is grounded and a signal is taken from the other end into a charge-sensitive preamplifier. The charge liberated by the passage of a particle divides inversely as the ratio of the resistances to the two ends of the counter. The preamplifier signal is therefore proportional to $\Delta E \cdot x/L$, where ΔE is the energy loss, L is the detector length and x is the distance from the grounded end to the point of entry of the particle. The energy loss ΔE is obtained as a second signal from the back of the detector. Division of the two signals in an analog or digital divider gives the position x/L.

The position resolution is, at best, about 0.5 - 1% of the detector length (0.25 - 0.5 mm/5 cm) for particles that lose a few MeV in the depletion depth. In a detector 1.4 cm long, Laegsgaard, Martin and Gibson (115) measured a position resolution of 0.16 mm for stopping 5 MeV α-particles. The system noise (30 keV) was equivalent to a position resolution of 0.08 mm. For particles

that lose small amounts of energy, the resolution is limited by the signal/noise ratio so that even in the thickest available counters (~ 600 μm depletion layer), the resolution becomes unacceptable (> 1 mm) for protons of E > 50 MeV. The theory of noise and resolution has been discussed by Owen and Awcock (118). The relatively small physical depth of silicon detectors (compared with gas-filled counters) makes their position resolution almost independent of the angle of entry of the particles.

The linearity of the silicon position-sensitive detector may be limited by the variation in rise time of the signals from the resistive surface as a function of position. The resistive surface and detector capacity act as a distributed RC line so, the further the particle from the preamplifier end, the slower is the pulse rise time. The characteristic RC is approximately 0.1 μs, or about 1/10 of the typical amplifier time constant so that a flat-topped pulse should be used to reduce the dependence of amplitude on rise-time. In practice, the linearity is about 1%. The theory of the charge-division process has been discussed by Kalbitzer and Melzer (119), Doehring et al. (120) and Kalbitzer and Stumpfi (121).

The position-sensitive gas proportional detector with charge-division readout is a device quite similar in principle to the silicon counter. The silicon

counter (a solid ion chamber with a resistive surface) is replaced by a gas-filled proportional chamber with a resistive central anode wire (111,122-123) having one end grounded or with a charge-sensitive preamplifier at each end as shown in Figure 28. The wire can be very thin (10 μm dia) nichrome (124) or carbon-coated quartz (25 - 75 μm) (123,125). The anode wire is stretched centrally between flat planes of thin aluminized plastic sheet which form the counter cathode, as shown in Figure 28. As with the silicon detector, the position signal at one end measures $\Delta E \cdot x/L$ and must be divided by a signal proportional to ΔE obtained either from the cathode or from the sum of the signals from the two ends of the anode wire. Compared with the silicon detector, the proportional chambers have the advantage that they can be made as long as required. By using several horizontal wires placed vertically one above the other, the sensitive vertical dimension can also be made as large as required. Further, the large gas multiplications that are achievable--as high as 10^5 while retaining proportionality (126)--maintain an excellent signal-to-noise ratio even for particles of very low specific ionization.

In an alternative read-out technique for the resistive-wire proportional chamber, Borkowski and Kopp (127-128) showed that the anode wire can be used as a

distributed RC line which slows down the rise time of the pulse as it travels in both directions away from its point of origin. The highly resistive wire is, in practice, a carbon-coated quartz fiber[†], diameter 25 μm and resistance 8000 Ω/mm. These fibers have excellent uniformity both in diameter and resistance and, having no tendency to curl, are easier to handle than metal wires of the same diameter. The rise-time method was first used in a spectrometer by Ford and co-workers (129).

Pulses are amplified at each end of the anode and differentiated to make bipolar pulses as shown in Figure 29. Crossover detectors generate pulses at the zero-crossing time, and the position of the particle is determined by measuring the time difference between these pulses, using a time-to-amplitude converter (TAC). The crossover pulse from one end passes through a fixed delay so that it always provides the stop signal for the TAC. A 25 μm anode fiber with a resistance of 8000 Ω/mm in a counter 1 cm deep gives a delay time of about 300 ns/cm. The energy-loss can be obtained by adding suitably shaped pulses from each end of the anode.

Unlike charge division read-out, the rise-time method has the advantage that the position signal, without additional processing, is independent of the

[†]Carl M. Zvanut Co., 14 Chetwynde Road, Paoli, Pennsylvania 19301.

amplitude of the event. The position resolution measured by charge division, where both the $\Delta E \cdot x/L$ and ΔE signals are of course amplitude-dependent, may depend on particle type when digital division is used. For example, if the pulse height given by α-particles is adjusted just to saturate the ADC, the proton pulses--20 times smaller--are not accurately measured by the limited number of ADC channels. Position resolution is therefore lost (124). In both methods, the position resolution may also be limited by the signal-to-noise ratio. In the rise-time method, noise causes a jitter in the zero-crossing time of the bipolar pulse. If the bipolar pulses cross zero at a rate dV/dt and the (uncorrelated) RMS noise on the signals is V_n, the time jitter in both the start and stop pulses to the TAC will be V_n dt/dV, and the position signal will be uncertain by $\sqrt{2}\ kV_n$ dt/dV where k is the distance corresponding to unit time difference. Of course, dt/dV is larger for particles making small amplitude pulses, so the position resolution may be dependent on particle type if it is noise limited. However, this is not usually the case. The position resolution and linearity of the rise-time method have been studied theoretically by Mathieson (130) who finds that both resolution and linearity degenerate rapidly near the ends of the resistive anode: particle detection should therefore be restricted to the central $\sim$ 75% of the length. The time constants of the

differentiating network that produces the bipolar pulses should be about $1/10^{th}$ of the RC of the anode. Mathieson assumes that the ends of the resistive wire are terminated in charge-sensitive preamplifiers which essentially short-out any voltage changes at the ends. Since many of the chambers used in experiments do not operate in this mode, his conclusions are of limited validity.

One disadvantage of the rise-time read-out method is the rather long resolving time (typically 10 - 15 μs). However, data rates are more likely to be limited by on-line computer speeds than by the chamber. It has been reported (131) that the position resolution of the rise-time read-out can be as good as 0.16 mm at 3×10^5 counts/sec. Of course, the coincidence losses at this rate would be unacceptably high in most experiments. The position resolutions reported in spectrometer focal planes are typically 0.5 mm/20 cm (charge division, (111)) and 0.6 mm/45 cm (rise time, (101,129,132)). Values as good as 0.15 mm are obtained in bench tests with collimated sources of radiation.

Neither charge-division nor rise-time read-out gives a response that can be assumed exactly linear with particle position (101,124). The rise-time method has been especially plagued by S-shaped response curves, but this problem can be cured by use of only the middle 75% of the anode length, by proper choice of the differentiating time constant (130), and by proper termination of the anode

line (101). Even so, the response must be calibrated by, for example, moving a strong elastic peak to different positions by changing the magnetic field of the spectrometer. In a counter with several wires, each wire will almost surely give a slightly different response: they must therefore all be calibrated separately and calibration data stored in an on-line computer.

In yet another read-out system, one or both of the cathode planes of a proportional detector are replaced with a single or double helical delay line whose axis (see Figure 30) is parallel with the anode wire or wires (133-135). The motion of the ion pairs near the anode induces a signal in several turns of the helical cathode. The pulse travels along the helix in both directions, delayed by about 30 ns/cm and the position is measured from the difference in arrival time of the pulse at the two ends.

For very long-range particles, the presence of helix wires in front of the anodes is unimportant, but it does cause trouble at lower particle energies (135). The configuration shown in Figure 30b is therefore preferable. In a typical helix (134), the wires are copper-clad aluminum, 75 μm diameter, 0.5 mm apart. The transparency of this helix to short-range particles is therefore only 85% but no doubt somewhat more transparent helices could be built. When

multiple detectors are required to measure ΔE or TOF, or for the virtually essential reduction of background by requiring multiple coincidences (123-124, 132), the helix detector would presumably have to be at the rear. Of course, the position-measuring device should be ahead of the other counters in order to avoid loss of position resolution from multiple scattering.

Although the delay-times in the helix--30 ns/cm--are about ten times shorter than in the rise-time system, pulses are reflected from the ends of the helix. In each reflection the pulse is inverted and attenuated about 5-fold. After the second reflection, the pulse has its original polarity but is attenuated by a factor of 30. To prevent double-counting, discriminators are used between the amplifiers and the TAC. Nevertheless, the pulse-storage time is only a factor of two or three shorter than in a rise-time system. The low transparency seems a high price to pay for this advantage. Position resolution is excellent--0.33 mm FWHM has been reported in a counter 25 cm long (135).

The helix read-out has the advantage that the position calibrations are identical for all the wires of a multiwire counter. The position calibration should be independent of time provided that the helix suffers no physical damage. Further, the position resolution appears to be independent of the angle of entry of the particles: this is discussed in more detail below.

Radeka (136) has made a theoretical analysis of the optimum performance to be expected from resistive wire charge-division chambers and delay-line read-out systems. He showed that dispersion in the delay-line causes the timing and hence the position resolution to become signal-to-noise limited in long lines. In charge-division read-out, the position resolution of an optimized system is determined only by the anode capacitance and not by its resistance. It should therefore be possible to use anodes of lower resistance than has been common, with consequent improvement in timing and energy resolution.

In the drift chamber (137) designed for the detection of 1 GeV protons (Figure 31), electrons liberated in the gas drift down a potential gradient in a direction normal to the trajectory of the particle. At the end of the drift they are detected in a simple proportional chamber. A time-zero signal is obtained from a scintillator, and drift time is measured to give the position of the particle. Detectors up to 50 cm in length are used with electric field gradients of 800 V/cm, requiring a high voltage supply of at least 40 kV. The drift velocity W depends on the field gradient E, the nature of the gas and its pressure p, but W becomes independent of the gradient when the quantity E/p is equal to about unity (in units of V/cm and Torr). The preferred gas is

pure methane, although neon-methane mixtures have been used. The limiting drift velocity is about 10 cm/μs in methane at a pressure of 1 atmosphere and somewhat less in neon-methane mixtures.

The line of electrons along the particle track is broadened by diffusion during the drift, which makes a contribution σ to the resolution:

$$\sigma = (2DL/W)^{1/2} \qquad 46.$$

where L is the drift length and D is the electron diffusion coefficient in the chosen gas. In pure methane, σ was found to be 0.4 mm (L = 12 cm) and 1.3 mm (L = 50 cm). The position resolution in a long drift-chamber is therefore not quite as good as for other systems.

The proportional chamber at the end of the drift space (137) was found to measure the energy loss of 1 GeV protons with no apparent loss of resolution even after a 25 cm drift. However, the measured resolution must have been limited entirely by energy loss straggling so that the sensitivity to such effects as electron attachment to impurities would be quite low. It remains to be shown that good energy resolution can be obtained for particles for which energy loss straggling is small.

When particles cross the gas space of a proportional or drift chamber at a non-normal angle there may be a serious loss of position resolution. The read-out systems correctly measure the center of ionization of the track, but especially for tracks of low ionization density, statistical fluctuations can move the center of ionization with respect to the geometrical center. This problem has been analyzed by Miller and co-workers (111). As might be expected, the loss of resolution is reduced when the counter is made shallower (but then the ΔE resolution becomes worse). Alternatively, the energy loss can be increased and the fluctuations reduced by increasing the gas pressure. Figure 32 shows the calculations of Miller et al. for particles incident at 45°.

The volume of the sensitive zone around a proportional counter anode wire can be controlled at will by the addition of gases that capture electrons to form negative ions of low mobility, such as ethyl bromide or freon (106). Parts of the particle track that are more than the desired distance from the wire do not contribute to the pulse so that the effective depth of the counter

is reduced. These gas mixtures have been used in multiwire proportional chambers but not so far in the ones described in this review. Of course it would be necessary to place the wires at a sufficiently close vertical spacing to avoid loss of events in dead spots. Further, good ΔE resolution would not be obtained, but as we shall discuss below it is usually advisable to use separate chambers for the position and ΔE measurements.

The helical delay line system is reported (135) to give a position resolution that is independent of angle of entry. This is because the read-out system responds only to the fastest rising part of the cathode pulse, which comes from charges formed in that part of the track closest to the anode wire. It follows that particles far from an anode wire in the vertical direction, having no section of track close to a wire, will be detected with much reduced pulse height (and therefore perhaps poorer resolution). In the counter of Flynn and co-workers (135), the vertical anode wire spacing was only 3 mm, whereas in the rise-time system the anode wires can be at least 15 mm apart without loss of position or ΔE resolution. The ΔE resolution of the helix system is about what would be expected for light particles where

energy loss straggling dominates but there are no reported results for highly ionizing particles such as heavy ions.

Measurement of ΔE and E

The measurement of particle energy E and energy loss ΔE with semiconductor detectors in addition to the magnetic rigidity provides a powerful method of particle identification (138-140). Since the counters are small, $B\rho$ is determined approximately, even in the absence of a position measurement. Vorob'ev et al. (140) used quadrupole lenses to define a small range of $B\rho$ (2 - 7%): they also measured TOF and E with a silicon detector.

Since

$$(B\rho)^2/E = 2A/q^2 \qquad 47.$$

measurement of $B\rho$ and E suffers from an A/q^2 ambiguity. For fully stripped ions (q = Z), the ambiguity is in A/Z^2. Measurement of E and ΔE leaves an ambiguity in AZ^2, since approximately

$$E \cdot \Delta E \propto AZ^2 \qquad 48.$$

For fully stripped ions (q = Z), Equations 47 and 48 give

$$A^2 \propto (B\rho)^2 \cdot \Delta E \qquad 49.$$

$$Z^4 \propto E^2 \Delta E/(B\rho)^2 \qquad 50.$$

In this case A and Z are completely determined by Bρ, E and ΔE measurements. Both E and Bρ are easy to measure with high resolution (at least over small areas and for particles of short range), but the resolution of ΔE measurements is usually limited by energy loss straggling. It is therefore fortunate that ΔE is proportional to A^2 (Equation 49) and Z^4 (Equation 50) so that the resolutions in the A and Z measurements are respectively twice and four times as good as they are in the ΔE determination. If Bρ is not measured, Equation 48 shows that ΔE depends only on the first and second powers of A and Z respectively.

Heckman et al. (141) used a combination of magnetic analysis, dE/dx and TOF measurements in a telescope of nine 3 - 5 mm-thick silicon counters to identify the products from the interaction of 2.1 GeV/A heavy ions with various target nuclei. Identification was simplified because all products were fully stripped and (for Z > 2) they all had the same velocity--equal to that of the beam particles. Hence varying the field of the spectrometer produced a sharp transmission maximum for a particle at

$$B\rho \propto M\beta\gamma/Z \qquad 51.$$

where $\gamma = (1 - \beta^2)^{-1/2}$ and $\beta\gamma$ was the same for all fragments. The various Z-values were separated by the counter telescope with a Z-resolution of ±0.12 units.

With the possible exception of very low energy heavy ions, particles do not stop in proportional counters, so that only energy loss is measured. It is important that the counters be designed so that the resolution in energy loss is limited only by the inevitable straggling rather than by instrumental problems. For small energy losses (e.g. with high-energy protons) the straggling is large (142), but for heavy ions, where the energy loss is large and energy loss straggling may be only a few percent, instrumental effects may limit the resolution.

It is important that the anode wires be smooth and uniform in diameter (143-144). Experimentally (143), the gas multiplication M at a 20 μm wire varies with change of radius dr as

$$dM/M = dr/k \qquad 52.$$

where $k \approx 1$ μm. Therefore a variation in M of ±1% requires that the wire radius uniformity be ±0.01 μm, which is only ±0.1%. This virtually impossible requirement can be relaxed in proportional counters in which position along

the wire is measured, for provided that the gas multiplication is sufficiently uniform over a length equal to the position resolution, a correction can be applied for slower diameter variations or for other effects by measuring the relative gas multiplication as a function of position. In counters with several wires the correction must be made for each position along each wire when the highest ΔE resolution is required.

Both energy loss and gas multiplication vary as a function of gas density, but in opposite directions. The resulting pulse height is approximately inversely proportional to the density. For 1% contributions to ΔE resolution, pressure must therefore be controlled to 1% and temperature to 3°C. In practice, pressures are controlled but temperatures usually are not, perhaps because they vary only slowly inside the spectrometer vacuum system.

The gas multiplication is, in addition, a complex function of the geometry of the counter (106,145-146). If several anode wires are used, they must be parallel, equally spaced from one another and at equal distances from the cathode planes if equal gas multiplications are required. The mutual electrostatic repulsion of the anode wires causes them to move out of the plane in alternate directions (147-148) by a distance Δy given by

$$\Delta y = 10^3 v^2 \ell^2 / T_S \text{ mm}$$

where V is the potential of the wires (kV), ℓ is the wire length (m), S is the distance between wires (cm) and T is the wire tension (dynes). Electrostatic stability and freedom from sustained vibrations is assured when the wire tension exceeds a critical value T_c:

$$T_c \geq V^2 \ell^2 / 4\pi^2 a^2 \qquad 53.$$

where 2a is the depth of the counter (147). The effects of wire displacement, and other geometrical errors, were reviewed by Charpak (106). The maximum tension that 25 μm diameter quartz fibers can reliably sustain is about 12 g. The 20 μm gold-plated tungsten anode wires of a helix detector (134) are tensioned to 50 g.

In a detector with several wires, electrons drift towards the nearest anode wire, where the multiplication then occurs. The (negative) signal on that wire induces a smaller positive signal on adjacent wires. A negative signal may appear on two or more wires if the projection of the track on the plane of the wires crosses from one wire to another. The ΔE signal is therefore most reliably measured by adding the signals from all the wires. Corrections for different gas multiplications can be made by relative gain

adjustments when each wire has a separate amplifier (135), by small adjustments (< 10 volts) in the positive bias of each wire (149), or in an on-line computer that receives a logic signal to identify the wire on which a pulse occurred (101,132).

Good ΔE resolution is especially important in the identification of heavy ions where the fractional difference between adjacent Z-values is small. It has been found by several groups (123,132,150) that the requirements of good position and ΔE resolution cannot be optimized simultaneously in a single proportional counter. Good position resolution requires that the detector be shallow, especially when particle trajectories are non-normal, whereas deep detectors give greater energy loss and less energy loss straggling. Good position resolution requires the greatest possible gas multiplication to obtain a very high signal-to-noise ratio. Good proportional behavior and energy resolution, on the other hand, are best obtained at low gas multiplications. The ideal system therefore consists of a shallow position-sensitive proportional counter in front of a deep ΔE counter. Harvey et al. (132) use a 1 cm-deep resistive wire rise-time position detector and a 4 cm-deep ΔE counter with nickel wires. The ΔE resolution in each counter is close to the value calculated from energy-loss straggling, but it is twice as good in

the deeper ΔE counter as in the position counter. Typical resolutions are 10% and 5% FWHM respectively for 100 MeV ^{16}O ions. The latter figure corresponds to a Z-resolution of about 2½% (since $\Delta E \approx Z^2$). Similar results have been obtained with the system at Argonne National Laboratory (150).

When the total charge density in the vicinity of an anode wire exceeds a certain value, the electric field is sufficiently perturbed that proportionality is lost (151). Since the total charge is proportional to the product of the energy-loss and the gas multiplication M, it follows that M must be kept quite low for detection of heavy ions where the energy loss may be several MeV especially when multiplication is confined to an extremely small volume as it will be in chambers at high gas pressures. In the Berkeley double counter (132), the gas multiplications in the position and ΔE chambers are only $\sim$ 100 and 10 respectively for detection of 100 MeV ^{16}O ions. When the product of energy loss and M exceeds very roughly 200 MeV, peaks in the ΔE spectrum begin to develop "tails" on the high energy loss side when the gas pressure is 1/3 atmosphere. This is of no consequence in a counter that is used only for a position measurement, but of course is highly undesirable for the ΔE counter.

In a chamber with horizontal wires spaced vertically one above another, guard wires must be used outside the upper and lower active anode wires,

otherwise the electric fields and gas multiplications of the outer wires may be considerably different from those of the inner wires (82,85). The maximum vertical spacing between wires consistent with good ΔE and position resolution is not well established. In one counter (132), the spacing is 15 mm so that particles up to 7.5 mm above or below a wire are detected. There appears to be no loss of position or ΔE resolution even in high resolution heavy ion measurements. In a 1-cm deep chamber with rise-time read-out, the position resolution (for a collimated x-ray beam) was constant up to at least 2.2 cm from the anode (152).

Table 1 gives some representative calculated values for energy loss and approximate energy loss straggling of heavy ions in Ar gas (153). The straggling arises both from multiple scattering which changes the path length in the gas, and from the statistical fluctuation in the charge state of the ion.

When ions of high Z and low velocity are detected, their energy loss is proportional to q_{eff}^2 rather than to Z^2, where q_{eff} is an effective ion charge $\leq Z$. The rate of energy loss $(dE/dx)_{A,Z,E/A}$ for an ion A, Z and energy E/A is related to the proton energy loss $(dE/dx)_{p,E}$ by

$$(dE/dx)_{A,Z,E/A} = q_{eff}^2 \, (dE/dx)_{p,E} \qquad 54.$$

Independent of stopping medium, q_{eff} is given (empirically) by (54):

$$q_{eff} = Z\{1 - 1.032 \exp[-v/(v_0 Z^{0.69})]\} \qquad 55.$$

for an ion of velocity v. The Bohr velocity v_0 equals 2.188×10^8 cm/sec. For the lighter heavy ions (e.g. ^{16}O), $q_{eff} \approx Z$ for energies above 5 MeV/A, see Figure 2, but for heavier ions and lower velocities, separation by ΔE measurement becomes more difficult. For example, for A = 90, E = 5 MeV/A:

$$\frac{(dE/dx)_{Z=40}}{(dE/dx)_{Z=39}} = \frac{(q^2_{eff})_{Z=40}}{(q^2_{eff})_{Z=39}} = 1.03$$

whereas

$$Z^2(40)/Z^2(39) = 1.05 \quad .$$

Thus Z-separation of these partially stripped ions requires a dE/dx resolution nearly twice as good as for fully stripped particles. For ^{24}Mg ions, q_{eff} rises from 9.6 at 50 MeV to 11.7 at 250 MeV. At the lower energy, the rate of energy loss is only 64% of what it would be for fully stripped ions of the same velocity.

Measurement of Particle Velocity

Particle velocity is measured by determination of the time of flight over a known distance. The great advantage of making the measurement in a spectrometer is that the focusing permits a long flight path (typically

several meters) with a much larger solid angle than would be possible in a simple evacuated pipe. The flight paths will be different for particles arriving at different points along the focal surface, but provided that position is measured, a correction can be applied to the TOF. There will be an additional dispersion in flight path for particles that leave the target at different angles and focus to a common radial point on the focal surface. A correction can be applied only if a particle's position is measured at two points. The amount of this dispersion decreases as the radial acceptance angle of the spectrometers is decreased: by operating at sufficiently small solid angles any required degree of isochronism can be obtained.

Since $B\rho \propto Av/q$, a two-dimensional plot of $B\rho$ vs TOF($\propto 1/v$) shows a series of lines corresponding to discrete values of A/q. After correcting TOF for focal plane position, these lines become horizontal, as in Figure 33. Events corresponding to a given value of A/q can then be selected by a single-channel analyzer or digitally in a computer. Particles with different Z-values but a common value of A/q can be separated by means of a ΔE measurement.

As discussed above, unambiguous identification is not obtained by measurement of $B\rho$, v, dE/dx. At a given value of $B\rho$ and v, two different species must satisfy:

$$A_1/q_1 = A_2/q_2$$

$$E_1/E_2 = A_1/A_2$$

If

$$dE/dx \propto AZ^2/E \propto Z^2/v^2 \quad ,$$

then

$$(dE/dx)_1 = (dE/dx)_2$$

when

$$Z_1 = Z_2 \quad .$$

Hence two ions of the same element Z are indistinguishable when they have the same ratio of mass number to charge state A/q, for example $^{16}O(8+)$ and $^{14}O(7+)$. In most experiments there will be a range of Bρ values where the two species do not overlap because of differences in Q-value and reaction kinematics.

In a two-dimensional spectrum of TOF vs ΔE, species are separated both by A and Z (except for the ambiguities mentioned above). Figure 34 shows such a plot for the species obtained by bombarding ^{24}Mg with 86 MeV ^{11}B ions.

Figure 35 shows an unidentified particle position spectrum and the spectra of three ion species that were identified and separated by measurement of Bρ, dE/dx and TOF.

Flight times for heavy ions in a spectrometer are typically 100 - 200 ns. Since adjacent A-values in typical heavy ion experiments ($A \approx 20$) differ by only 5%, the TOF resolution should be at least 1 - 2 ns.

When the beam is obtained from a cyclotron or other pulsed accelerator, TOF differences can be measured by starting a TAC with the signal from a fast plastic scintillator in the focal plane and stopping it with a signal from the cyclotron oscillator (101,154). The TOF resolution is then at best just the time width of the accelerator beam microstructure. With special precautions this has been reduced to 200 ps at the Michigan State University cyclotron (154), but in most cyclotrons the pulse width is about 5 - 10 ns which is unacceptably long. Moreover, the time structure of the beam pulses in most machines is very sensitive to almost all the parameters of the cyclotron, such as the magnitude and shape of the magnetic field, the dee voltage and frequency, the ion source position and so on. The time width of the microstructure is therefore not very stable, and the tuning conditions that give the sharpest time structure almost axiomatically produce less than the maximum amount of beam.

For most cyclotron work, or for experiments with D.C. beams, a time-zero detector between the target and the spectrometer entrance must be used. It

should be sufficiently thin that energy-loss straggling and multiple scattering cause acceptably small losses of energy resolution. The effect of multiple scattering is minimized when the detector is placed as close as possible to the target. If it were actually at the target position (clearly impossible in practice), its effect would be exactly the same as the addition of the same material to the target. When the detector is placed downstream from the target, the change of direction due to multiple scattering makes the particle appear to have originated from a different part of the target. If the spectrometer is operated with a momentum dispersed beam rather than an analyzed (monoenergetic) beam, the multiple scattering causes a loss of the correlation between beam energy and its position on the target that is essential for the dispersion matching in the spectrometer (100). Moreover, the change in angle of the trajectory causes a loss of the kinematic compensation. A particle emitted from the target at angle θ with respect to the beam, and having the kinematically correct energy E_θ will appear, after multiple scattering and energy loss in the time-zero detector, to have been emitted at $\theta \pm \Delta\theta$ with energy $E_\theta - \Delta E$. The new energy and the apparent angle are no longer related by the kinematics of the nuclear reaction. For heavy ions of energies used for nuclear reaction

studies, the energy loss straggling effect would seem to dominate. The straggling δE is given approximately by

$$\delta E(\text{FWHM})(\text{keV}) = 0.924\ Z_1 (Z_2 t/A_2)^{1/2}$$

where Z_2, A_2 refer to the foil material of thickness t $\mu g/cm^2$. For a 50 $\mu g/cm^2$ carbon foil, δE is approximately 40 keV for ^{16}O ions.

The multiple scattering half-angle $\delta\theta$ can be calculated from tables given by Meyer (155). For 100 MeV ^{16}O and a 50 $\mu g/cm^2$ carbon foil, $\delta\theta$ is about 0.3 mrad, but detailed calculations are required to estimate the effect of $\delta\theta$ upon the energy resolution of a specific spectrometer system. Only about one third of the multiply scattered particles are contained in the cone of half-angle $\delta\theta$. For a given type of particle in a given foil, $\delta\theta$ is roughly proportional to q_{eff}^2 and inversely proportional to the energy. Experimental values for the RMS multiple scattering angles for ^{16}O and ^{32}S in C, BeO and Al_2O_3 foils have been measured by Cline and coworkers (156). By extrapolating their results, a value of 1 mrad is obtained for $\langle \delta\theta^2 \rangle^{1/2}$ for 100 MeV ^{16}O in a 50 $\mu g/cm^2$ carbon foil.

The time-zero detector will frequently be required to operate at an extremely high count rate, for regardless of what particles are detected at the focal surface, it will always be exposed to the elastically scattered beam

particles. The best position for it is therefore immediately behind the entrance slits of the spectrometer. The detector should not be placed between magnetic elements when heavy ions are to be detected. The fields of the elements achieve proper focusing or deflection of particles of a fixed charge state, so that any ion that emerges from the detector with a charge state different from its value in the first element will behave incorrectly in subsequent magnetic elements. In spite of all these difficulties, the time-zero detector seems likely to become a standard feature in particle-identifying spectrometer systems although at the present time it is rarely used.

The system of Vorob'ev et al. (140) uses two quadrupole doublets to focus light nuclei formed in the thermal neutron fission of ^{235}U on to an energy-measuring silicon detector, thus selecting a range of $B\rho$ values 2 - 7% wide depending on the size of the detector. Time of flight is measured between the silicon detector and a thin (0.5 μm) aluminum foil placed at the focus of the first doublet. The foil is biased at -20 kV and secondary electrons are accelerated towards two scintillation-photomultiplier detectors. A coincidence between the two photomultiplier signals is used as the time-zero pulse. The time resolution

of the system is 2 ns (FWHM). Combined with the 1% energy resolution, this gives a mass resolution of 2%.

The Berkeley spectrometer (101,132) uses a thin NE III scintillator foil observed by two photomultipliers through a bi-conical light guide (Figure 36). For detection of heavy ions, foils of about 50 $\mu g/cm^2$ prepared by the method of Muga and co-workers (157) give a detection efficiency close to 100%. It is unfortunate that the very great quenching of the light output makes plastic scintillators basically unsuitable for detection of heavy ions: the high efficiency is obtained by setting the threshold for detection at a single photoelectron, and the count rate in the system is typically in the range of 10^5 - 10^6 counts/sec. The scintillator foil is extremely sensitive to electrons coming from the target so that an electrostatic deflector must be placed between the target and the foil. Time of arrival of a particle at the focal surface is measured with a 45 × 6 cm plastic scintillator placed behind the rise-time position-measuring proportional counter and the energy-loss counter. The intrinsic time resolution of the system is about 0.7 ns, but flight path length dispersion degrades it to 2 ns at a solid angle of 1 msr. The flight time for 100 MeV heavy ions is about 150 ns, so the time and mass resolution is typically better than 2%.

The use of a four-fold coincidence between the time-zero detector, two proportional counters and the focal surface scintillator reduces the system background virtually to zero. In a study of the reaction $^{208}Pb(^{20}Ne,\alpha)^{224}Th$, no α-events were observed between 0 and 5 MeV of excitation in ^{224}Th. A single event would have corresponded to a cross section of 70 nb/sr.

As already mentioned, the channel-plate secondary electron detector offers the possibility of simultaneously measuring the time and the position of the particle. With the apparatus shown in Figure 22b, Gabor, Homeyer, and Kovar (158) obtained a position resolution of about 1.5 mm. The position-sensitive silicon counter that they used is not ideal for fast timing, but it could be replaced by an array of anodes to give both position and fast timing. The accelerating grid--transparency 99%--caused background problems in the position spectrum at the focal surface by scattering heavy ions. Muga (159) has shown that a low-resolution position measurement ($\sim$ 7.5 mm) can be obtained from a thin plastic scintillator by comparing the light output from the two ends in a system similar to that of Figure 36.

A radial position measurement at the entrance of a spectrometer would be enormously valuable. If the radial width of the beam spot on the target

is sufficiently small, a position measurement at a point downstream is equivalent to a determination of the angle at which a particle enters the spectrometer. Corrections can then be made for the angular dependence of the flight path length, for radial spectrometer aberrations and for the angular variation of the energy of nuclear reaction products. The spectrometer designer would be liberated from concern with isochronism, radial aberration control and kinematic compensation with multipole elements or by focal plane displacement. Moreover, angular distributions of reaction products measured in a spectrometer with a large radial acceptance angle could be broken down into measurements over small angular increments.

With increasing interest in the study of heavy ion reactions, the designer of spectrometers and particle-identifying instruments will be presented with many fascinating new problems. Fortunately, the field has never contained so many potentially fruitful new ideas, nor has the rate of advance ever been so high.

LITERATURE CITED

1. Price, P. B., Fleischer, R. L. 1971. Ann. Rev. Nucl. Sci. 21:295

2. Livingston, M. S., Bethe, H. A. 1937. Rev. Modern Phys. 9:261

3. Hudson, G. M. 1970. Nucl. Instr. Methods 77:197

4. Bichsel, H. 1970. Nucl. Instr. Methods 78:277

5. Turner, J. E. 1964. Nat. Acad. Sci. Publ. 1133:99

6. Northcliffe, L. C. 1963. Ann. Rev. Nucl. Sci. 13:67

7. Northcliffe, L. C. 1970. Nucl. Data Tables A7:233

8. Stokes, R. G., Northrop, J. A., Boyer, K. 1958. Rev. Sci. Instr. 29:61

9. Griffiths, R. J., et al. 1962. Nucl. Instr. Methods 15:309

10. Sachs, M. W., Chasman, C., Bromley, D. A. 1966. Nucl. Instr. Methods 41:213

11. Mark, S. K., Moore, R. B. 1966

12. Broadhurst, J. H., Pyle, G. J. B. 1967. Nucl. Instr. Methods 48:117

13. Gupta, S. K. 1971. Nucl. Instr. Methods 92:33

14. Goulding, F. S., Landis, D. A., Cerny, J., Pehl, R. H. 1964. Nucl. Instr. Methods 31:1

15. Cerny, J., et al. 1966. Nucl. Instr. Methods 45:237

16. Alderson, P. R., Bearpark, K. 1968. Nucl. Instr. Methods 62:217

17. Harmanci, A. D. 1970. Nucl. Instr. Methods 86:109

18. Fischer, P. S., Scott, D. K. 1967. Nucl. Instr. Methods 49:301

19. Armstrong, D. W., et al. 1969. Nucl. Instr. Methods 70:69

20. Skyrme, D. J. 1967. Nucl. Instr. Methods 57:61

21. Butler, G. W., Poskanzer, A. M., Landis, D. A. 1970. Nucl. Instr. Methods 89:189

22. Chaminade, R., Faivre, J-C., Pain, J. 1967. Nucl. Instr. Methods 49:217

23. Bird, B., Ollerhead, R. W. 1968. Nucl. Instr. Methods 71:231

24. Chulick, E. T., Natowitz, J. B., Schnatterly, C. 1973. Nucl. Instr. Methods 109:171

25. Radeka, V. 1964. IEEE Trans. Nucl. Sci. NS-11:302

26. Sah, C. T., Noyce, R. N., Shockley, W. 1957. Proc. IRE 45:1228

27. Muga, M. L. 1971. Nucl. Instr. Methods 95:349

28. Anderson, C. E., Bromley, D. A., Sachs, M. 1961. Nucl. Instr. Methods 13:238

29. Goulding, F. S., Stone, Y. 1970. Science 170:280

30. Ewan, G. T. 1968. Progress in Nuclear Techniques and Instrumentation ed. F. J. M. Farley. Amsterdam: North Holland. 3:69

31. Dabbs, J. W. T, Walter, F. J. 1961. Nat. Acad. Sci. Publ. 871

32. Entire volume of Nucl. Instr. Methods 1966, 43

33. Brown, W. L., et al. 1969. Nat. Acad. Sci. Publ. 1593

34. Gibson, W. M., et al. 1965. Alpha, Beta and Gamma Ray Spectroscopy ed. K. Siegbahn. Amsterdam: North Holland. 1:343

35. Bertolini, G., Coche, A. ed. 1968. Semiconductor Detectors. New York: Wiley

36. Dearnaley, G., Northrop, D. C. 1966. Semiconductor Counters for Nuclear Radiations 2nd Edition. New York: Wiley

37. Bertolini, G., Cappellini, F., Restelli, G. 1973. Nucl. Instr. Methods 12:219

38. Meek, R. L., Gibson, W. M., Brown, R. H. 1971. Nucl. Instr. Methods 94:435

39. Ponpon, J. P., Siffert, P. 1973. Nucl. Instr. Methods 112:465

40. Elad, E., to be published in IEEE Trans. Nucl. Sci. 1974

41. Forcinal, G., Siffert, O., Coche, A. 1968. IEEE Trans. Nucl. Sci. NS-15:275

42. Hansen, N. J. 1971. Nucl. Instr. Methods 96:378

43. Wilkins, B. D., et al. 1971. Nucl. Instr. Methods 92:381

44. Wegner, H. E. 1965. Nucleonics 23

45. Dearnaley, G. 1964. IEEE Trans. Nucl. Sci. NS-11:249

46. Gibson, W. M. 1966. IEEE Trans. Nucl. Sci. NS-13:162

47. Fairstein, E., Hahn, J. 1965. Nucleonics 23

48. Goulding, F. S. 1966. Nucl. Instr. Methods 43:1

49. Dabbs, J. W. T. See Ref. 31, 375-742

50. Van Roosebroeck, W. 1965. Phys. Rev. 139:A1702

51. Klein, C. A. 1966. J. Phys. Soc. Japan 21:307

52. Eberhart, J. E. 1970. Nucl. Instr. Methods 80:291

53. Northcliffe, L. C. 1960. Phys. Rev. 120:1744

54. Betz, H. D. 1972. Rev. Mod. Phys. 44:466

55. Landau, W. 1944. J. Phys. USSR 8:201

56. Symon, K. 1958. Harvard Thesis; also see High Energy Particles 1952. Prentice Hall

57. Vavilov, P. V. 1957. Zh.E.T.P. 32:920; transl. J.E.T.P. 5:749, 1957

58. Maccabee, H. D., Raju, M. J., Tobias, C. A. 1966. IEEE Trans. Nucl. Sci. NS-13:76

59. Gooding, T. J., Eisberg, R. M. 1957. Phys. Rev. 105:357

60. Selzer, S. M., Berger, M. J. 1964. Nat. Acad. Sci. Publ. 1133:187

61. Bohr, N. 1915. Phil. Mag. 30:581

62. Linhard, J., Nielson, V. 1962. Phys. Letters 2:209

63. Haines, E. L., Whitehead, A. B. 1966. Rev. Sci. Instr. 37:190

64. Sternberg, E. P., et al. 1972. Nucl. Instr. Methods 99:309

65. Finch, E. C. 1973. Nucl. Instr. Methods 113:29 (also p. 41)

66. Goulding, F. S., Landis, D. A., Cerny, J., Pehl, R. H. 1966. IEEE Trans. Nucl. Sci. NS-13:514

67. Greiner, D. E. 1972. Nucl. Instr. Methods 103:308

68. Jackson, H. G. 1973. IEEE Trans Nucl. Sci. NS-20:3

69. Gedke, D. A., McDonald, W. J. 1967. Nucl. Instr. Methods 55:377

70. Gedke, D. A., McDonald, W. J. 1968. Nucl. Instr. Methods 58:253

71. Chase, R. L. 1968. Rev. Sci. Instr. 39:1318

72. Maier, M. R., Sperr, P. 1970. Nucl. Instr. Methods 87:13

73. Maier, M. R., Landis, D. A., to be published in Nucl. Instr. Methods

74. Jaffe, L. 1962. Ann. Rev. Nucl. Sci. 12:153

75. Muga, M. L., Burnsed, D. J., Steeger, W. D., Taylor, H. E. 1970. Nucl. Instr. Methods 83:135

76. Gelbke, C. K., et al. 1971. Nucl. Instr. Methods 95:397

77. Schneider, W. F. W., Kohlmeyer, B., Bock, R. 1970. Nucl. Instr. Methods 87:253

78. Stern, W. E., Leachman, R. B. 1950. Rev. Sci. Instr. 27:1049

79. Milton, J. D., Frazer, J. S. 1962. Can. J. Phys. 40:1626

80. Grachev, V. T., et al. 1968. Bull. Acad. Sci. USSR Ser. 32:653

81. Deitz, E., et al. 1971. Nucl. Instr. Methods 97:581

82. Pfeffer, W., Kohlmeyer, B., Schneider, W. F. W. 1973. Nucl. Instr. Methods 107:121

83. Gabor, G. unpublished report (Lawrence Berkeley Laboratory, Berkeley, California)

84. Parkinson, E. R., Bodansky, D. 1965. Nucl. Instr. Methods 35:347

85. Pleyer, H., et al. 1971. Nucl. Instr. Methods 96:263

86. Blignaut, E., et al. 1967. Nucl. Instr. Methods 51:102

87. Emerson, S. T., et al. 1967. Nucl. Instr. Methods 52:229

88. Mak, H. B., Jenson, H. B., Barnes, C. A. 1973. Nucl. Instr. Methods 109:529

89. Watson, B. A., Chang, C. C., Tabor, S. L. 1971. Particles and Nuclei 2:376

90. Henning, W., Zeidman, B., Kovar, D. unpublished report (Argonne National Laboratory, Chicago, Illinois)

91. Poskanzer, A. M., Cosper, S. W., Hyde, E. K., Cerny, J. C. 1966. Phys. Rev. Letters 17:1271

92. Poskanzer, A. M., et al. 1968. Phys. Rev. Letters 27B:414

93. Davids, C. M., Laumer, H., Austin, S. M. 1969. Phys. Rev. Letters 22:1388

94. Davids, C. M., Laumer, H., Austin, S. M. unpublished; Production of Light Elements Li, Be and B by Proton Spallation of ^{12}C (Center for Nuclear Studies, University of Texas, Austin, Texas)

95. Raisbeck, G. M., et al. unpublished report (Princeton University, Princeton, N. J.)

96. Klapish, R., unpublished report; Special Experimental Techniques in the Study of Nuclei Far from Stability (Centre de Spectrometric Nucleaire et de Spectrometric de Masse du C.N.R.S., Orsay, France)

97. Laumer, H., Austin, S. M., Panggabean, L. M., Davids, C. N. 1973. Phys. Rev. C 8:483

98. Bowman, J. D., Poskanzer, A. M., Korteling, R. G., Butler, G. W. 1973. Lawrence Berkeley Laboratory Report LBL-1967

99. Bowman, J. D., Poskanzer, A. M., Korteling, R. G., Butler, G. W. 1973. Phys. Rev. Letters 31:614

100. Hendrie, D. L. 1974. Magnetic Detection of Charged Particles, ed. J. Cerny. Nuclear Spectroscopy and Reactions. New York: Academic Press, Vol. A

101. Harvey, B. G., et al. 1972. Nucl. Instr. Methods 104:21

102. Wiedner, C. A., Goldschmidt, M., Rieck, D., Enge, H. A., Kowalski, S. B. 1972. Nucl. Instr. Methods 105:205

103. Matsuda, K., Nonaka, I., Omata, K., Yagi, K., Koike, M. 1967. Nucl. Instr. Methods 53:82

104. Cohen, B. L., Rubin, A. G. 1958. Nucl. Instr. Methods 111:1568

105. Kobayashi, T., Takayanagi, S. 1967. Nucl. Instr. Methods 53:77

106. Charpak, G. 1970. Ann. Rev. Nucl. Sci. 20:195; and references therein

107. Becker, H., Kalbitzer, S., Rieck, D., Wiedner, C. A. 1971. Nucl. Instr. Methods 95:525

108. Saudinos, J., Vallois, G., Laspalles, C. 1967. Nucl. Instr. Methods 46:229; Specht, H. J. 1968. Bull. Am. Phys. Soc. 13:1363

109. Hardacre, A. 1967. Nucl. Instr. Methods 52:309

110. Fulbright, H. W., Robbins, J. A. 1969. Nucl. Instr. Methods 71:237

111. Miller, G. L., Williams, N., Senator, A., Stensgaard, R., Fischer, J. 1971. Nucl. Instr. Methods 91:389

112. Grove, R., Lee, K., Perez-Mendez, V., Sperinde, J. 1970. Nucl. Instr. Methods 89:257

113. Grove, R., Ko, I., Leskovar, B., Perez-Mendez, V. 1972. Nucl. Instr. Methods 99:381

114. Grove, R., Perez-Mendez, V., Sperinde, J. 1973. Nucl. Instr. Methods 106:407

115. Laegsgaard, E., Martin, F. W., Gibson, W. M. 1968. Nucl. Instr. Methods 60:24

116. Jolly, R. K., Trentelman, G. E., Kashy, E. 1970. Nucl. Instr. Methods 87:325

117. Bock, R., Duhm, H. H., Melzer, W., Pühlhofer, F., Stadler, B. 1966. Nucl. Instr. Methods 41:190

118. Owen, R. B., Awcock, M. L. 1968. IEEE Trans. Nucl. Sci., no. 3, 15:290

119. Kalbitzer, S., Melzer, W. 1967. Nucl. Instr. Methods 56:301

120. Doehring, A., Kalbitzer, S., Melzer, W. 1968. Nucl. Instr. Methods 59:40

121. Kalbitzer, S., Stumpfi, W. 1970. Nucl. Instr. Methods 77:300

122. Kuhlmann, W. R., Lauterjung, K. H., Schimmer, B., Sistermich, K. 1966. Nucl. Instr. Methods 40:118

123. Williams, M. E., Kruse, T., Bayer, D., Williams, N., Savin, W. 1972. Nucl. Instr. Methods 102:201

124. Fulbright, H. W., Markham, R. G., Lanford, W. A. 1973. Nucl. Instr. Methods 108:125

125. Williams, N., Kruse, T. H., Williams, M. E., Fenton, J. A. 1971. Nucl. Instr. Methods 93:13

126. Fuzesy, R. Z., Jaros, J., Kaufman, L., Marriner, J., Parker, S., Perez-Mendez, V., Redner, S. 1972. Nucl. Instr. Methods 100:267

127. Borkowski, C. J., Kopp, M. K. 1968. Rev. Sci. Instr. 39:1515

128. Borkowski, C. J., Kopp, M. K. 1970. IEEE Trans. Nucl. Sci., no. 3, NS-17:340

129. Ford, J. L. C., Stelson, P. H., Robinson, R. L. 1972. Nucl. Instr. Methods 98:199

130. Mathieson, E. 1971. Nucl. Instr. Methods 97:171

131. Gabriel, A., Dupont, Y. Unpublished report. Inst. des Sciences Nucléaires, Univ. Grenoble, France

132. Harvey, B. G., Homeyer, H., Mahoney, J. A. 1974. Ann. Rep. Nucl. Chem. Div. Lawrence Berkeley Lab.; Report LBL-2366

133. Lee, D. M., Sobottka, S. E., Thiessen, H. A. 1972. Nucl. Instr. Methods 104:179

134. Lee, D. M., Sobottka, S. E., Thiessen, H. A. 1973. Nucl. Instr. Methods 109:421

135. Flynn, E. R., Orbesen, S., Stein, N., Thiessen, H. A., Lee, D. M., Sobottka, S. E. 1973. Nucl. Instr. Methods 111:67

136. Radeka, V. 1973. IEEE Trans. Nucl. Sci. To be published. Brookhaven Nat'l. Lab.; Report BNL-18377

137. Saudinos, J., Duchazeaubeneix, J-C., Laspalles, C., Chaminade, R. 1973. Nucl. Instr. Methods 111:77

138. Artukh, A. G., Avdeichikov, V. V., Erö, J., Gridnev, G. F., Mikheev, V. L., Volkov, V. V. 1970. Nucl. Instr. Methods 83:72

139. Jackmart, J. C., Liu, M., Mazloum, F., Riou, M. 1966. Int. Conf. Heavy Ion Physics. Dubna, U.S.S.R.

140. Vorob'ev, A. A., et al. 1969. Atomnaya Energiya 27:31; 1969. Soviet Atomic Energy 27:713

141. Heckman, H. H., Greiner, D. E., Lindstrom, P. J., Bieser, F. S. 1972. Phys. Rev. Letters 28:926

142. Studies in Penetration of Charged Particles in Matter. 1964. NAS-NRC Nuclear Science Series Report No. 39; and references therein

143. Peterson, V. Z., Yount, D. 1971. Nucl. Instr. Methods 97:181

144. Charles, M. W., Cooke, B. A. 1968. Nucl. Instr. Methods 61:31

145. Waligorski, M. P. R. 1973. Nucl. Instr. Methods 109:43

146. Tomitani, T. 1972. Nucl. Instr. Methods 100:179

147. Schilly, P., et al. 1971. Nucl. Instr. Methods 91:221

148. Walenta, A. H. 1973. Nucl. Instr. Methods 111:467

149. Parker, S., et al. 1971. Nucl. Instr. Methods 97:181

150. Greenwood, L. R., et al. 1972. Argonne Nat'l. Lab., Physics Division; Report PHY-1972b; Kovar, D. G., private communication

151. Hanna, G. C., Kirkwood, D. H. W., Pontecorvo, B. 1949. Phys. Rev. 75:985

152. Mahoney, J. 1974. Private communication

153. Maples, C. C. 1974. Private communication

154. Benenson, W., Kashy, E., Proctor, I. D., Preedom, B. M. 1973. Phys. Letters 43B:117

155. Meyer, L. 1971. Phys. Stat. Sol. (b) 44:253

156. Cline, C. K., Pierce, T. E., Purser, K. H., Blann, M. 1969. Phys. Rev. 180:450

157. Muga, L., Burnsed, D. J., Steeger, W. E. 1972. Nucl. Instr. Methods 104:605

158. Gabor, G., Homeyer, H., Kovar, D. G. 1973. Private communication

159. Muga, L. 1972. Nucl. Instr. Methods 105:61

TABLE 1. Energy losses ΔE(MeV) and energy loss straggling (%) in Ar gas (153). A four-fold increase in stopping power improves straggling by about a factor of 2.

E(MeV)	^{11}B		^{12}C		^{16}O		^{20}Ne	
	ΔE	%	ΔE	%	ΔE	%	ΔE	%
				1 cm-atmosphere				
50	2.19	5.80	3.29	4.63	6.45	3.15	9.90	2.56
100	1.30	9.81	2.01	7.61	4.29	4.74	7.34	3.46
150			1.48	10.3	3.20	6.37	5.73	4.44
200					2.59	7.86	4.68	5.44
250							4.00	6.37
				4 cm-atmosphere				
50	9.15	2.78	14.2	2.15	28.5	1.42	46.7	1.09
100	5.27	4.83	8.21	3.72	18.00	2.26	31.4	1.62
150	4.06	6.29	5.86	5.22	13.1	3.11	23.9	2.13
200					10.4	3.93	19.2	2.65
250							16.2	3.16

FIGURE CAPTIONS

Fig. 1. Block diagram of $\Delta E,E$ identifier system.

Fig. 2. Stopping power (in aluminum) for various ions. (Adapted from Reference 6.) The stopping power axis is normalized in terms of Z-1 where Z-1 is the nuclear charge of the particular ion. The energy scale is normalized in terms of the energy/nucleon of the ion. The slope lines at the top of the figure show the slopes corresponding to various power laws.

Fig. 3. Behavior of the components of the output in a $E,\Delta E$ multiplier type of identifier.

Fig. 4. A) Basic circuit of a logarithmic function generator.

B) Basic circuit of an exponential function generator.

Fig. 5. A) Function generator to develop the power function:

$$\text{output} \propto (\text{input})^{b}.$$

B) Schematic of the system used in an identifier based on the range algorithm.

Fig. 6. Measured response of a function generator of the type shown in Figure 5A.

Fig. 7. The range of hydrogen and helium ions in silicon.

Fig. 8. Range-energy curves for various heavy ions in silicon (note that the energy scale is in MeV/amu.

Fig. 9. Energy lost by monoenergetic 40-MeV alpha particles passing through a 100-micron silicon crystal in two directions. (See Reference 44.)

Fig. 10. ^{3}He and ^{4}He identifier output distributions for detectors cut normal to the ⟨111⟩ axis and at 5° with respect to the previous cut. (See Reference 44.)

Fig. 11. Plot of MZ^2 for ions of $Z <= 10$ known to be stable against particle break-up. A fixed percentage error in determining MZ constitutes a fixed vertical error in this plot.

Fig. 12. Block diagram of the triple-detector identifier system.

Fig. 13. Diagram of the triple-detector identifier circuit showing waveforms.

Fig. 14. Heavy-ion particle identifier spectrum using $\Delta E,E$ multiplier algorithm. This experiment used a gas proportional ΔE detector (Reference 10).

Fig. 15. Early identifier spectrum using a silicon $\Delta E,E$ detector telescope and the range (power law) algorithm.

Fig. 16. Comparison between the particle identifier spectrum achieved using the simple $\Delta E,E$ telescope and a triple-detector telescope and identifier.

Fig. 17. Identifier spectrum obtained in an experiment to measure the mass of ^{8}He. The reaction studied was $^{26}Mg(\alpha,^{8}He)^{22}Mg$ at an alpha particle energy of 80 MeV.

Fig. 18. ^{8}He energy spectrum achieved in the experiment described in the caption to Figure 17.

Fig. 19. Plot of the velocity of ions as a function of E/M.

Fig. 20. Plot of the mass resolution as a function of E/M for various resolutions (Δt) in the time-of-flight measurement. d is the length of the flight path.

Fig. 21. Two dimensional picture of MZ^2 particle identifier output combined with mass determination by measurement of time-of-flight. A 10-cm flight path, 100-MeV ions and 250-ps timing accuracy are assumed.

Fig. 22. Diagram of a detector using electron emission from a carbon foil into a channel multiplier. A shows a fast timing detector using a Chevron plate. B shows a system using a position-sensitive detector to provide an image of the emission pattern from the foil.

Fig. 23. Input circuit of a silicon fast-timing detector.

Fig. 24. Block diagram of an identifier system using both MZ^2 and time-of-flight measurements.

Fig. 25. Identifier output spectrum for heavy ions covering a very broad energy range:

a) With the output calculated from $R = a E$ but with the value of b too high.

b) As (a) but with the value of b adjusted to 1.40.

c) Computer processed with an energy-dependent exponent. (See Equations 43-44.)

Fig. 26. Two-dimensional contour plot of particle identifier output (MZ^2) versus mass (derived from time-of-flight measurement).

Fig. 27. This figure indicates practical limits of identification using silicon detector telescopes for both MZ^2 and time-of-flight mass determination.

Fig. 28. Position sensitive proportional counter with charge division readout.

Fig. 29. Position sensitive proportional counter with rise-time readout.

Fig. 30. (a) Chamber with helical cathode wound around anode ground plane.

(b) Chamber with helical cathode wound around ground plane separate from the anode plane. Particles enter chamber without passing through the helix.

Fig. 31. Drift counter (see Reference 137).

Fig. 32. Position resolution as a function of detector thickness, (a) for 1 atm. of argon, (b) for 3 atm. of argon (see Reference 111).

Fig. 33. Plot of time of flight vs. position on detector. Time of flight has been corrected for differences in flight path.

Fig. 34. Plot of time of flight vs. ΔE showing separated particle groups.

Fig. 35. Total position spectrum with gated particle spectra below.

Fig. 36. Schematic diagram of thin scintillator foil holder and light guide.

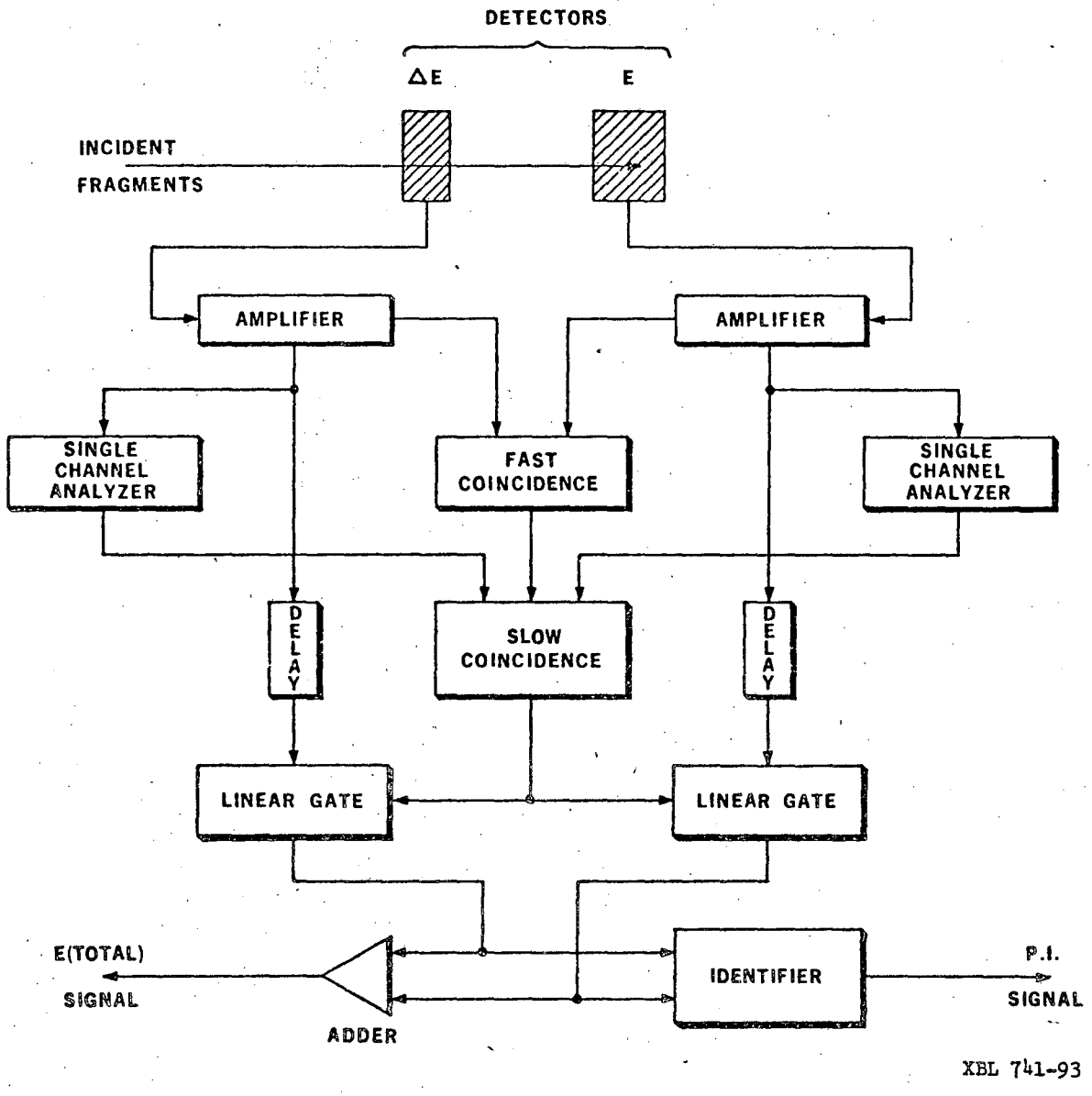
DETECTORS
ΔE
E
INCIDENT
FRAGMENTS
AMPLIFIER
AMPLIFIER
SINGLE CHANNEL ANALYZER
FAST COINCIDENCE
SINGLE CHANNEL ANALYZER
DELAY
SLOW COINCIDENCE
DELAY
LINEAR GATE
LINEAR GATE
E(TOTAL)
SIGNAL
ADDER
IDENTIFIER
P.I.
SIGNAL
XBL 741-93

Fig. 1

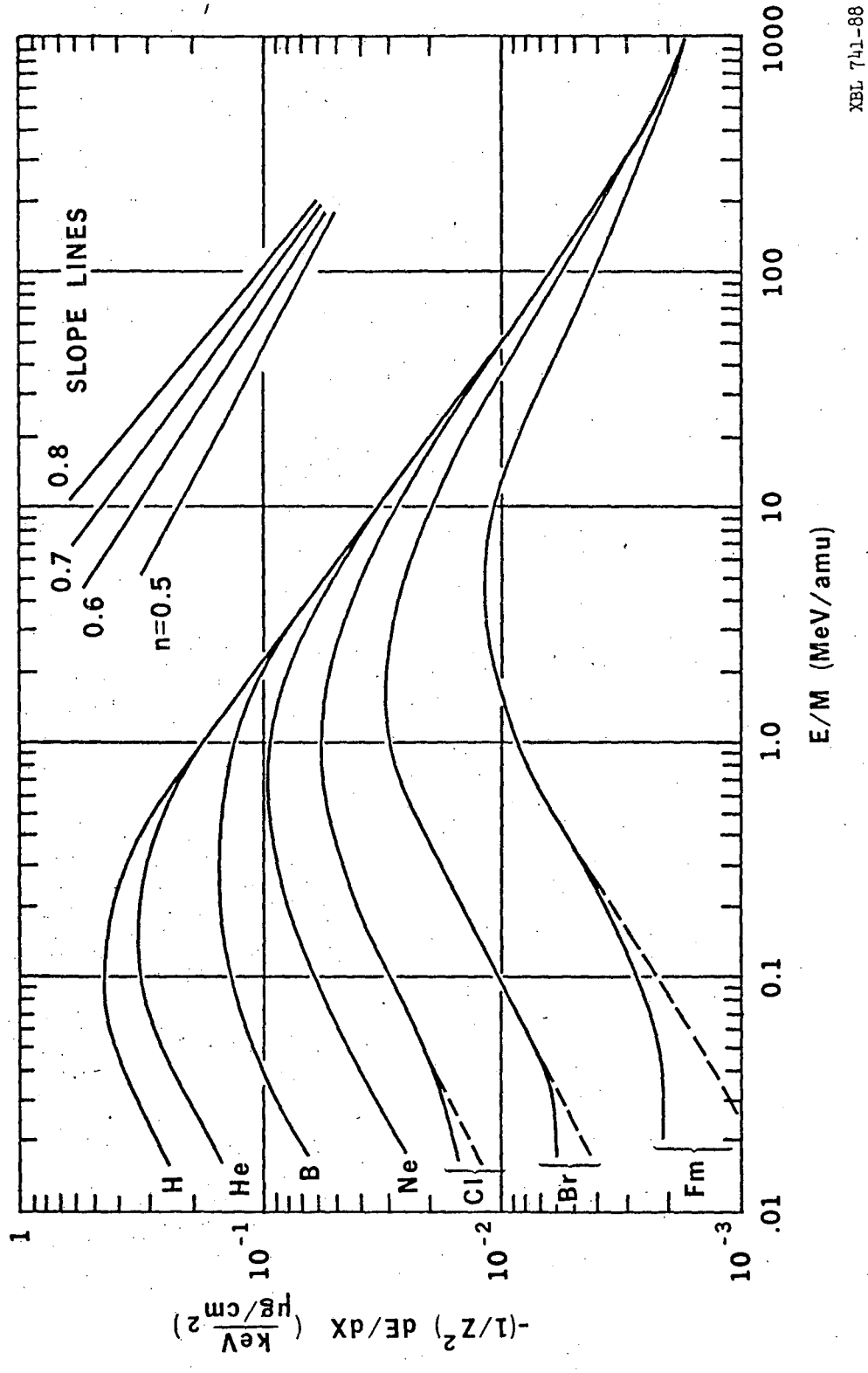
SLOPE LINES
0.8
0.7
0.6
n=0.5
H
He
B
Ne
Cl
Br
Fm
1
10^{-1}
10^{-2}
10^{-3}
.01
0.1
1.0
10
100
1000
E/M (MeV/amu)
$-(1/Z^2)\ dE/dx\ \left(\frac{keV}{\mu g/cm^2}\right)$
XBL 741-88

Fig. 2

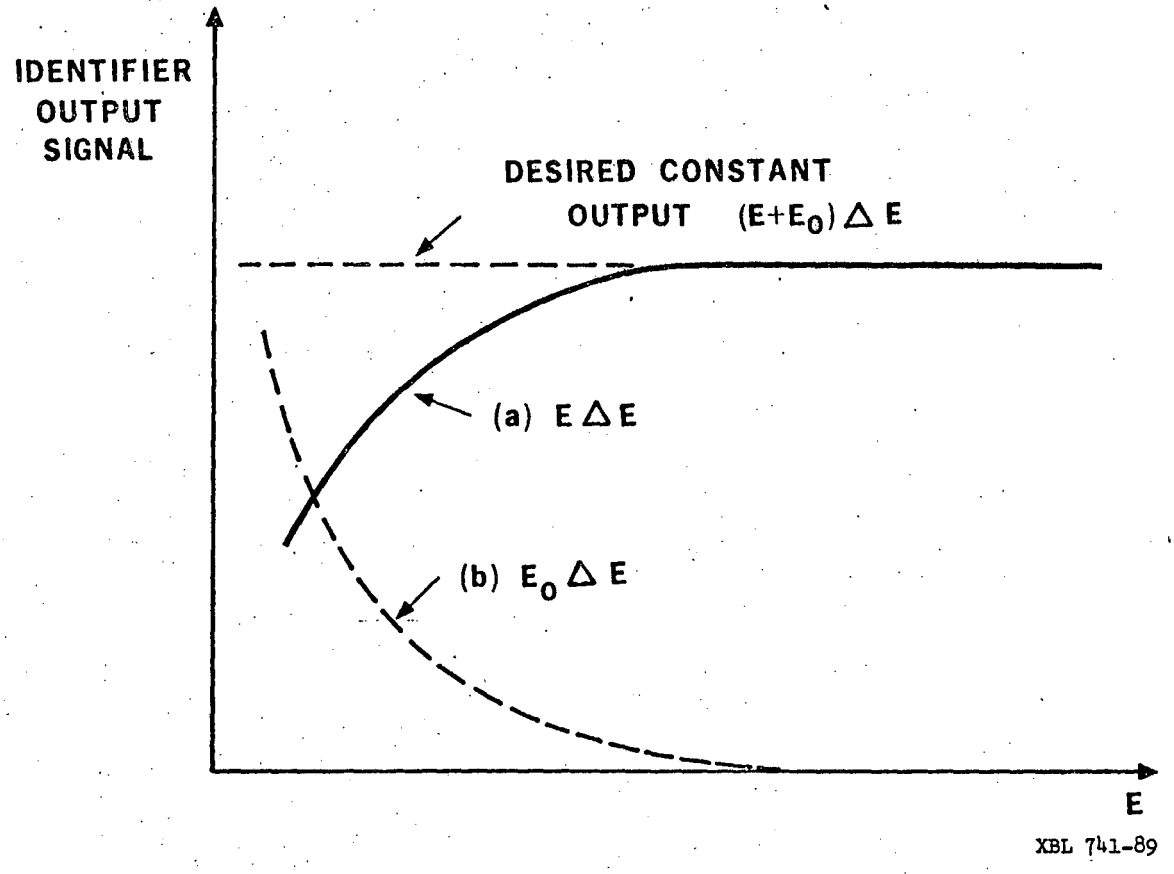
IDENTIFIER
OUTPUT
SIGNAL
DESIRED CONSTANT
OUTPUT (E+E0) Δ E
(a) E Δ E
(b) E0 Δ E
E
XBL 741-89

Fig. 3

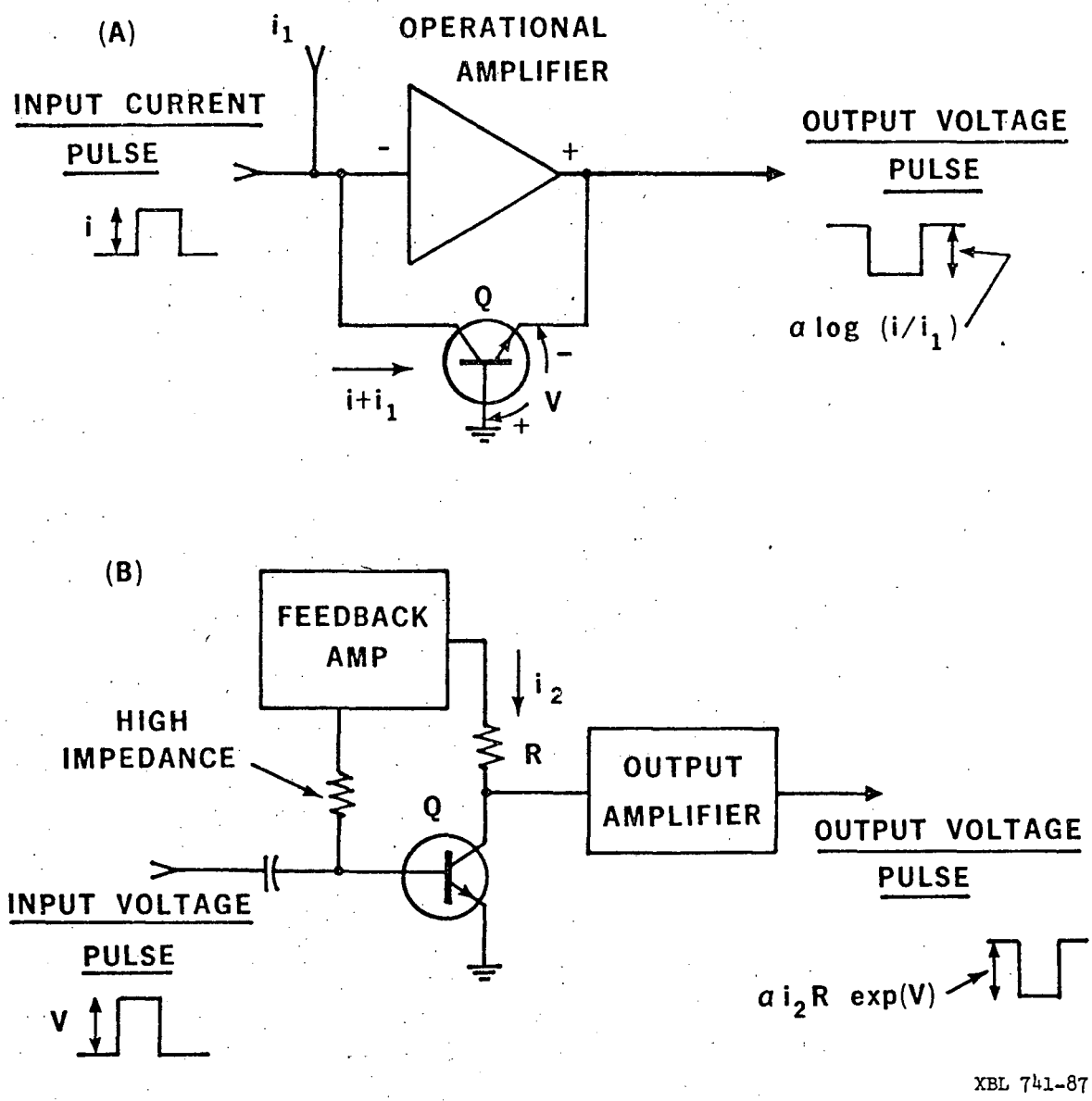
(A)
i_1
OPERATIONAL AMPLIFIER
INPUT CURRENT PULSE
i
OUTPUT VOLTAGE PULSE
Q
$i+i_1$
V
$a \log (i/i_1)$
(B)
FEEDBACK AMP
i_2
HIGH IMPEDANCE
R
OUTPUT AMPLIFIER
Q
INPUT VOLTAGE PULSE
V
OUTPUT VOLTAGE PULSE
$a\, i_2 R \exp(V)$
XBL 741-87

Fig. 4

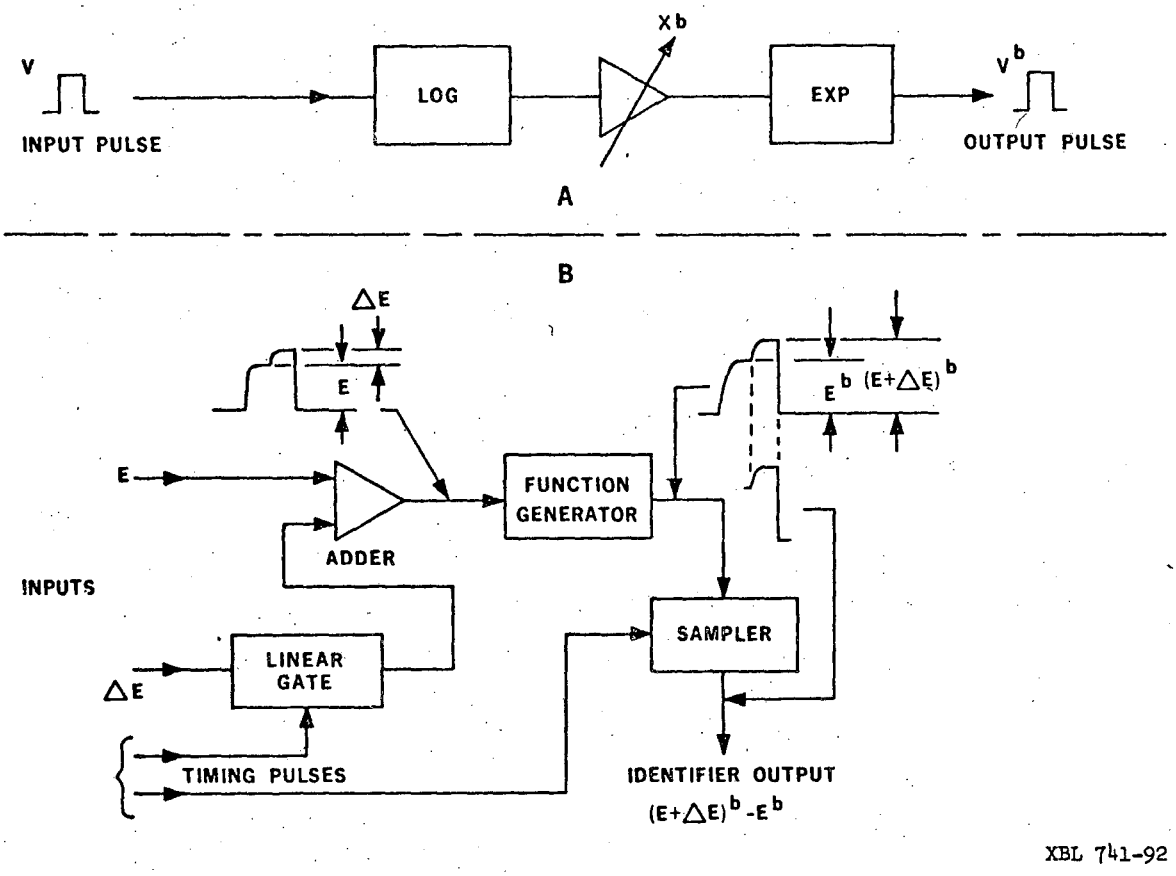
V
INPUT PULSE
LOG
Xb
EXP
V b
OUTPUT PULSE
A
B
ΔE
E
E b (E+ΔE) b
E
ADDER
FUNCTION GENERATOR
INPUTS
SAMPLER
LINEAR GATE
ΔE
TIMING PULSES
IDENTIFIER OUTPUT
(E+ΔE) b -E b
XBL 741-92

Fig. 5

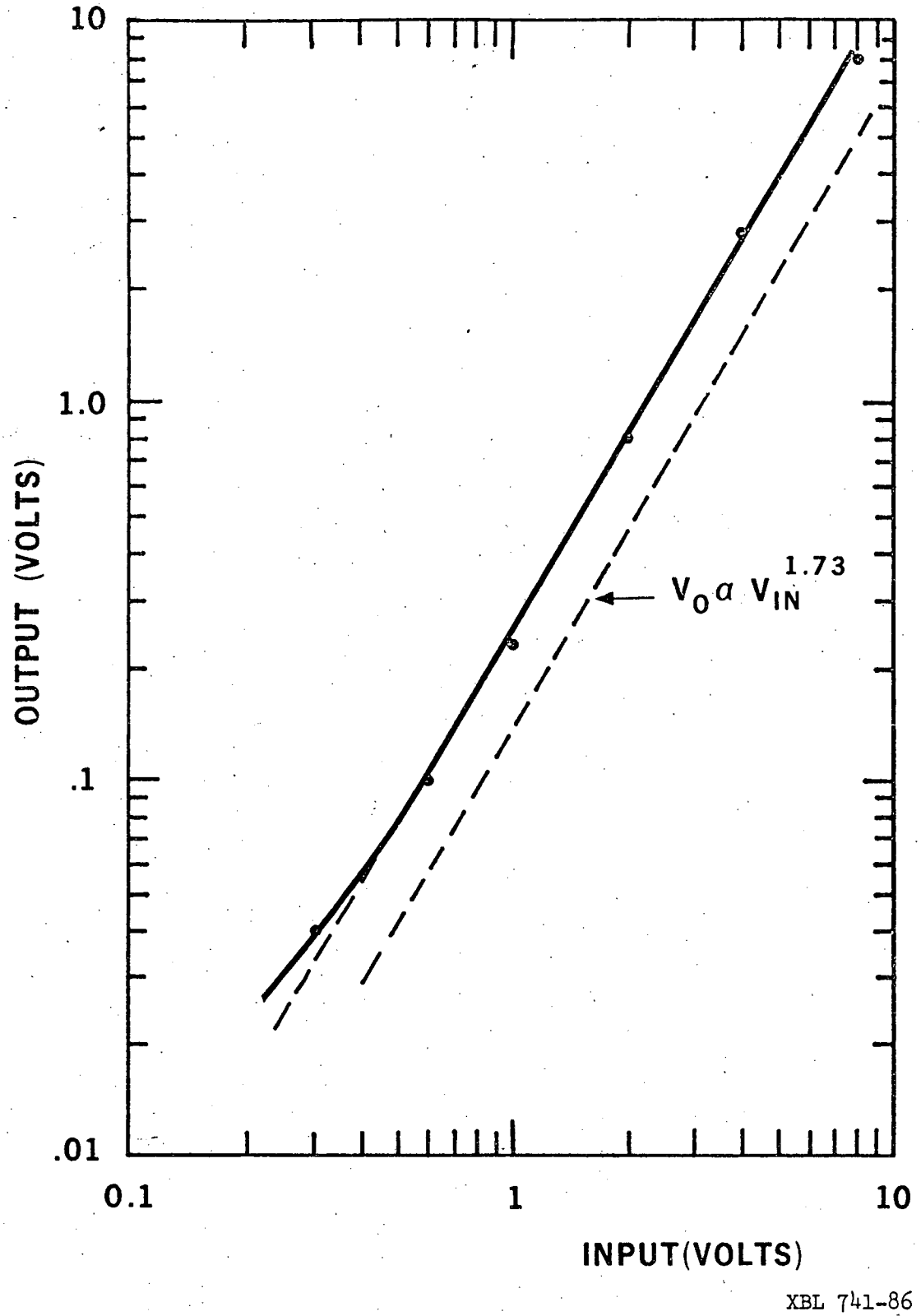
10
1.0
.1
.01
0.1
1
10
OUTPUT (VOLTS)
INPUT(VOLTS)
$V_O \alpha V_{IN}^{1.73}$
XBL 741-86

Fig. 6

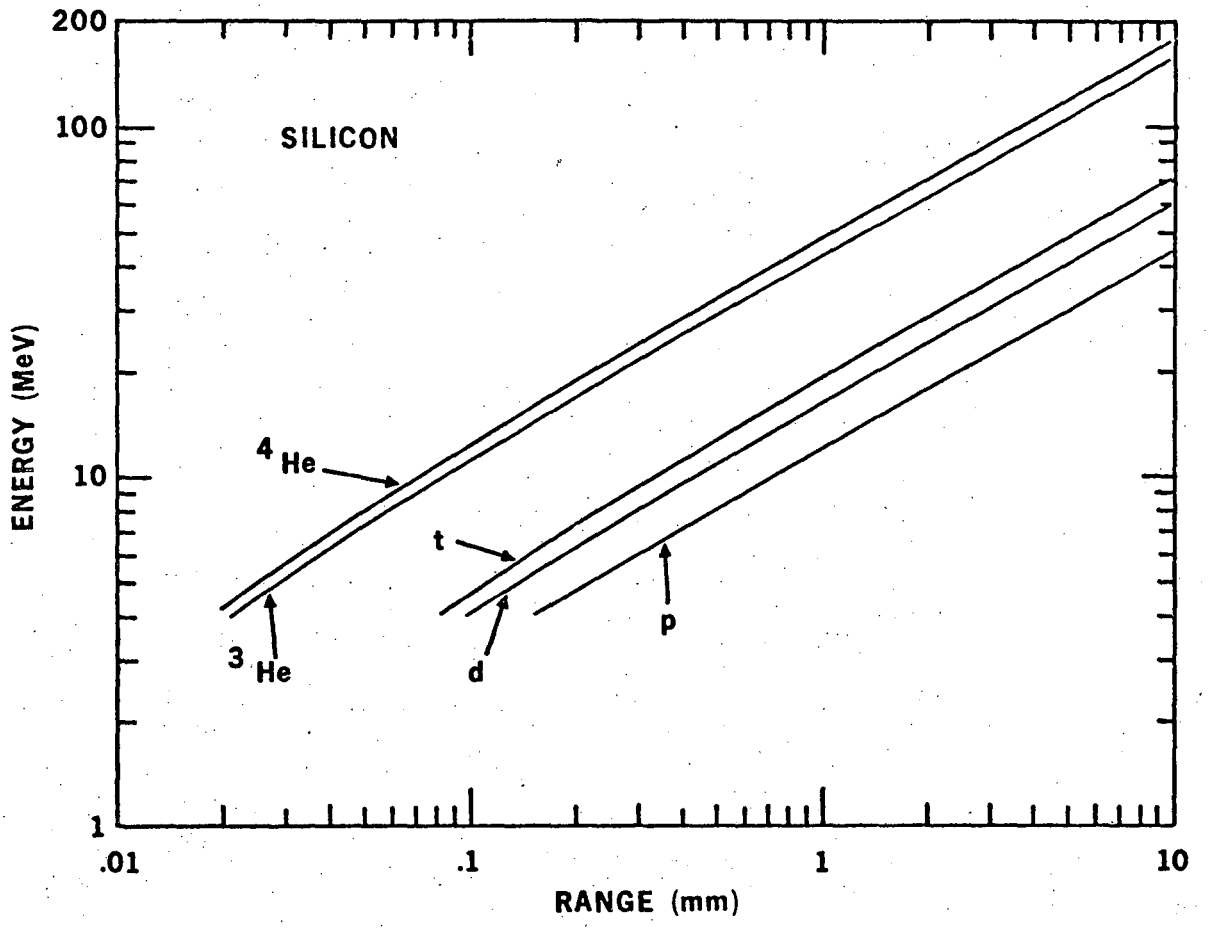

XBL 728-1391

Fig. 7

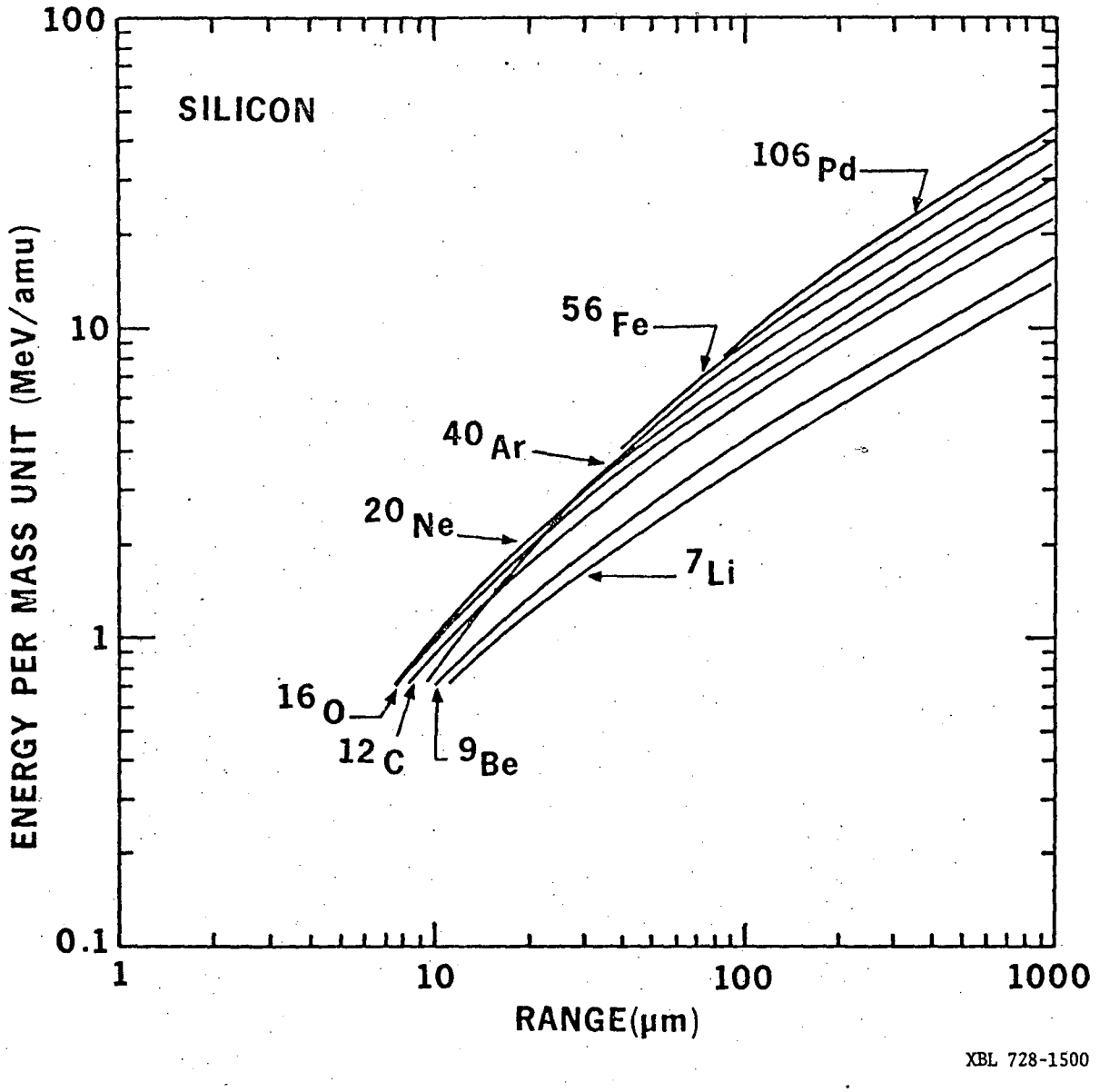
SILICON
106 Pd
56 Fe
40 Ar
20 Ne
7 Li
16 O
12 C
9 Be
ENERGY PER MASS UNIT (MeV/amu)
RANGE(μm)
100
10
1
0.1
1
10
100
1000
XBL 728-1500

Fig. 8

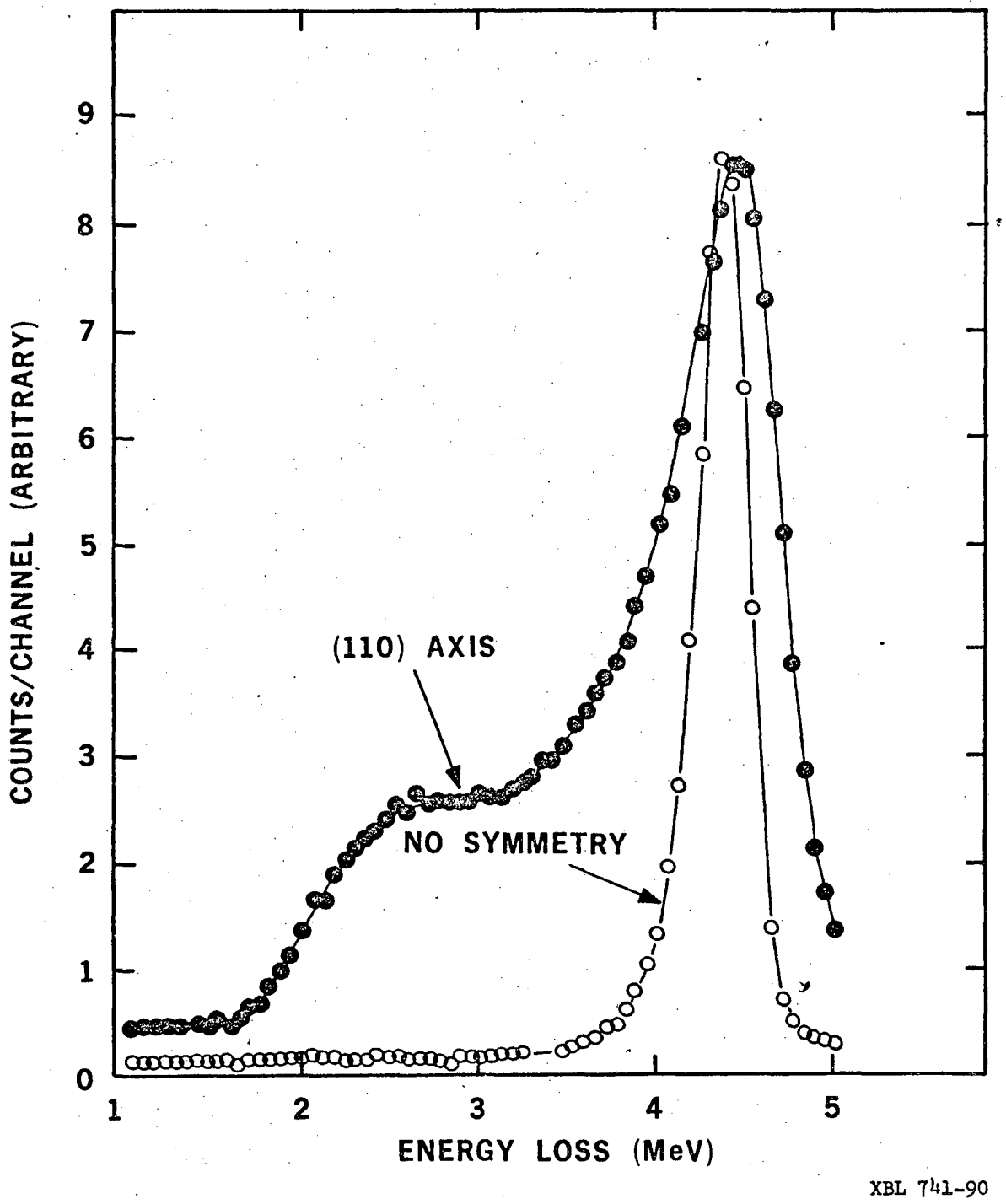
COUNTS/CHANNEL (ARBITRARY)
0
1
2
3
4
5
6
7
8
9
1
2
3
4
5
ENERGY LOSS (MeV)
(110) AXIS
NO SYMMETRY
XBL 741-90

Fig. 9

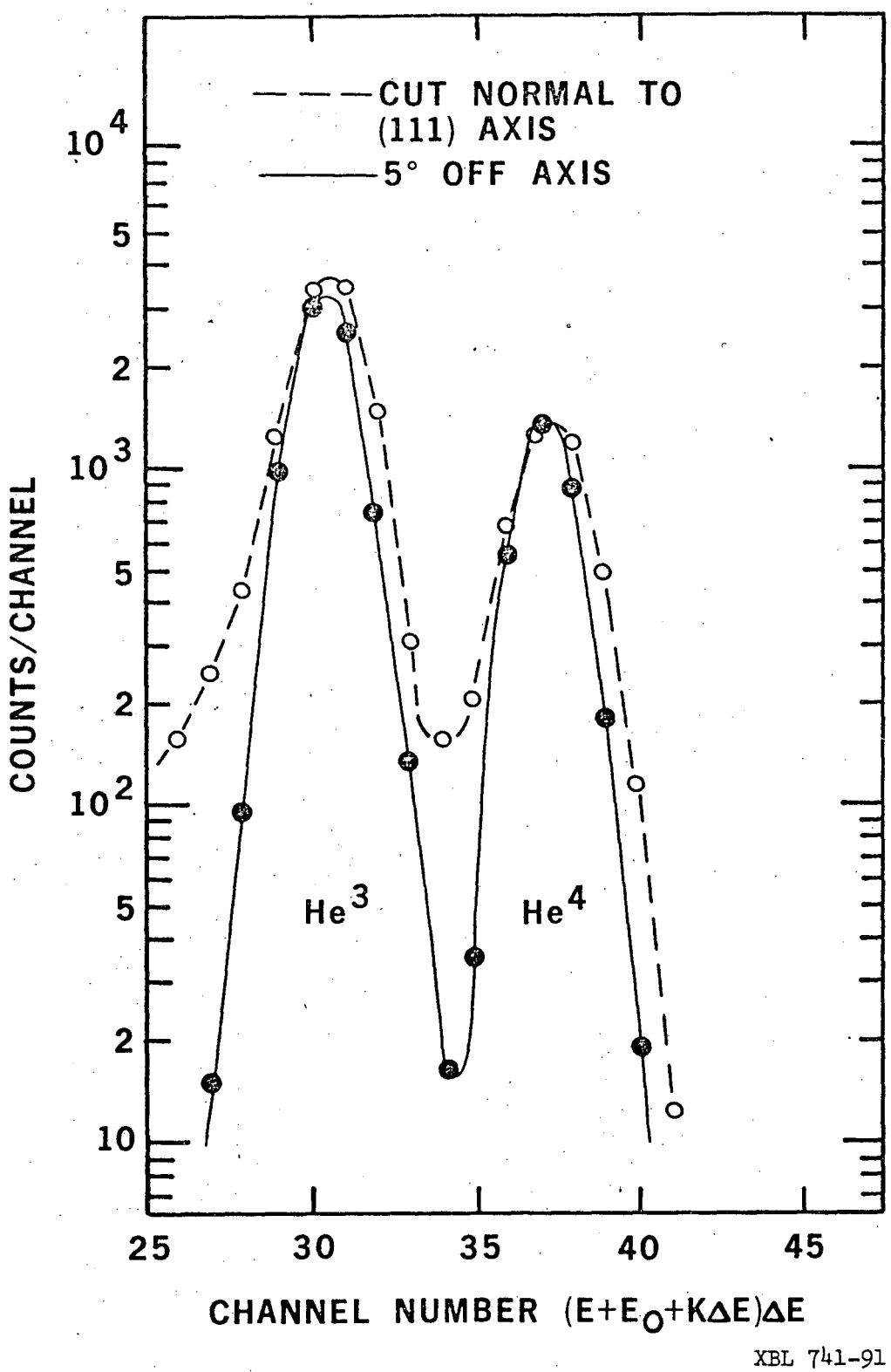
CUT NORMAL TO
(111) AXIS
5° OFF AXIS
COUNTS/CHANNEL
10^4
5
2
10^3
5
2
10^2
5
2
10
He^3
He^4
25
30
35
40
45
CHANNEL NUMBER (E+E_O+KΔE)ΔE
XBL 741-91

Fig. 10

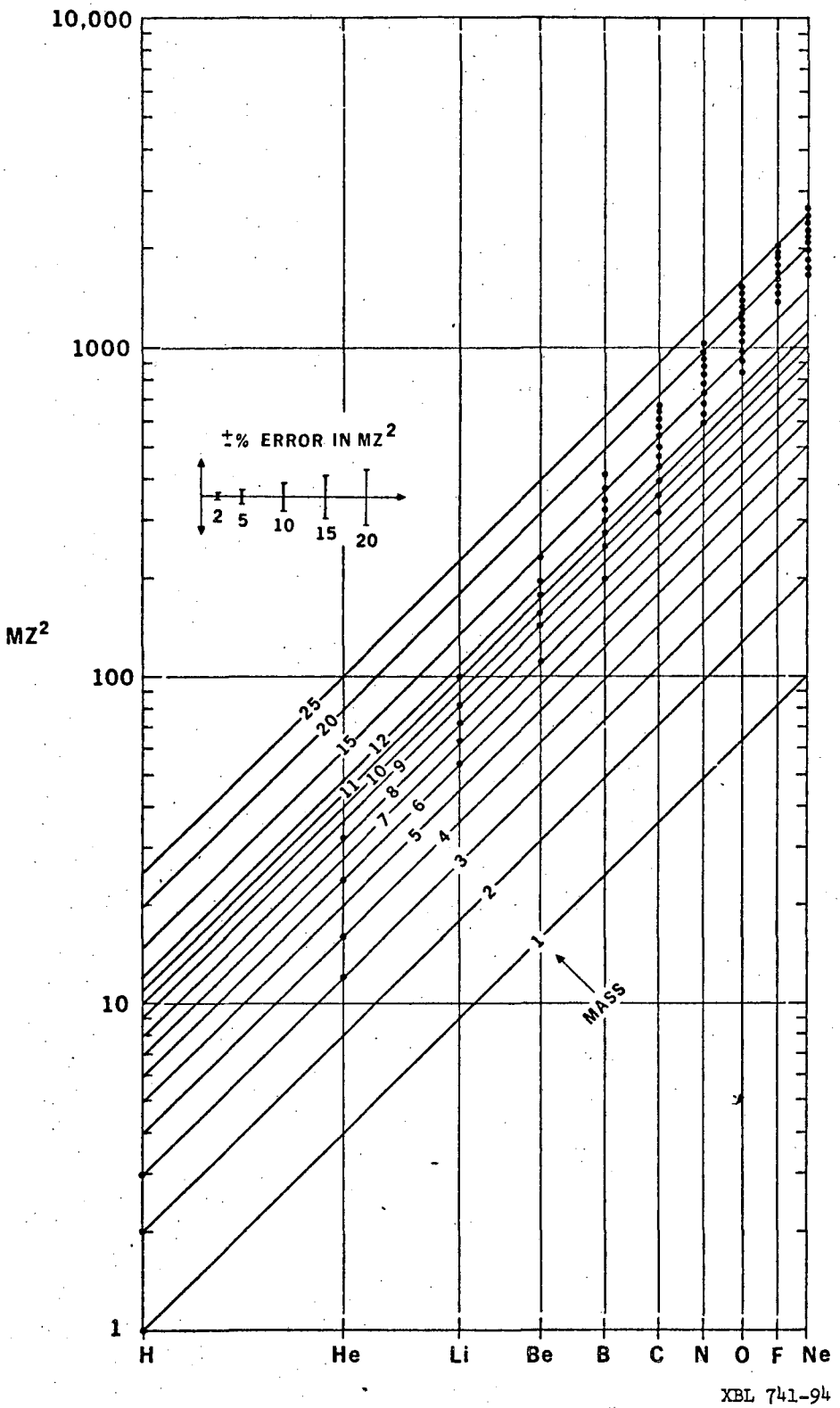
10,000
1000
100
10
1
MZ²
±% ERROR IN MZ²
2
5
10
15
20
25
20
15
12
11
10
9
8
7
6
5
4
3
2
1
MASS
H
He
Li
Be
B
C
N
O
F
Ne
XBL 741-94

Fig. 11

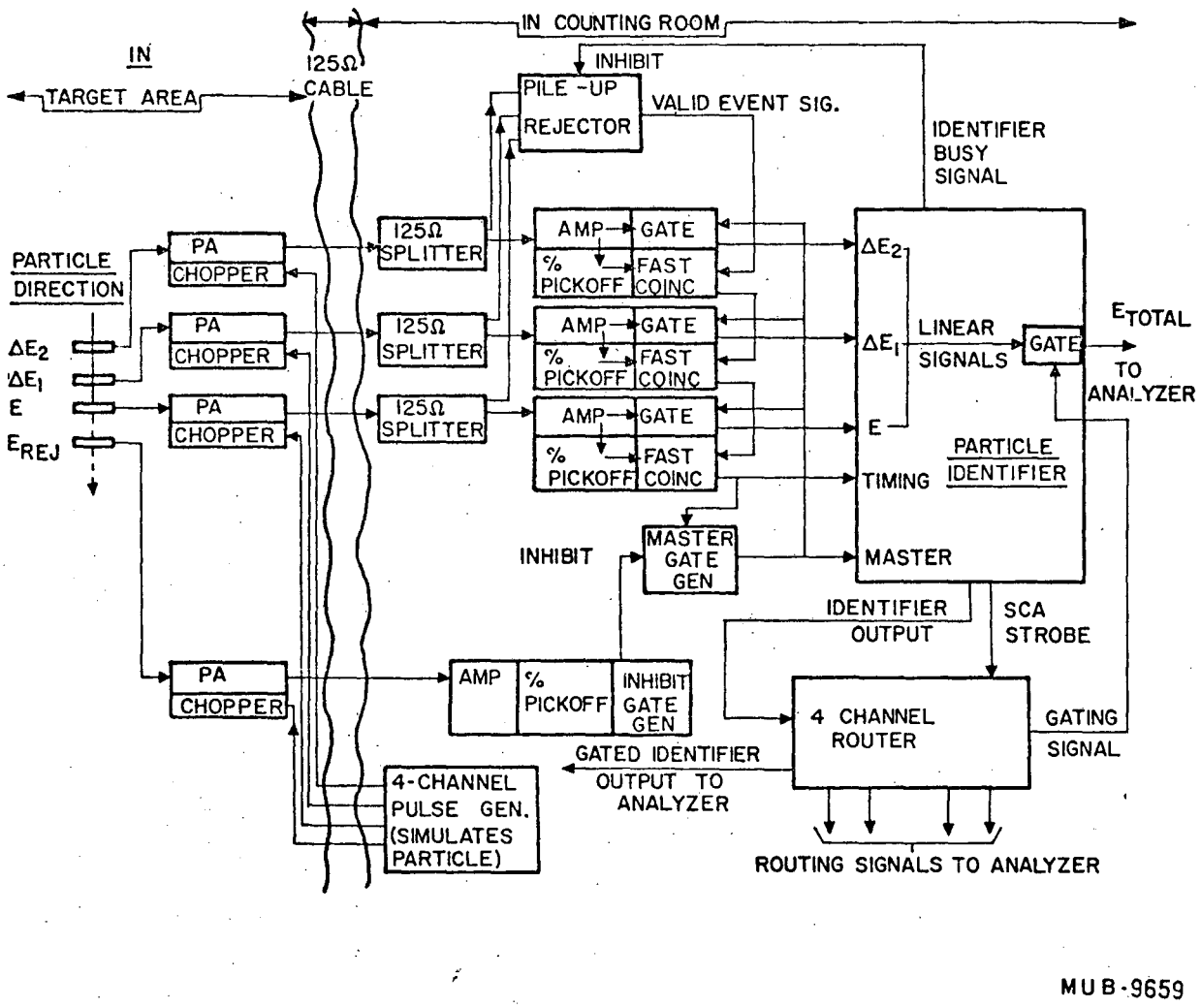
IN COUNTING ROOM
IN
TARGET AREA
125Ω CABLE
INHIBIT
PILE -UP REJECTOR
VALID EVENT SIG.
IDENTIFIER BUSY SIGNAL
PARTICLE DIRECTION
ΔE2
ΔE1
E
EREJ
PA CHOPPER
125Ω SPLITTER
AMP
GATE
% PICKOFF
FAST COINC
ΔE2
ΔE1
E
TIMING
LINEAR SIGNALS
GATE
ETOTAL
TO ANALYZER
PARTICLE IDENTIFIER
MASTER GATE GEN
INHIBIT
MASTER
IDENTIFIER OUTPUT
SCA STROBE
AMP
% PICKOFF
INHIBIT GATE GEN
4 CHANNEL ROUTER
GATING SIGNAL
GATED IDENTIFIER OUTPUT TO ANALYZER
4-CHANNEL PULSE GEN. (SIMULATES PARTICLE)
ROUTING SIGNALS TO ANALYZER
MUB-9659

Fig. 12

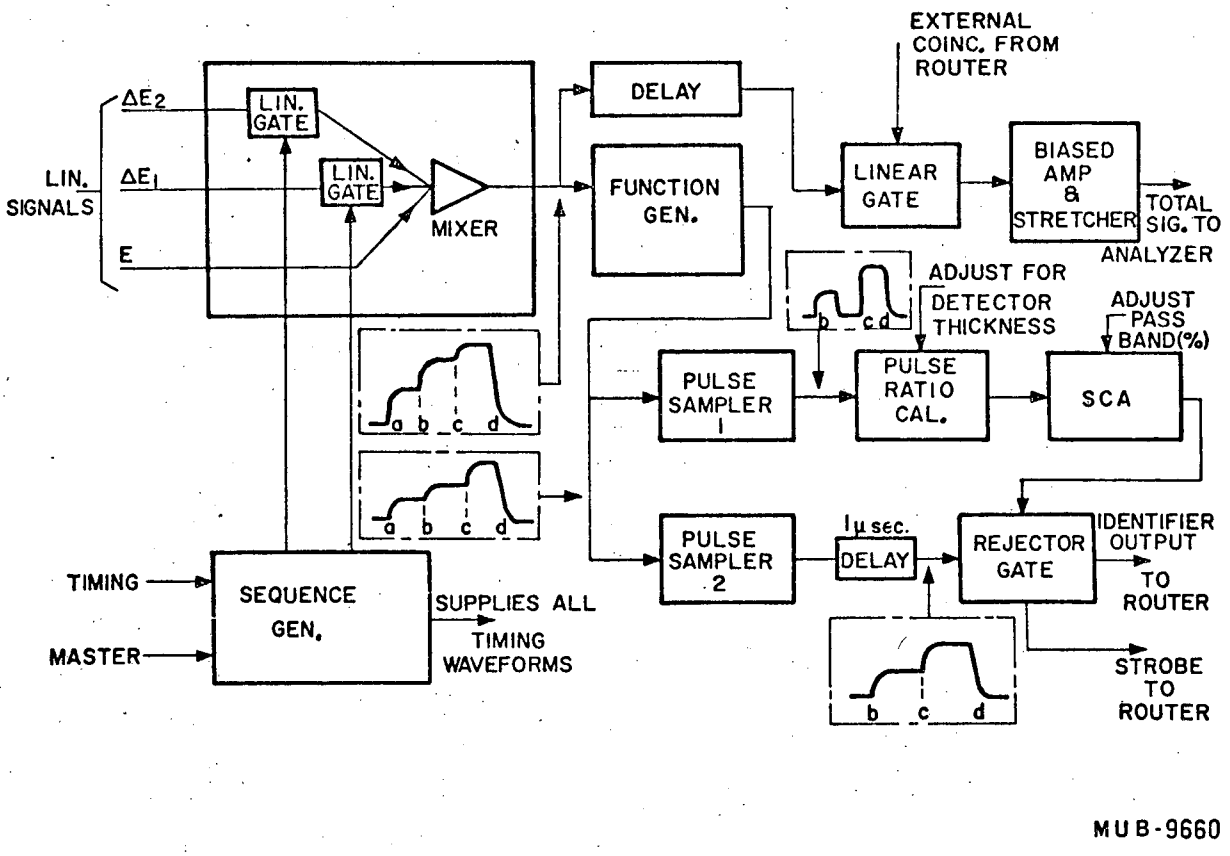
EXTERNAL
COINC. FROM
ROUTER
ΔE2
LIN.
GATE
LIN.
SIGNALS
ΔE1
LIN.
GATE
E
MIXER
DELAY
FUNCTION
GEN.
LINEAR
GATE
BIASED
AMP
&
STRETCHER
TOTAL
SIG. TO
ANALYZER
ADJUST FOR
DETECTOR
THICKNESS
ADJUST
PASS
BAND(%)
a b c d
b c d
PULSE
SAMPLER
1
PULSE
RATIO
CAL.
SCA
a b c d
PULSE
SAMPLER
2
1μ sec.
DELAY
REJECTOR
GATE
IDENTIFIER
OUTPUT
TO
ROUTER
TIMING
MASTER
SEQUENCE
GEN.
SUPPLIES ALL
TIMING
WAVEFORMS
b c d
STROBE
TO
ROUTER
MUB-9660

Fig. 13

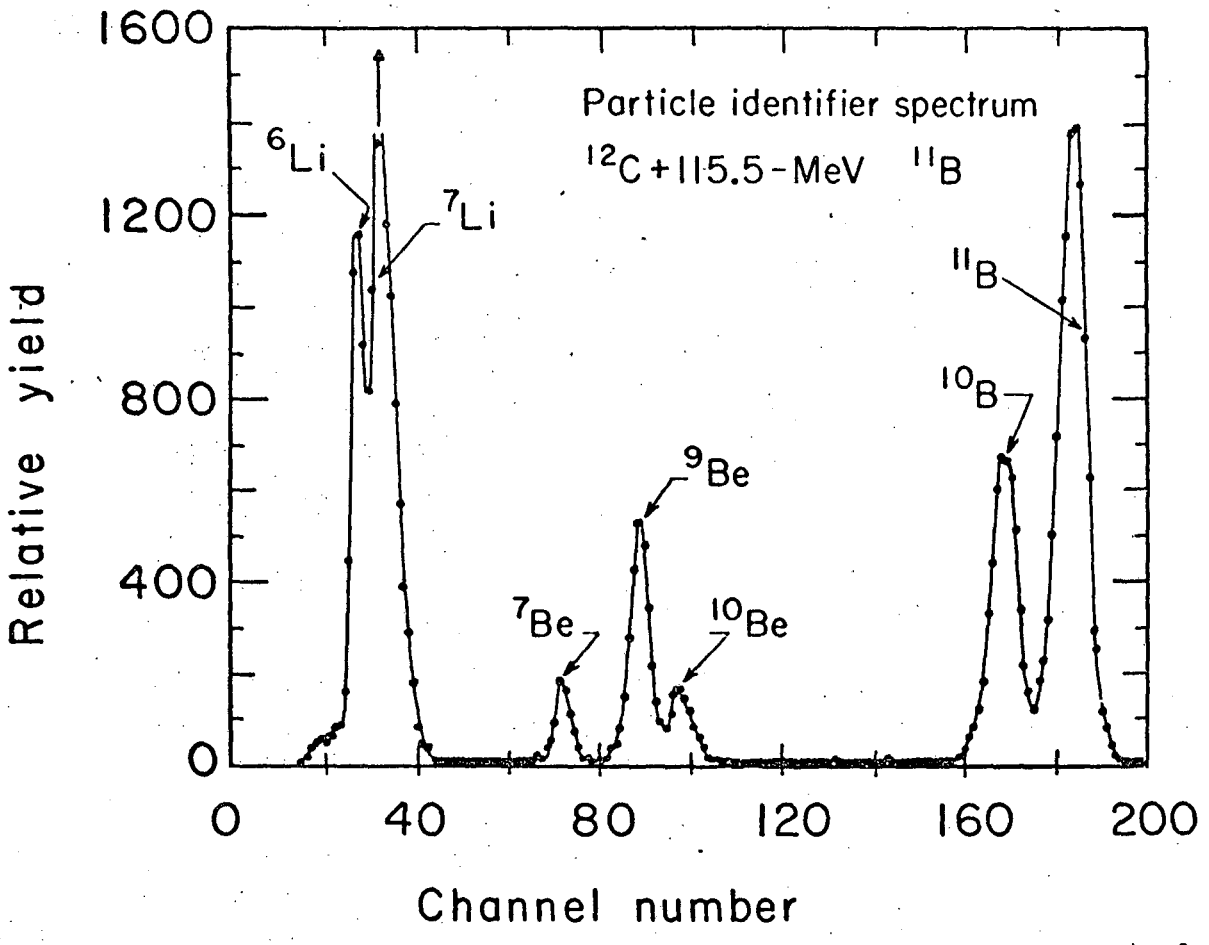

XBL 741-183

Fig. 14

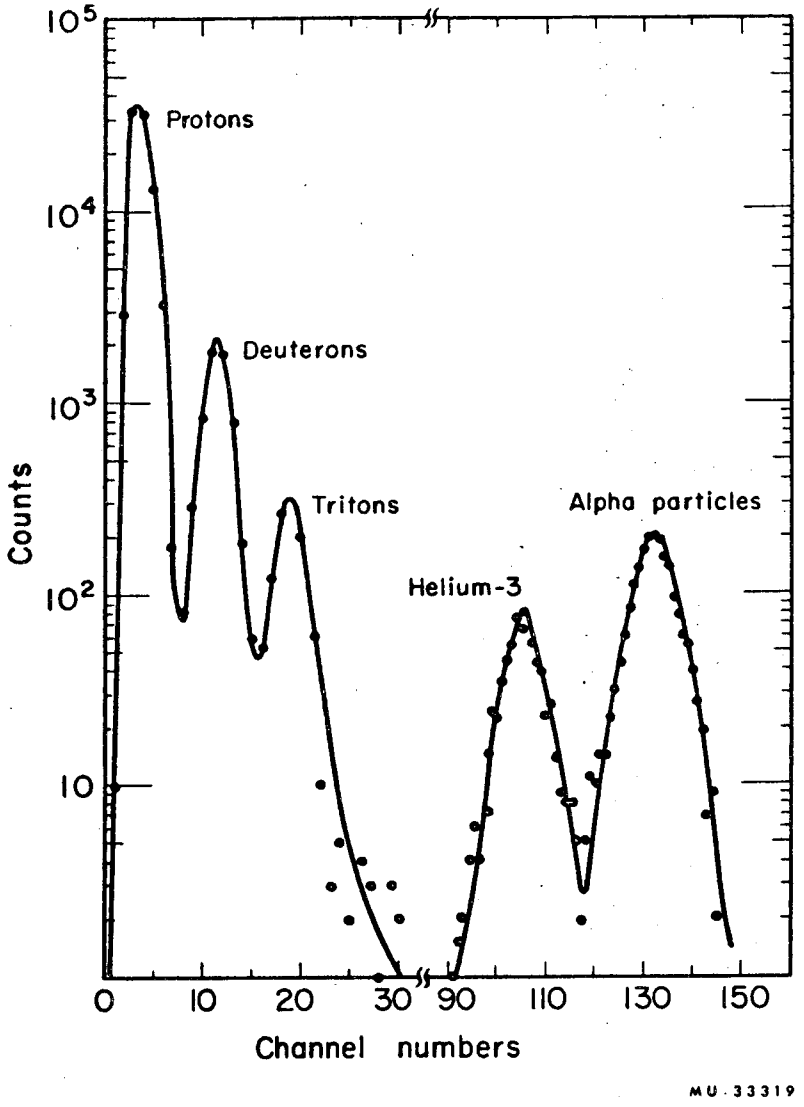
Protons
Deuterons
Tritons
Helium-3
Alpha particles
Counts
Channel numbers
MU-33319

Fig. 15

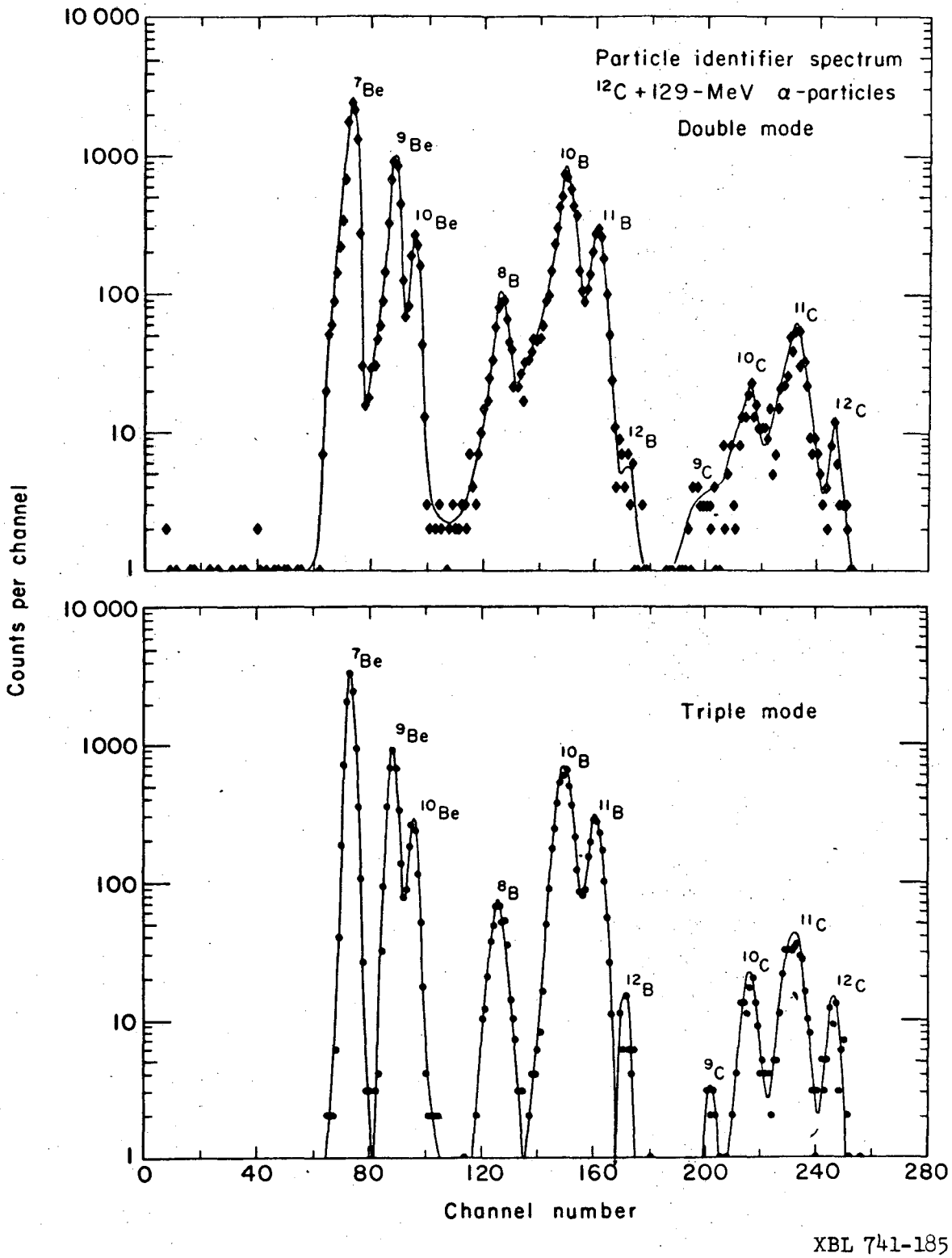
Particle identifier spectrum
^{12}C + 129-MeV α-particles
Double mode
Triple mode
Counts per channel
Channel number
^{7}Be
^{9}Be
^{10}Be
^{8}B
^{10}B
^{11}B
^{12}B
^{9}C
^{10}C
^{11}C
^{12}C
10 000
1000
100
10
1
0
40
80
120
160
200
240
280
XBL 741-185

Fig. 16

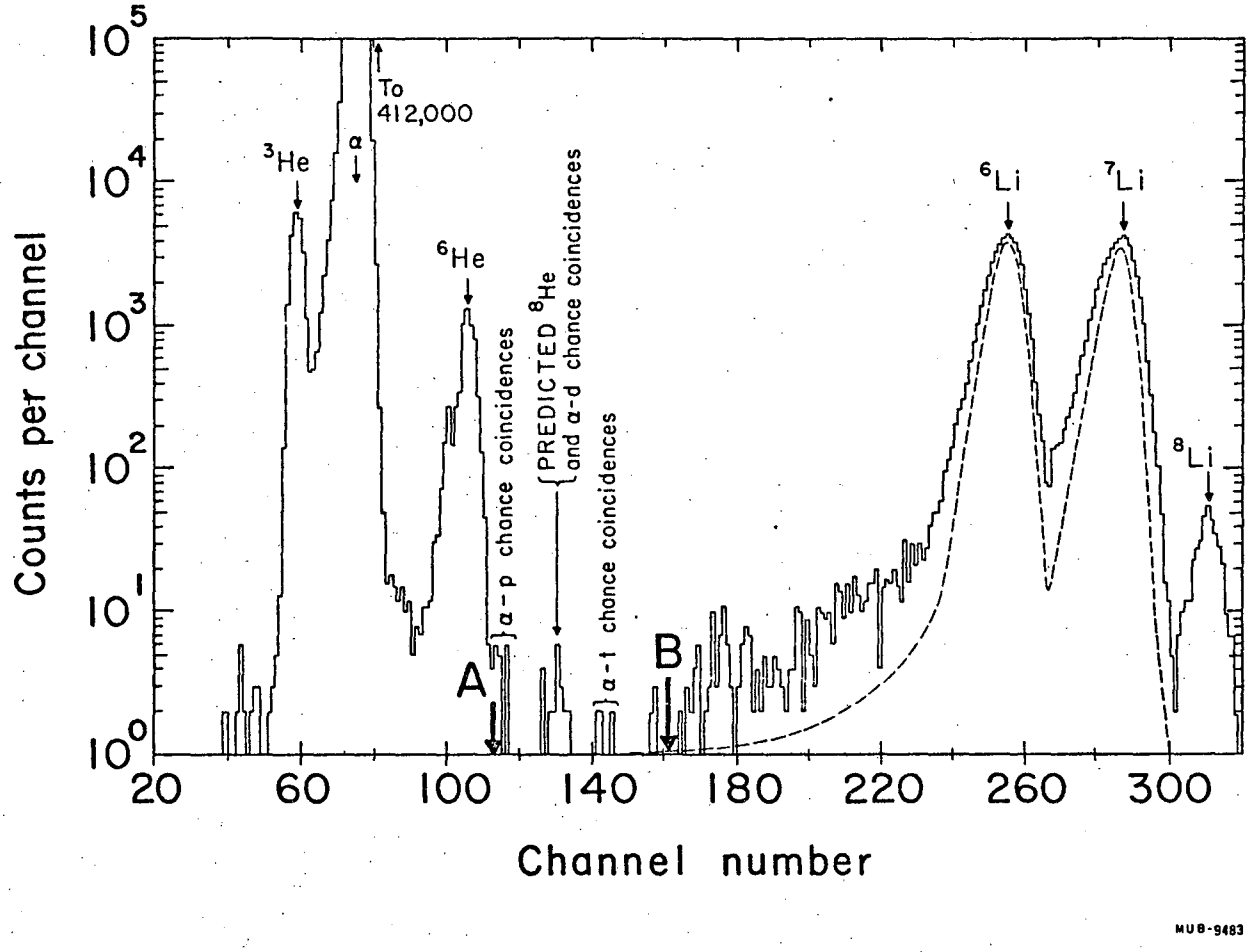
Counts per channel
Channel number
10^5
10^4
10^3
10^2
10^1
10^0
20
60
100
140
180
220
260
300
To 412,000
α
^{3}He
^{6}He
α-p chance coincidences
PREDICTED ^{8}He and α-d chance coincidences
α-t chance coincidences
A
B
^{6}Li
^{7}Li
^{8}Li
MUB-9483

Fig. 17

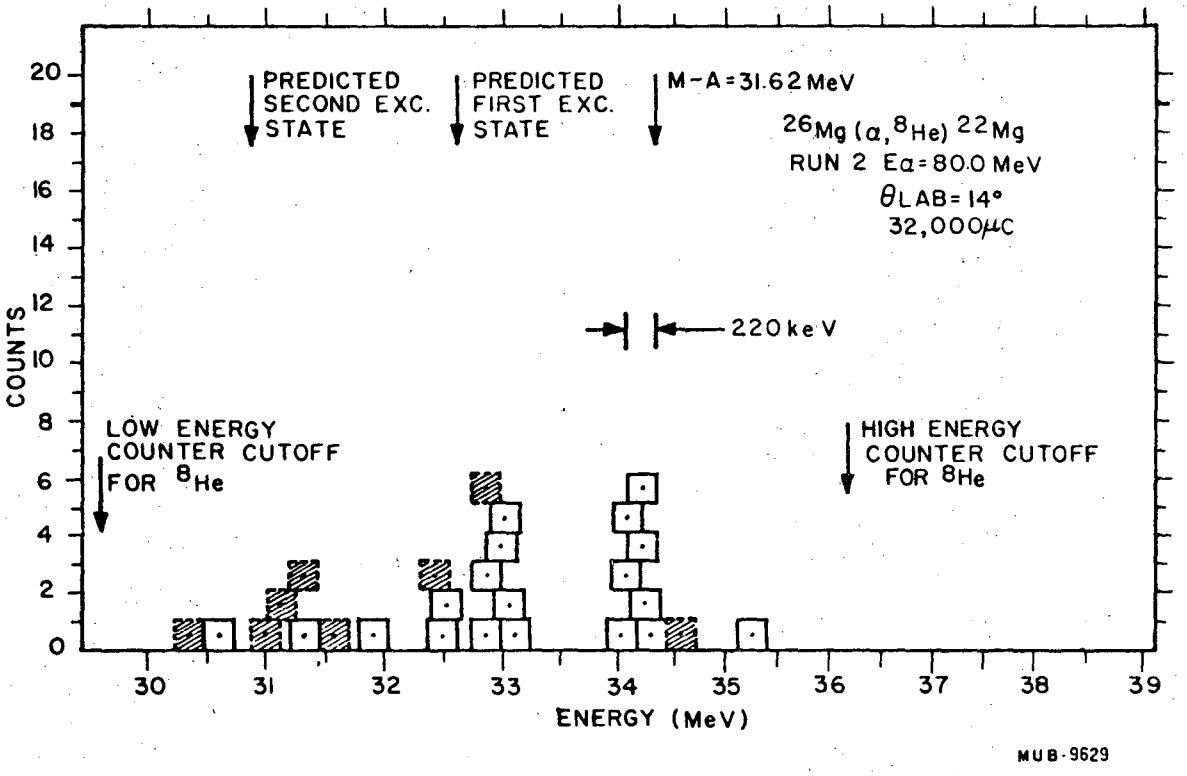
PREDICTED SECOND EXC. STATE
PREDICTED FIRST EXC. STATE
M-A=31.62 MeV
26Mg (α, 8He) 22Mg
RUN 2 Eα=80.0 MeV
θLAB=14°
32,000μC
220 keV
LOW ENERGY COUNTER CUTOFF FOR 8He
HIGH ENERGY COUNTER CUTOFF FOR 8He
COUNTS
ENERGY (MeV)
MUB-9629

Fig. 18

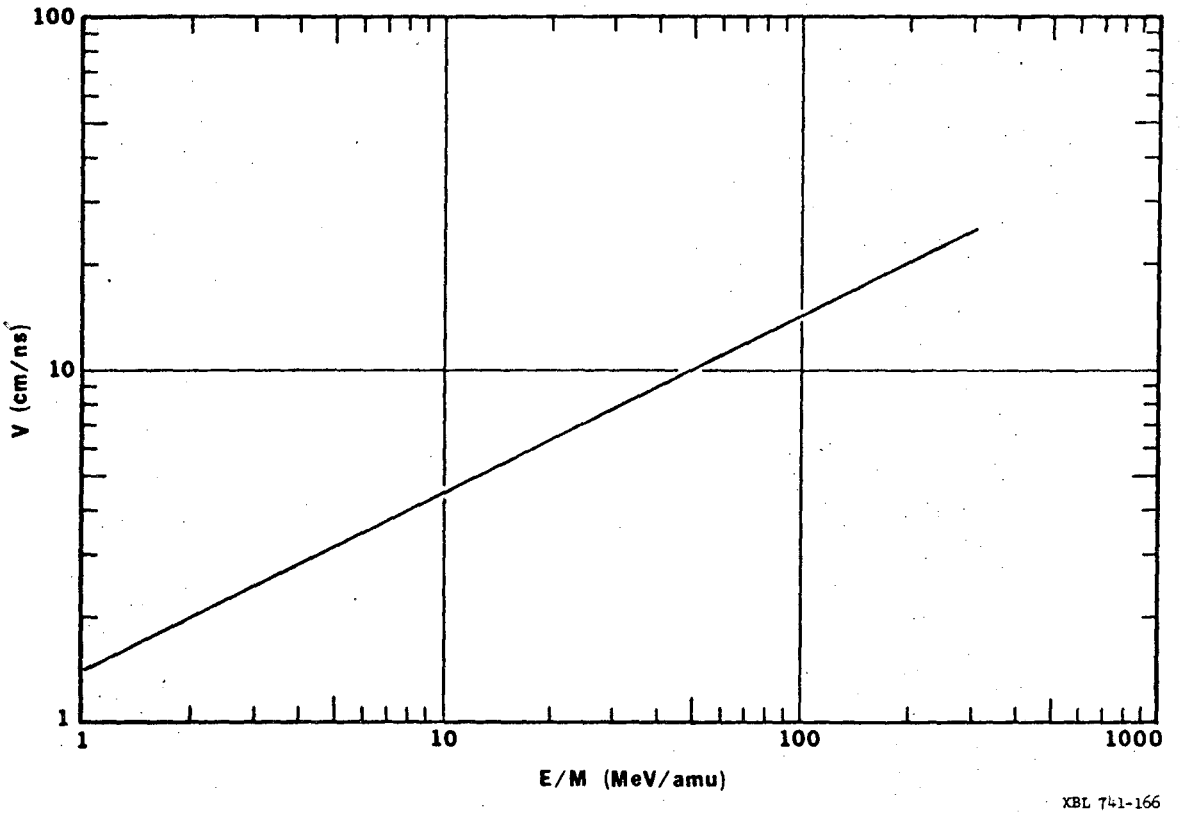

Fig. 19

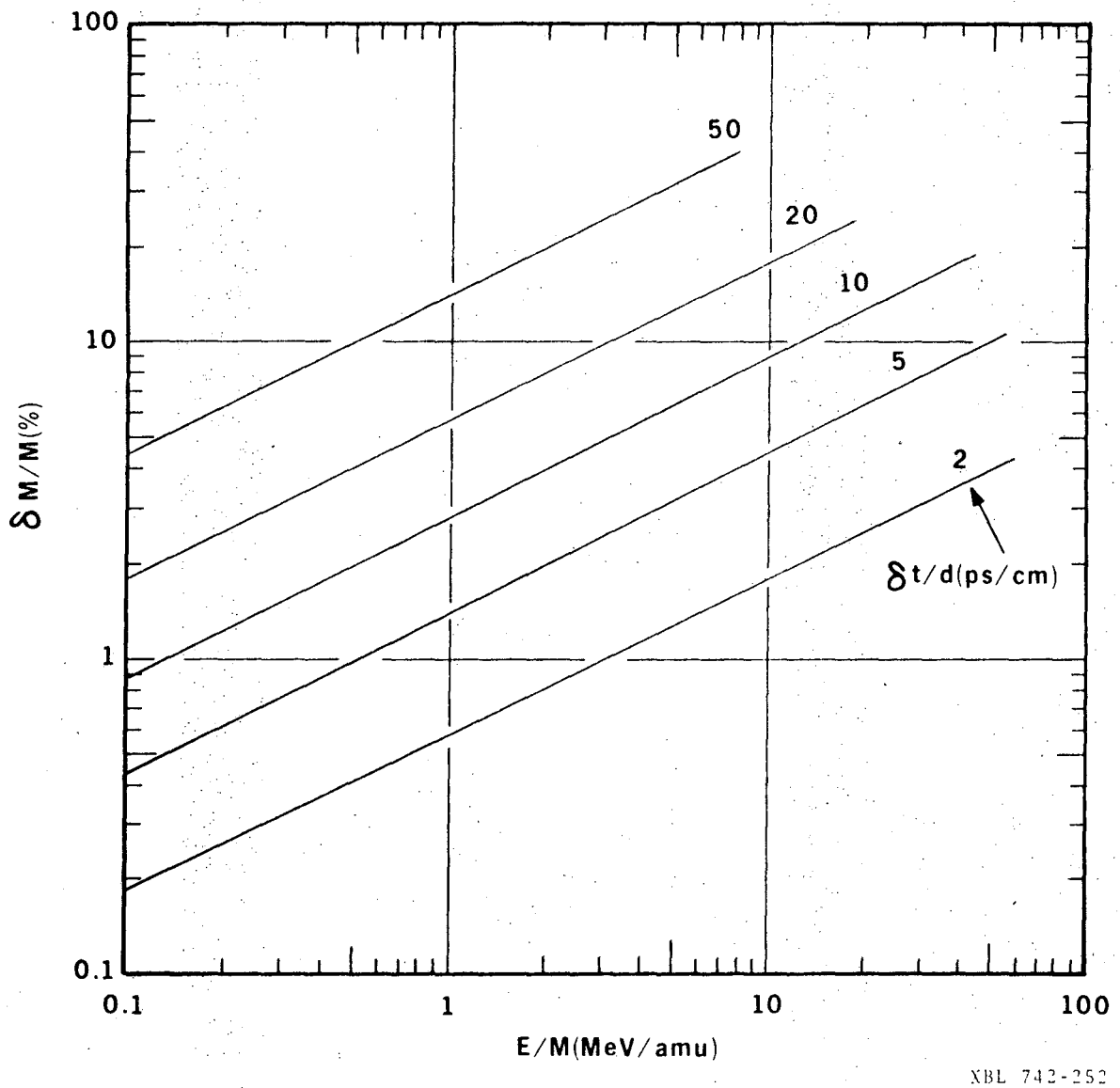
100
10
1
0.1
0.1
1
10
100
δ M/M(%)
E/M(MeV/amu)
50
20
10
5
2
δt/d(ps/cm)
XBL 742-252

Fig. 20

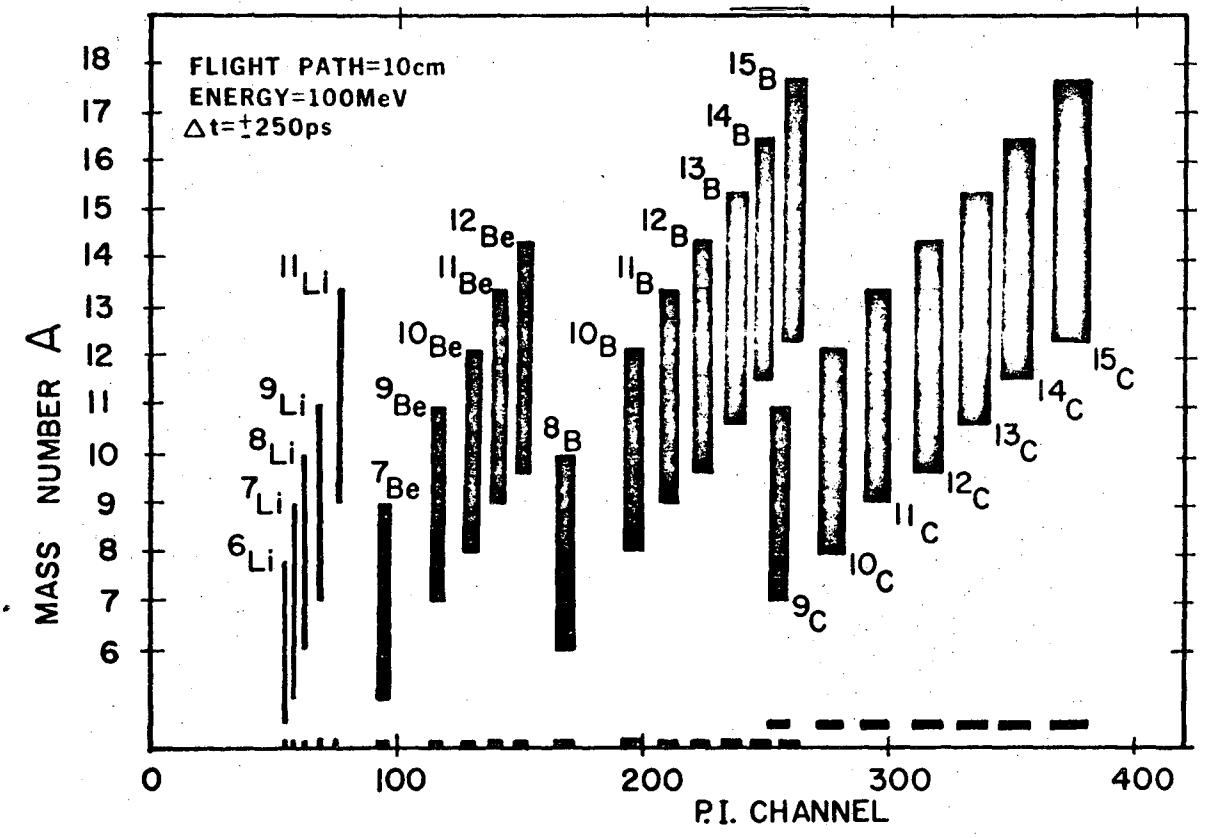

XBL 675-1459A

Fig. 21

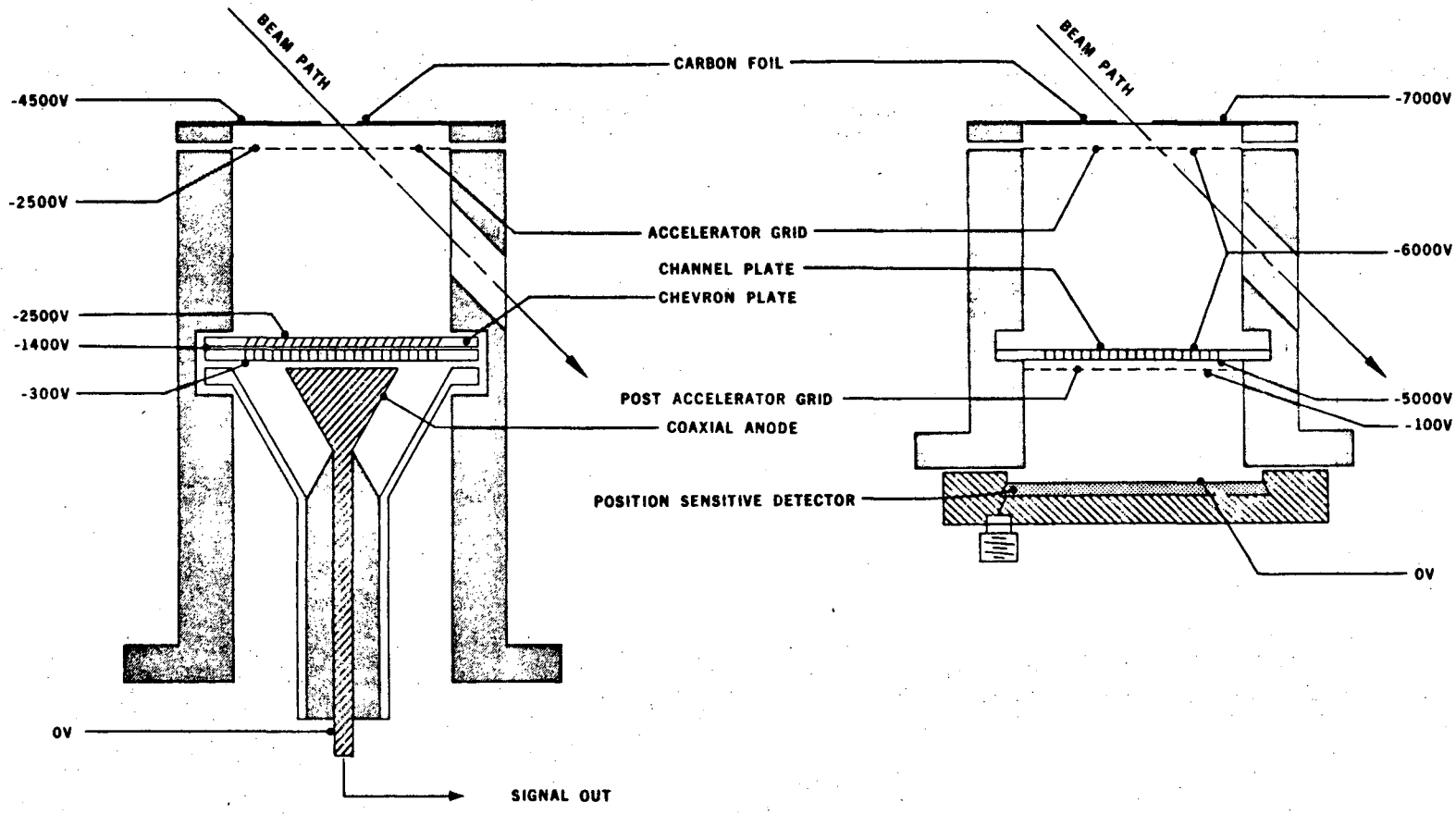

XBL 741-184

Fig. 22

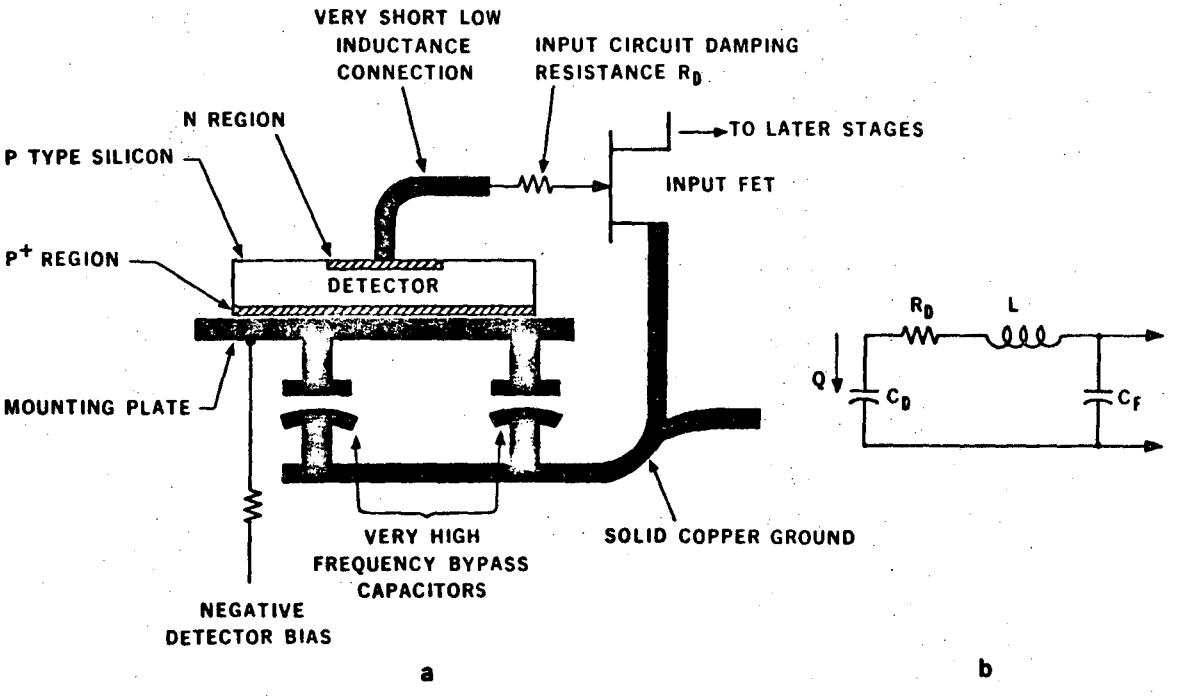

XBL 723-596

Fig. 23

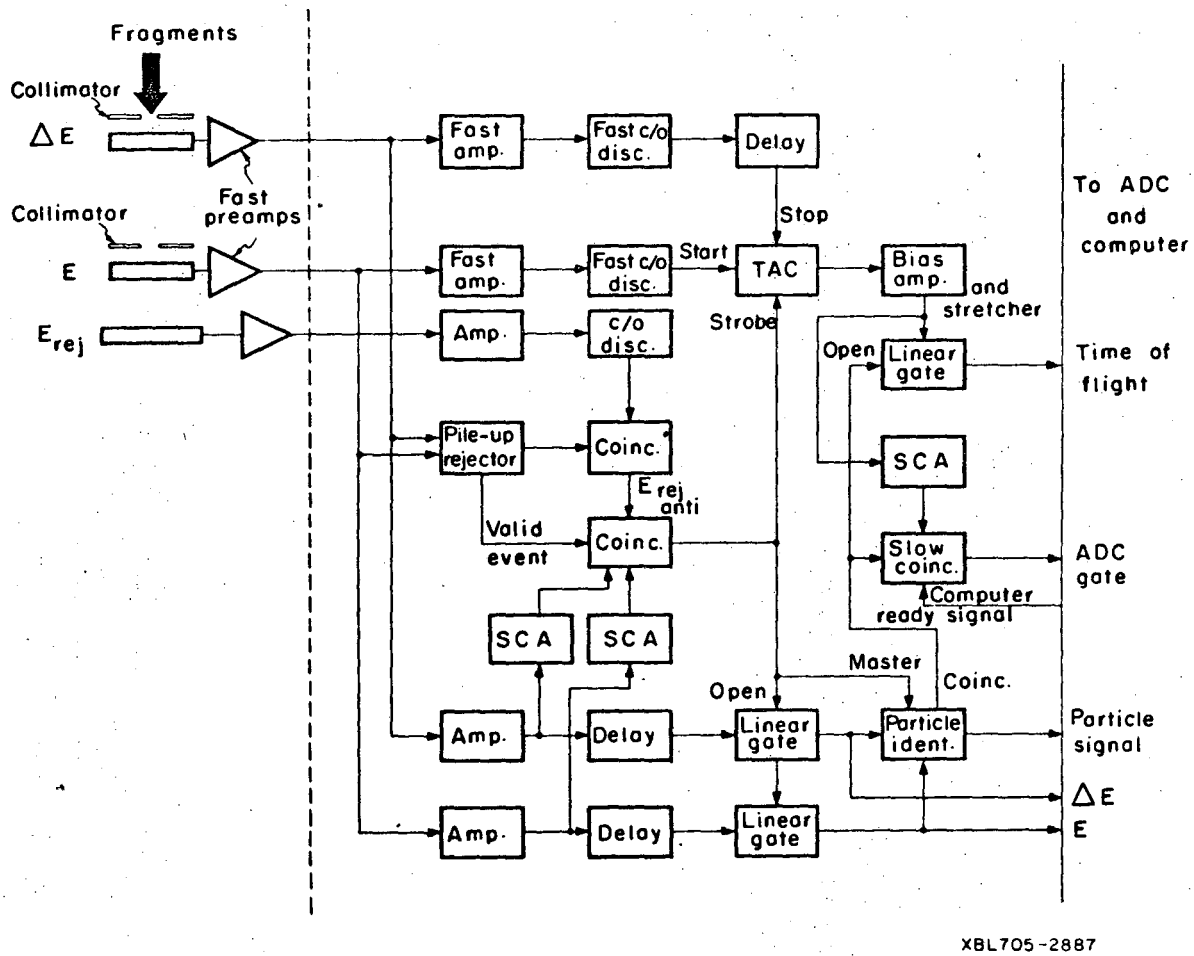
Fragments
Collimator
ΔE
Fast preamps
Collimator
E
E rej
Fast amp.
Fast c/o disc.
Delay
Stop
Fast amp.
Fast c/o disc.
Start
TAC
Bias amp.
and stretcher
Strobe
Amp.
c/o disc.
Open
Linear gate
Time of flight
Pile-up rejector
Coinc.
SCA
E rej anti
Valid event
Coinc.
Slow coinc.
ADC gate
Computer ready signal
SCA
SCA
Master
Coinc.
Open
Amp.
Delay
Linear gate
Particle ident.
Particle signal
ΔE
Amp.
Delay
Linear gate
E
To ADC and computer
XBL705-2887

Fig. 24

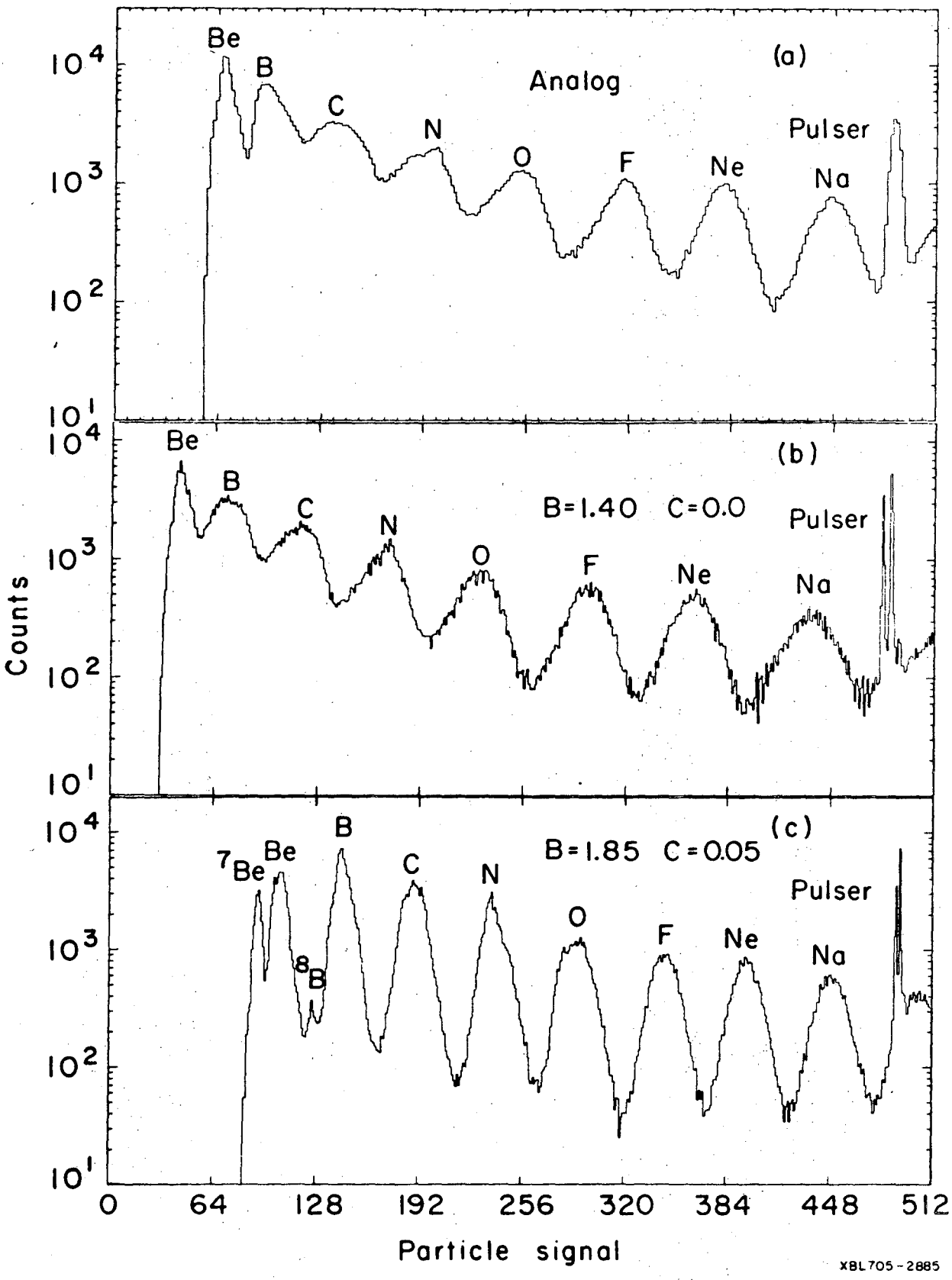
Be
B
C
N
O
F
Ne
Na
Analog
Pulser
(a)
(b)
B=1.40 C=0.0
(c)
B=1.85 C=0.05
^{7}Be
^{8}B
Counts
Particle signal
XBL705-2885

Fig. 25

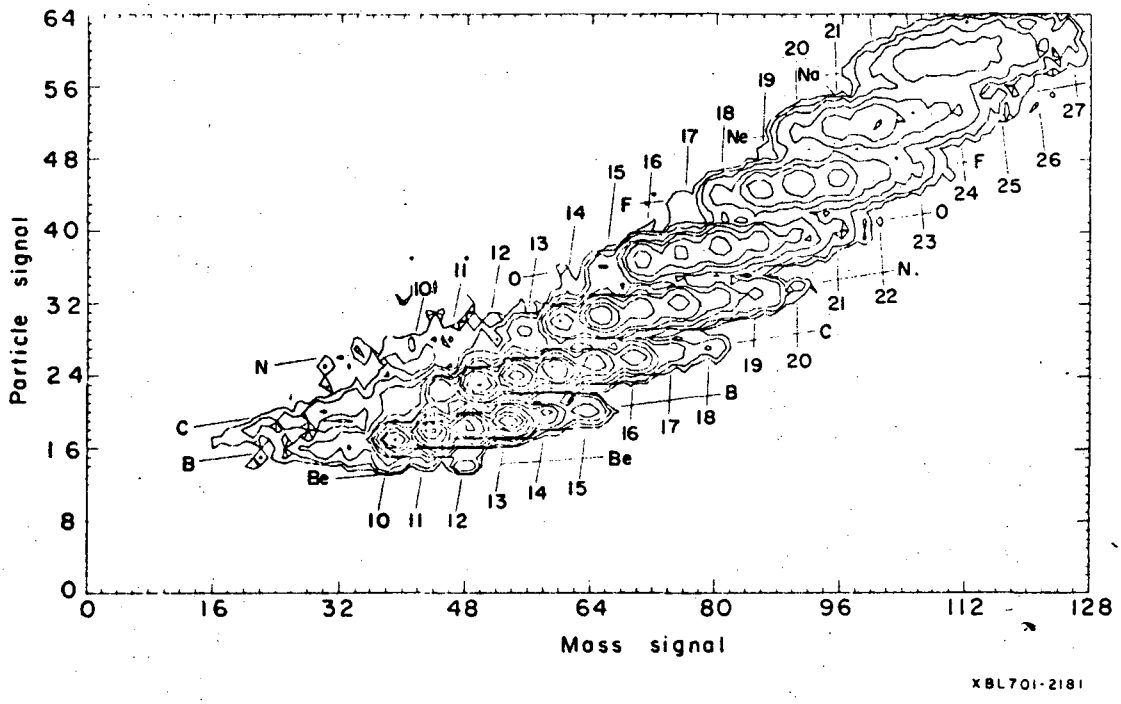
Particle signal
Mass signal
0
8
16
24
32
40
48
56
64
0
16
32
48
64
80
96
112
128
N
C
B
Be
10
11
12
13
14
15
16
17
18
19
20
21
Na
Ne
F
O
22
23
24
25
26
27
XBL701-2181

Fig. 26

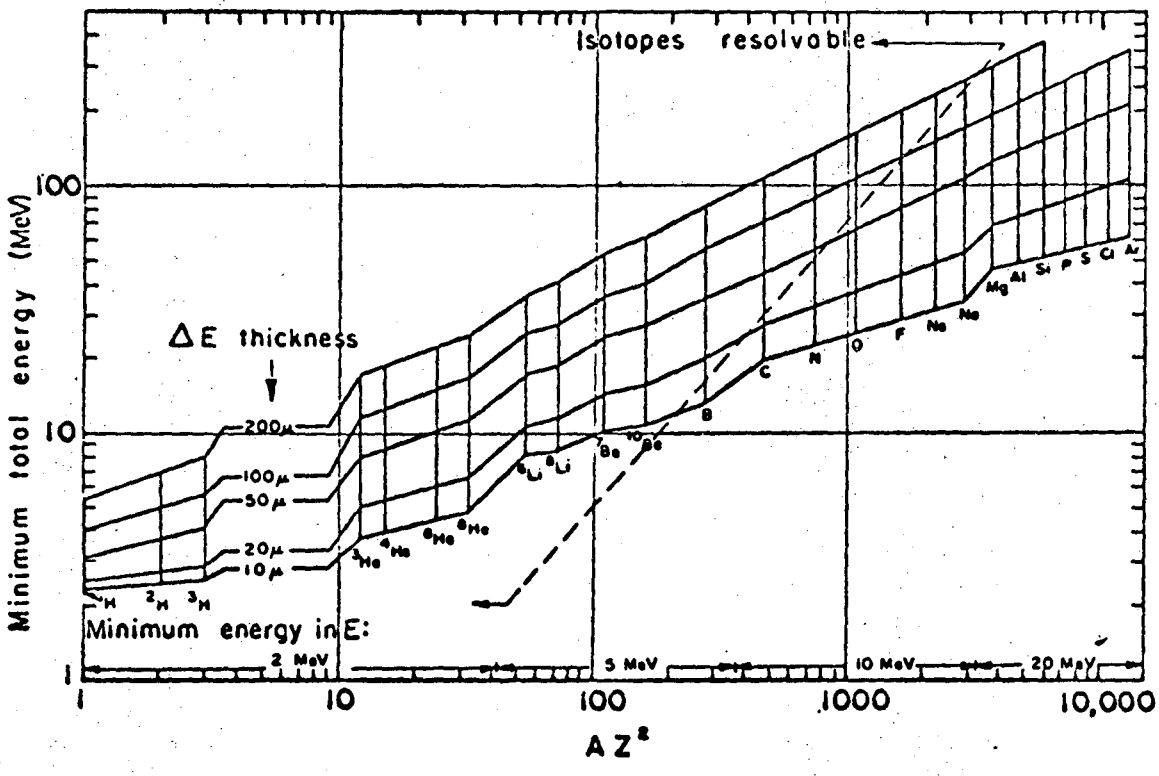
Isotopes resolvable
Minimum total energy (MeV)
ΔE thickness
200μ
100μ
50μ
20μ
10μ
Minimum energy in E:
2 MeV
5 MeV
10 MeV
20 MeV
AZ²
XBL697-3342

Fig. 27

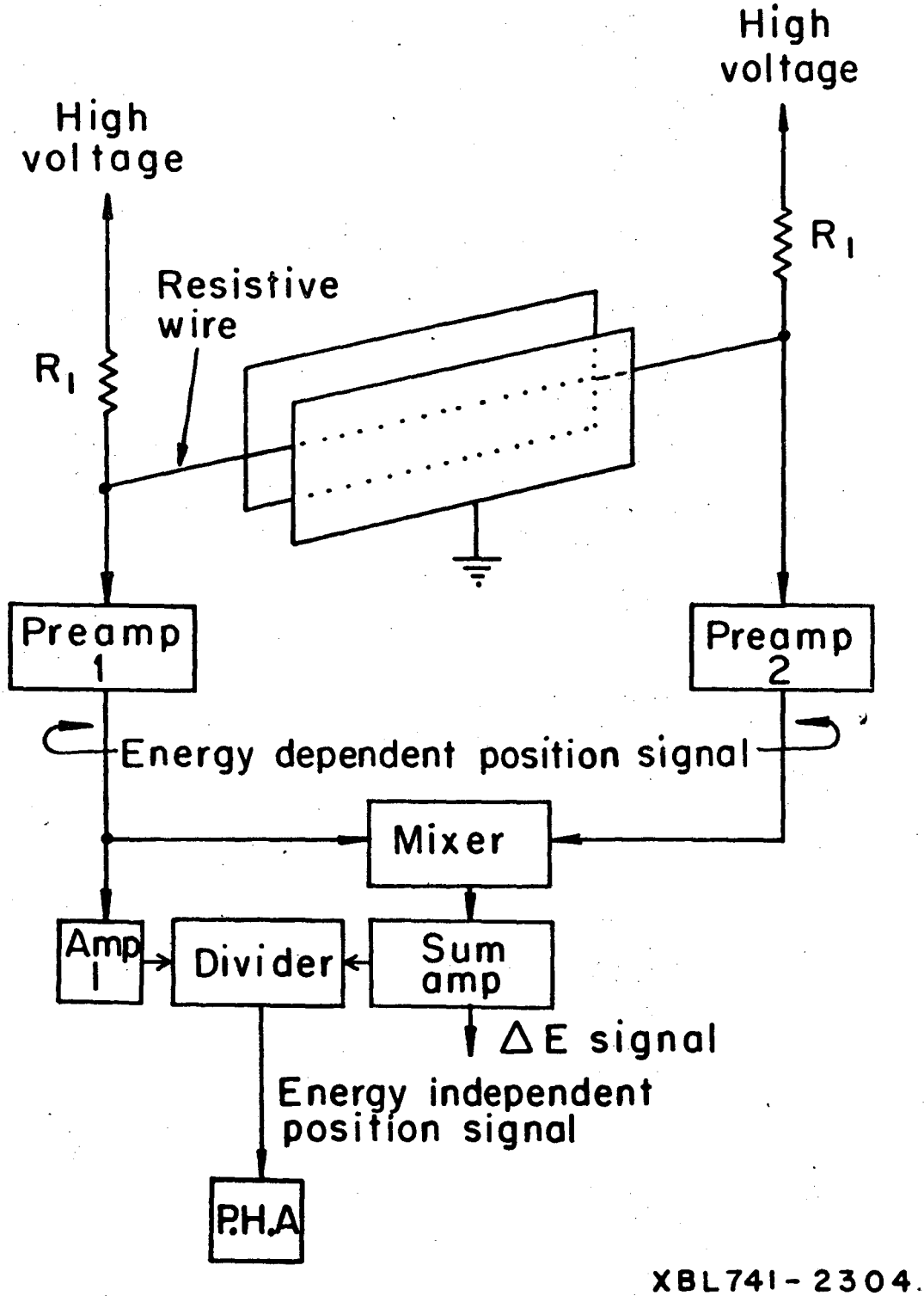
High voltage
High voltage
R1
Resistive wire
R1
Preamp 1
Preamp 2
Energy dependent position signal
Mixer
Amp 1
Divider
Sum amp
ΔE signal
Energy independent position signal
P.H.A
XBL741-2304

Fig. 28

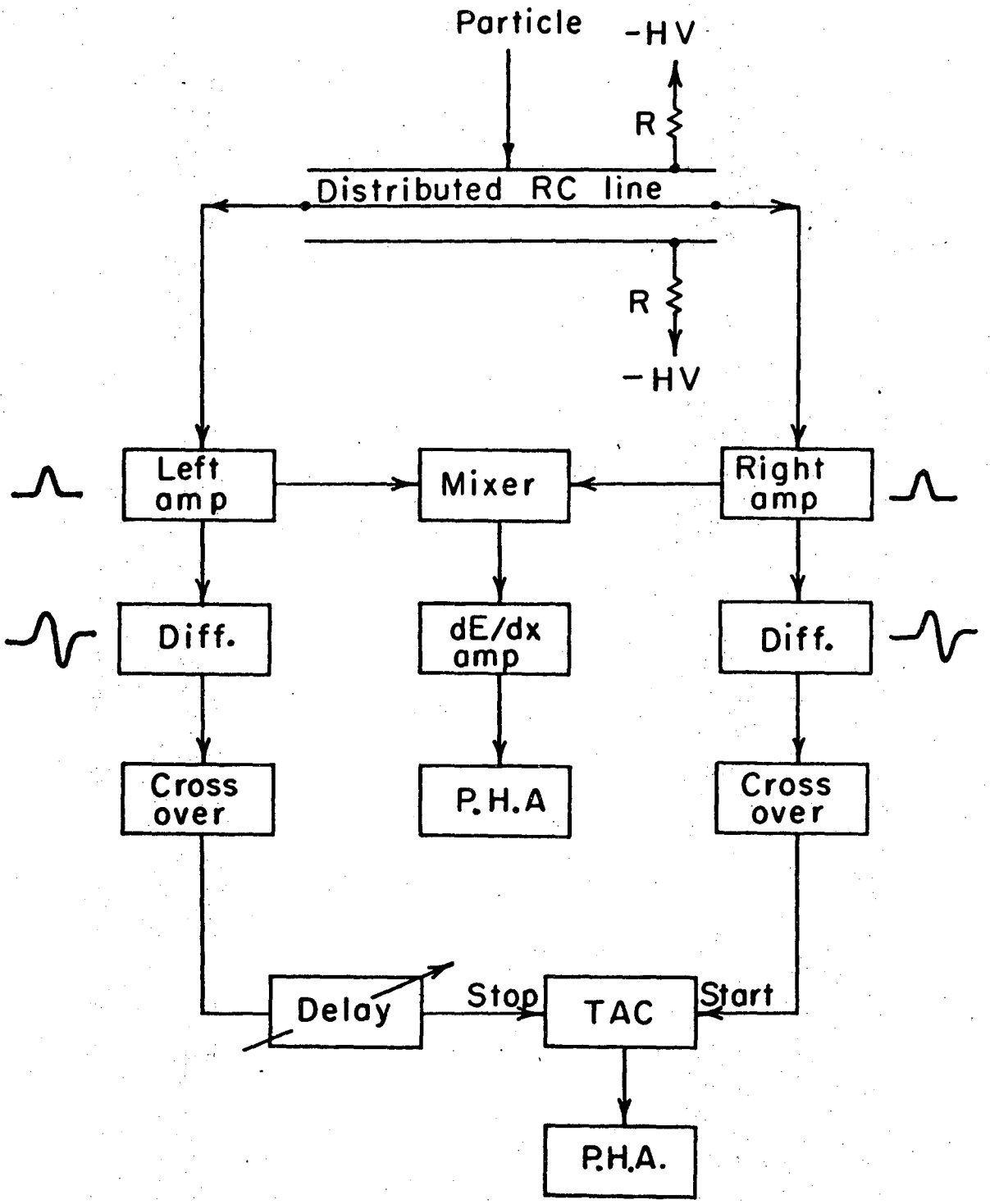
Particle
-HV
R
Distributed RC line
R
-HV
Left amp
Mixer
Right amp
Diff.
dE/dx amp
Diff.
Cross over
P.H.A
Cross over
Delay
Stop
TAC
Start
P.H.A.
XBL741-2305

Fig. 29

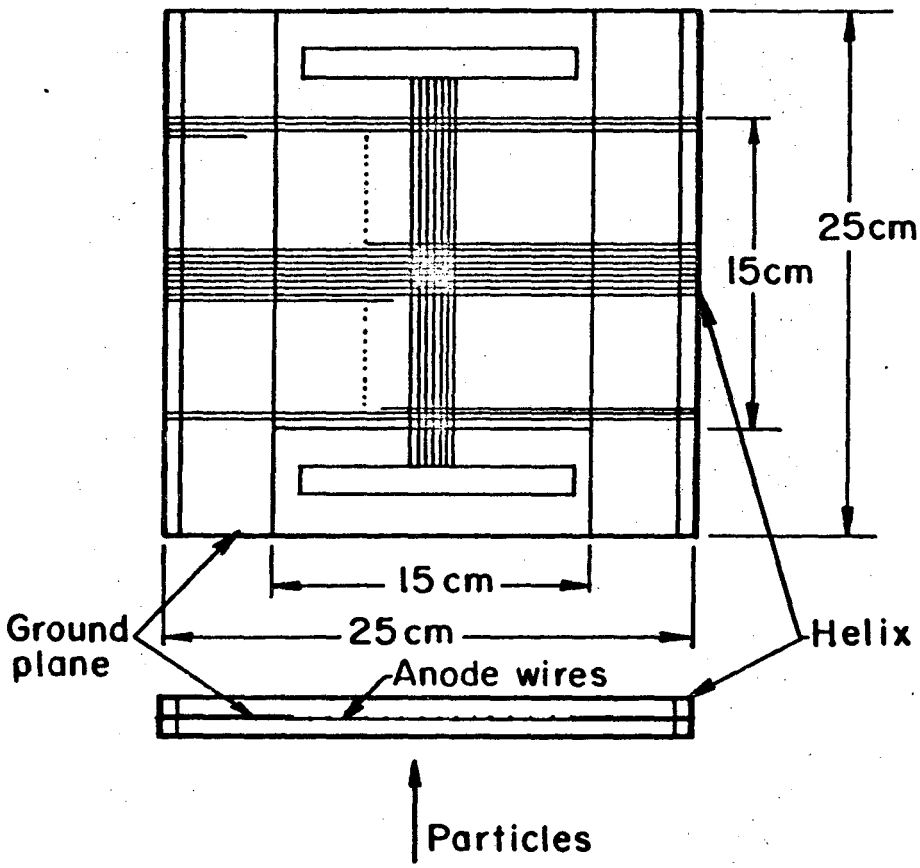

XBL 742-2306

Fig. 30a

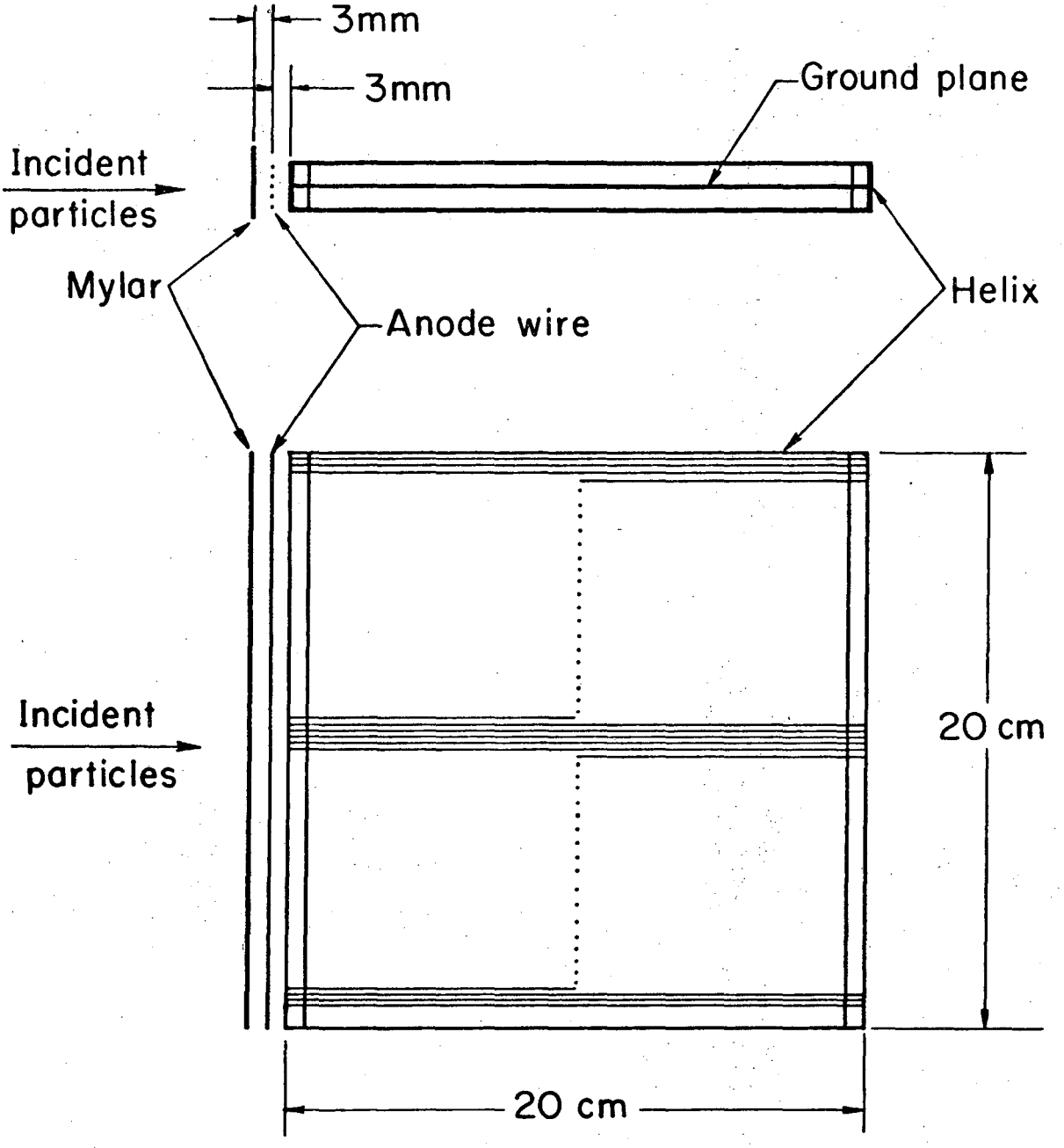
3mm
3mm
Ground plane
Incident
particles
Mylar
Anode wire
Helix
Incident
particles
20 cm
20 cm
XBL 742 - 2307

Fig. 30b

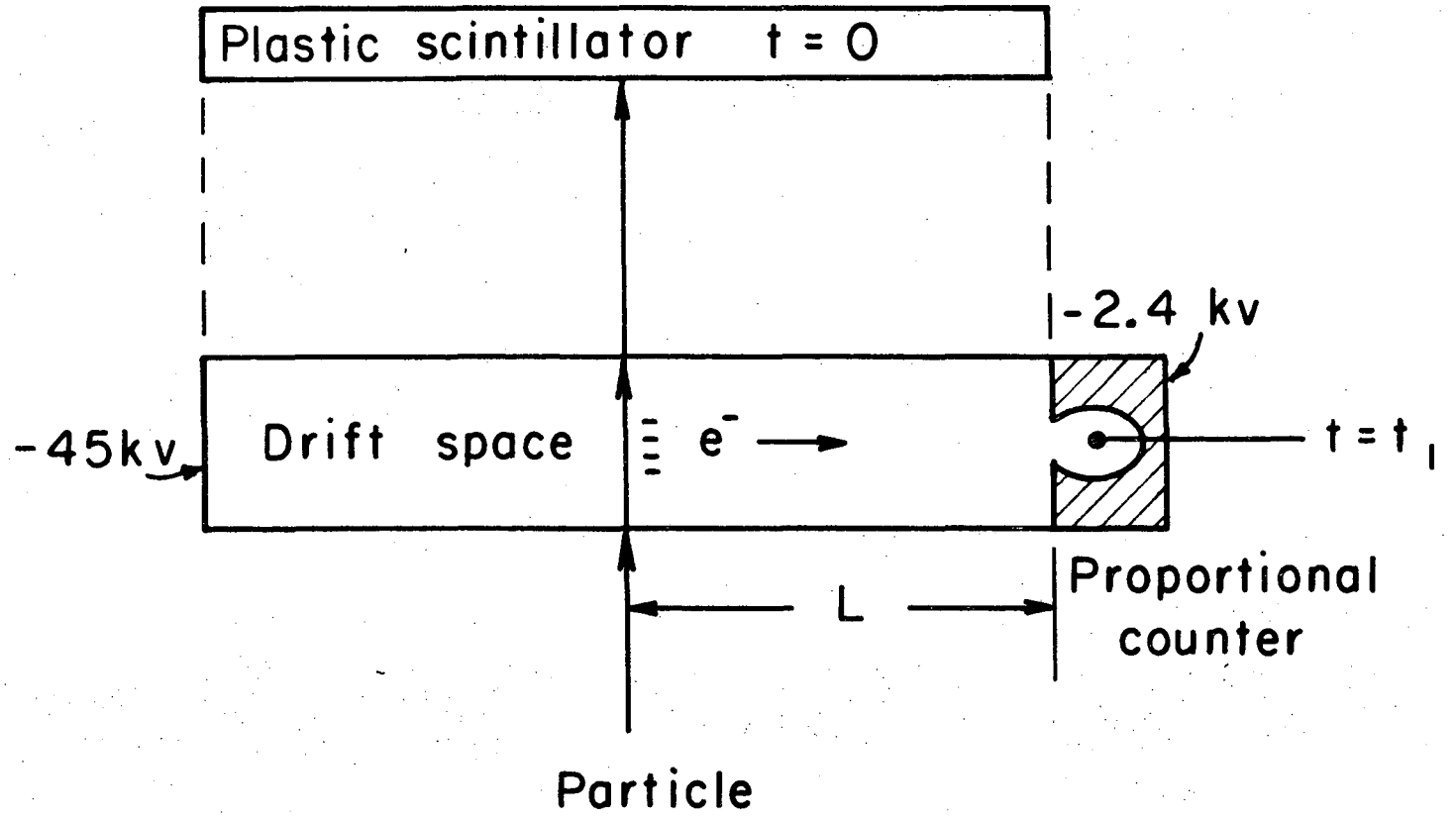

XBL741-2303

Fig. 31

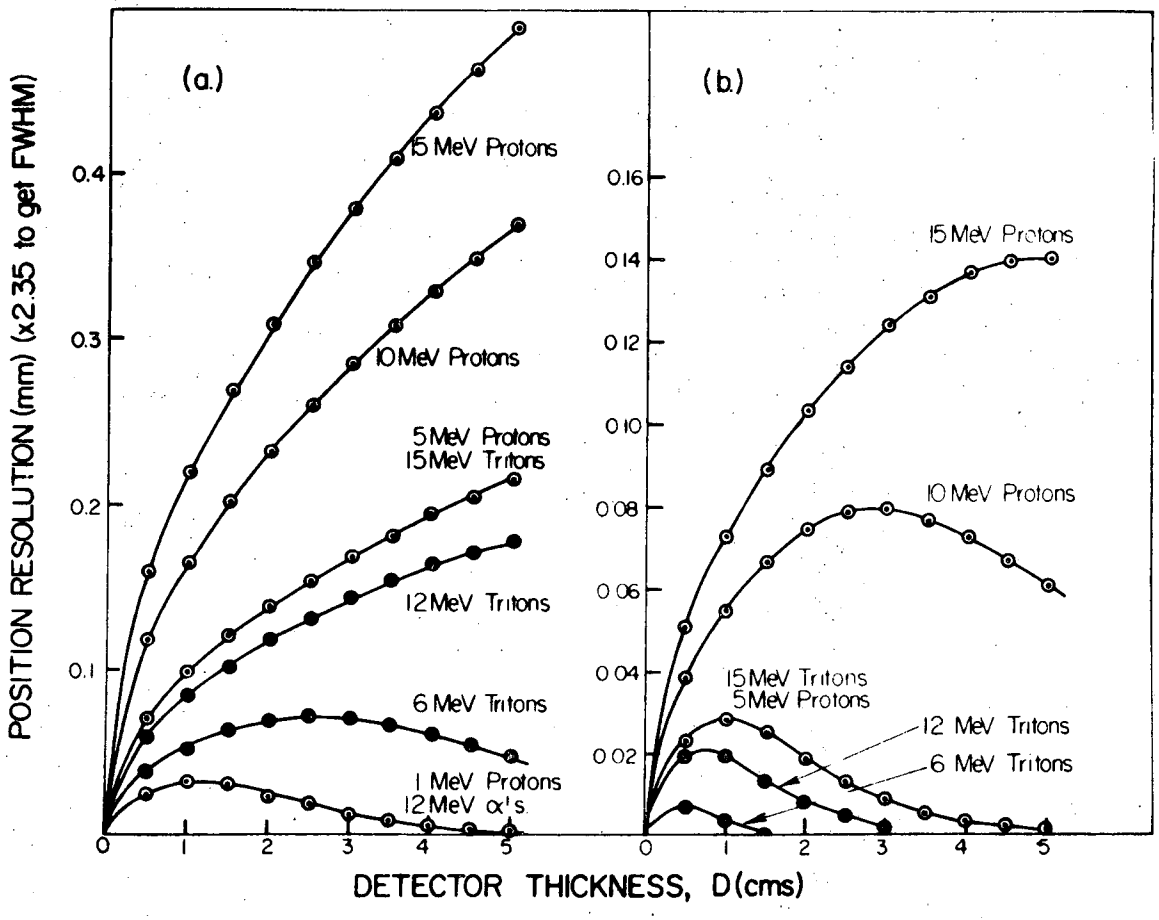

XBL 742-290

Fig. 32

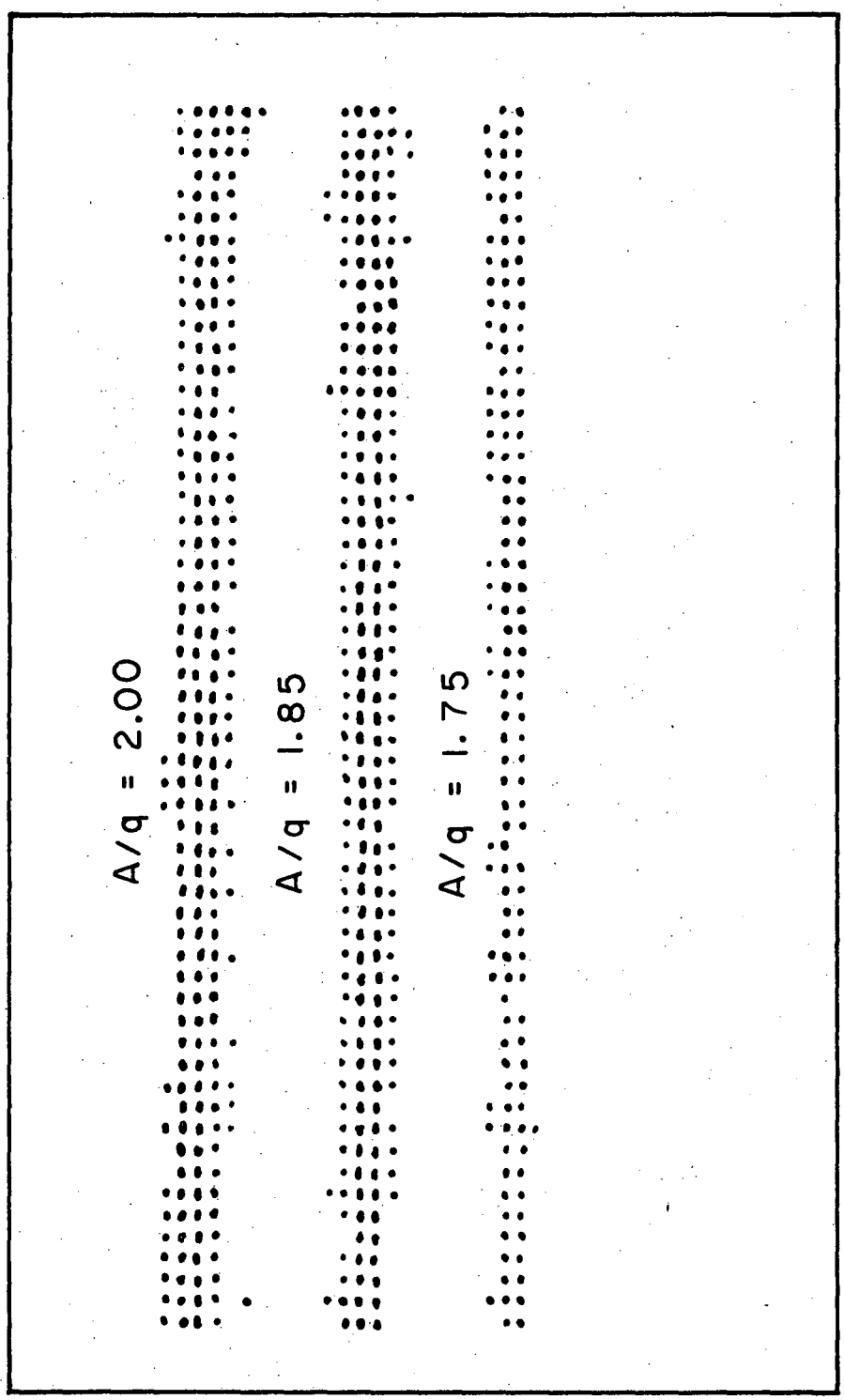

XBL741-2308

Fig. 33

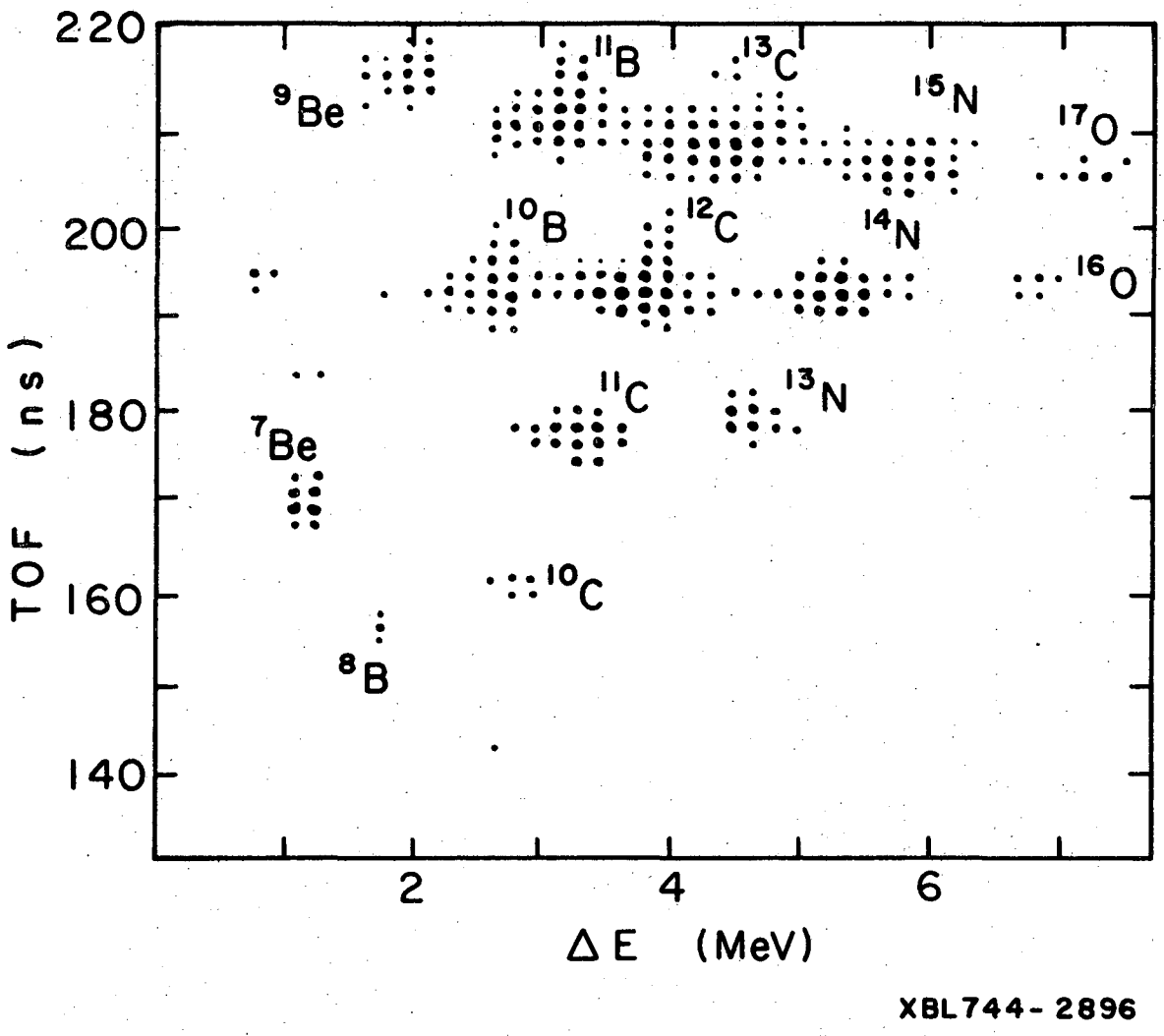
220
200
180
160
140
TOF (ns)
2
4
6
ΔE (MeV)
^{9}Be
^{11}B
^{13}C
^{15}N
^{17}O
^{10}B
^{12}C
^{14}N
^{16}O
^{7}Be
^{11}C
^{13}N
^{10}C
^{8}B
XBL744-2896

Fig. 34

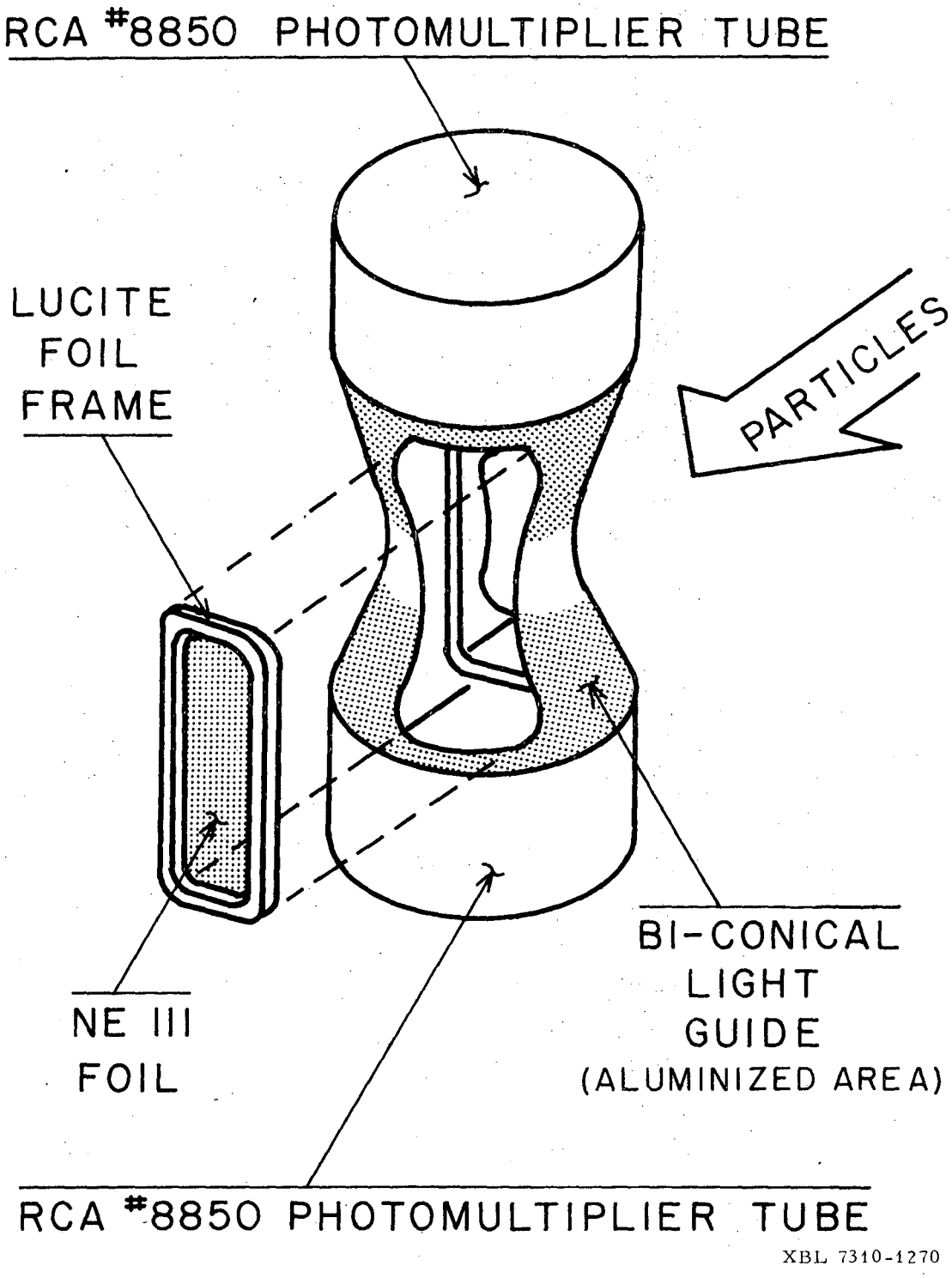
RCA #8850 PHOTOMULTIPLIER TUBE
LUCITE FOIL FRAME
PARTICLES
NE III FOIL
BI-CONICAL LIGHT GUIDE (ALUMINIZED AREA)
RCA #8850 PHOTOMULTIPLIER TUBE
XBL 7310-1270

Fig. 36

TECHNICAL INFORMATION DIVISION
LAWRENCE BERKELEY LABORATORY
UNIVERSITY OF CALIFORNIA
BERKELEY, CALIFORNIA 94720